



UNIVERSIDAD DE GRANADA

DEPARTAMENTO DE FÍSICA TEÓRICA Y DEL COSMOS

PROGRAMA OFICIAL DE POSGRADO EN FÍSICA Y MATEMÁTICAS

Characterisation of an isolated galaxy sample: Astrophysical implications

Maria del Carmen Argudo Fernández

Instituto de Astrofísica de Andalucía - CSIC



Directores:

Dr. Simon Verley

Dr. Gilles Bergond

Dr. Jack Sulentic

Editor: Editorial de la Universidad de Granada
Autor: María del Carmen Argurdo Fernández
D.L.: GR 721-2014
ISBN: 978-84-9028-878-8

La doctoranda Maria del Carmen Argudo Fernández y los directores de tesis Dr. Simon Verley, Dr. Gilles Bergond y Dr. Jack Sulentic, garantizamos, al firmar esta tesis doctoral, que el trabajo ha sido realizado por la doctoranda bajo la dirección de los directores de la tesis y hasta donde nuestro conocimiento alcanza, en la realización del trabajo, se han respetado los derechos de otros autores a ser citados, cuando se han utilizado sus resultados o publicaciones.

Granada, 24 de Septiembre de 2013



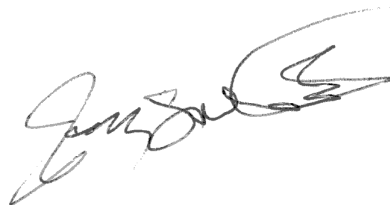
Fdo.:
La Doctoranda:
Maria del Carmen Argudo Fernández



Fdo.:
El Director:
Dr. Simon Verley



Fdo.:
El Director:
Dr. Gilles Bergond



Fdo.:
El Director:
Dr. Jack Sulentic

A mis padres Paco y Mari Carmen, a mi abuelo Manolo, y a Germán

Contents

Resumen	11
Abstract	13
Thesis outline	15
1 Introduction	17
1.1 Introduction to the thesis work	18
1.1.1 Cosmological scenario	18
1.1.2 The distribution of galaxies in the Universe	19
1.1.3 Isolated galaxies	22
1.2 The AMIGA project	22
1.2.1 The AMIGA project	22
1.2.2 The AMIGA data revision	23
1.2.3 Optical characterisation of the AMIGA sample	25
1.2.4 Previous revision of the environment	27
2 Revision of the isolation degree for galaxies in the CIG	31
2.1 Introduction	32
2.2 Data and methodology	33
2.2.1 CIG galaxies in the SDSS	34
2.2.2 Catalogues of neighbours	34
2.2.3 Estimation of apparent diameters from the SDSS	36
2.3 Quantification of the isolation	38
2.3.1 Isolation parameters	38
2.3.2 Comparison with denser environments	39
2.4 Results	40
2.4.1 Photometric study	40
2.4.2 Spectroscopic study	43
2.5 Discussion	46
2.5.1 Photometric study	46
2.5.2 Spectroscopic study	51
2.5.3 Photometric versus spectroscopic studies	52

2.6	Summary and conclusions	55
3	Effects of the environment on galaxies in the CIG	57
3.1	Introduction	58
3.2	The sample and the data	59
3.3	Identification of physical companions	60
3.3.1	Escape speed	60
3.3.2	Gaussian distribution of physical satellites	61
3.4	Quantification of the environment	61
3.4.1	Tidal strength parameter	61
3.4.2	Projected number density parameter	64
3.5	Results	64
3.5.1	Spectroscopic identification of physical satellites around galaxies in the CIG	64
3.5.2	Large Scale Structure	65
3.5.3	Local environment versus large scale environment	65
3.5.4	Correction for the redshift incompleteness	68
3.6	Discussion	68
3.6.1	The construction of the CIG	68
3.6.2	Identification of satellites	70
3.6.3	Local and large scale environments around CIG galaxies	71
3.6.4	Influence of the environment on the evolution of the primary galaxies	72
3.7	Summary and conclusions	74
4	Isolated galaxies, isolated pairs, and isolated triplets	79
4.1	Introduction	80
4.2	Data and definition of the samples	81
4.3	Physical definition	82
4.4	Quantification of the environment	83
4.4.1	Tidal strength	83
4.4.2	Projected density	83
4.5	Results	85
4.5.1	The catalogues	85
4.5.2	Relation to the Large Scale Structure	93
4.5.3	Morphology	93
4.6	Discussion	96
4.6.1	The catalogues	96
4.6.2	Relation with the Large Scale Structure	96
4.6.3	Euclidean Minimum Spanning Tree	100
4.6.4	Morphology	100
4.7	Summary and conclusions	103
5	Conclusions	105

A	Interactive 3D visualisation software	107
A.1	Interactive 3D visualisation software: pie chart	108
A.2	Interactive 3D visualisation software: Mollweide projection	110
B	Collaborations	113
B.1	Effect of the interactions and environment on nuclear activity	114
B.2	The stellar mass-size relation for the most isolated galaxies in the local Universe	116
B.3	Highly perturbed molecular gas in the Abell 1367 ram pressure stripping spiral archetype CGCG 97-079	118
C	CasJobs queries	119
C.1	SQL queries	120
C.1.1	Query 1: cross-ID for CIG galaxies in the SDSS	120
C.1.2	Query 2: searching for photometric SDSS neighbours	120
C.1.3	Query 3: cleaning photometric SDSS neighbours	120
C.1.4	Query 4: searching for spectroscopic SDSS neighbours	120
C.1.5	Query 5: photometric data for spectroscopic SDSS neighbours	122
D	Tables	123
D.1	Summary of the samples used in the photometric and spectroscopic studies for CIG galaxies	124
D.2	Quantification of the local and large scale environment	125

Resumen

Con objeto de entender cómo evolucionan las galaxias es necesario tener una muestra de referencia en la que los efectos del entorno estén minimizados y cuantificados. Los últimos avances en las grandes fuentes de datos espectroscópicos, como el Sloan Digital Sky Survey (SDSS), permiten visualizar el entorno tridimensional de las galaxias. En las dos primeras partes de esta tesis, y en el marco del proyecto AMIGA (Análisis del Medio Interestelar en Galaxias Aisladas), presentamos la revisión del grado de aislamiento de las galaxias pertenecientes al catálogo de galaxias aisladas (CIG; Karachentseva 1973) y el estudio tridimensional de su entorno. En la tercera parte de la tesis hemos construido nuevos catálogos de galaxias aisladas, pares aislados y tripletes aislados haciendo uso de información tridimensional.

Los principales objetivos de la tesis son:

- Refinar la muestra de galaxias en el CIG, la cual está definida visualmente a partir de placas fotográficas, proporcionando una mejora de la cuantificación del grado de aislamiento con respecto a los trabajos anteriores llevados a cabo en el proyecto, usando tanto datos de fotometría como de espectroscopía;
- Identificar y cuantificar los efectos de las galaxias satélites físicamente ligadas alrededor de galaxias en el CIG, así como los efectos de la estructura a gran escala del universo (LSS);
- Construir un catálogo nuevo de galaxias aisladas, así como catálogos de pares y tripletes de galaxias físicamente ligadas, pero aislados en su conjunto de otras estructuras.

Para llevar a cabo los objetivos planteados hemos desarrollado un método automático para la búsqueda de galaxias en el entorno de cada una de las galaxias en el CIG, en un área de hasta 3 Mpc de radio, haciendo uso de la novena publicación de datos del SDSS (SDSS-DR9). A la hora de identificar las galaxias vecinas físicamente ligadas, nos enfocamos en las galaxias satélites que no podrían escapar de la influencia gravitatoria de la galaxia central, definida a partir de su velocidad de escape. Con el fin de cuantificar el grado de aislamiento, tanto local como en relación a la LSS, se han estimado el parámetro de densidad hasta el quinto vecino más cercano y las fuerzas de marea que afectan a la galaxia central.

Por primera vez se han usado datos digitales para caracterizar el entorno alrededor de las galaxias en el CIG y cuantificar su grado de aislamiento. Además, la disponibilidad de los datos

espectroscópicos nos permite verificar la validez de los criterios de aislamiento usados para compilar el CIG, concluyendo que no es totalmente eficiente. Alrededor del 50% de los vecinos considerados como compañeros potenciales en el estudio fotométrico son, de hecho, galaxias del fondo. También encontramos que un 92% de las galaxias vecinas con velocidades de recesión similares a la de la galaxia CIG correspondiente, no son consideradas como compañeros potenciales por los criterios de aislamiento del CIG, y sin embargo pueden tener una influencia no despreciable sobre la evolución de la galaxia CIG central. Esto se traduce en una variedad de entornos para las galaxias en el CIG, que abarcaría desde galaxias en interacción con satélites físicos a galaxias sin ningún vecino dentro de 3 Mpc.

Aparece una clara separación entre galaxias CIG en interacción, que son más bien de tipo temprano, y galaxias aisladas, que preferentemente son de tipo tardío. Las galaxias aisladas son en general más azules, con poblaciones estelares probablemente más jóvenes y con mayor formación estelar, con respecto a las galaxias CIG más viejas y rojas que se encuentran en interacción. Recíprocamente, los satélites alrededor de galaxias CIG de tipo temprano, son más rojos y con poblaciones de estrellas más viejas, mientras que alrededor de galaxias CIG de tipo tardío, las galaxias satélites tienen un contenido estelar más joven. Esto sugiere que el CIG se compone de una población heterogénea de galaxias. Las galaxias CIG en interacción son marginalmente más masivas (0.3-0.4 dex), lo que podría indicar una mayor frecuencia de fusiones en el pasado.

A la luz de estos resultados, las grandes fuentes de datos espectroscópicos son la herramienta óptima para la construcción de nuevos catálogos de galaxias así como para el posterior estudio de su entorno. La información espectroscópica permite hacer distinción entre galaxias satélites (débiles y pequeñas, pero que pueden estar afectando la evolución de la galaxia central), y galaxias de fondo, teniendo así una clara visión del entorno tridimensional. Con esta idea y cómo última parte del trabajo de tesis, presentamos nuevos catálogos de galaxias aisladas, pares de galaxias aislados y tripletes de galaxias aislados en el universo local ($z \leq 0.080$), creados de forma homogénea usando la información tridimensional del SDSS. Los catálogos están compuestos por 4,191 galaxias aisladas, 1,270 pares aislados y 300 tripletes aislados. Para caracterizar su relación con el entorno local y a gran escala usamos el parámetro de densidad y el parámetro de fuerza de marea. Las asociaciones físicas en pares aislados y tripletes aislados suelen dar cuenta de más del 98% del total de las fuerzas de marea sobre la galaxia central. En relación con la LSS no hay diferencia entre galaxias aisladas, pares aislados y tripletes aislados, lo que sugiere que su formación y evolución podrían tener un origen común. La mayoría de las galaxias aisladas, pares aislados y tripletes aislados pertenecen a partes externas de filamentos, paredes y cúmulos, diferenciándose generalmente de la población de galaxias en entornos vacíos. Los tres catálogos están disponibles públicamente para la comunidad científica. Para las galaxias incluidas en estos catálogos proporcionamos sus posiciones, redshifts y grados de aislamiento con respecto tanto a su entorno físico local como a gran escala.

Abstract

In order to understand the evolution of galaxies, it is necessary to have a reference sample where the effects of the environment are minimised and quantified. Recent advances in large redshift galaxy surveys, such as the Sloan Digital Sky Survey (SDSS), allow to reach a 3-dimensional picture of the environment. In the first two parts of the thesis, we present, in the framework of the AMIGA project (Analysis of the interstellar Medium of Isolated GALaxies), a revision of the isolation degree and a study of the 3-dimensional environment for galaxies in the Catalogue of Isolated Galaxies (CIG, Karachentseva 1973). Using the 3-dimensional information, new catalogues of isolated galaxies, isolated pairs, and isolated triplets are assembled in the third part of the thesis.

The main aims of this thesis are:

- to refine the photographic-based CIG and to provide an improvement of the quantification of the isolation degree with respect to previous works, using both photometry and spectroscopy;
- to identify and quantify the effects of the physical satellite distribution around galaxies in the CIG, as well as the effects of the Large Scale Structure (LSS);
- to construct a catalogue of galaxies isolated in 3-dimension, and build catalogues of physically associated isolated pairs and isolated triplets.

We develop an automatic method to search for neighbours around each CIG galaxy in the SDSS (Ninth Data Release, DR9), within a projected area up to 3 Mpc. To recover the physically bound neighbour galaxies we focus on the satellites which are within the escape speed of each CIG galaxy. The local number density, at the 5th nearest neighbour, and the tidal strength affecting the CIG galaxy are estimated to quantify the local and LSS isolation degrees.

For the first time, the environment and the isolation degree of CIG galaxies are quantified using digital data. Besides, the availability of the spectroscopic data allows us to check the validity of the CIG isolation criterion, and shows that it is not fully efficient. Indeed, about 50% of the neighbours considered as potential companions in the photometric study are in fact background objects. We also find that about 92% of neighbour galaxies showing recession velocities similar to the corresponding CIG galaxy are not considered by the CIG isolation criterion as potential companions, and may have a non negligible influence on the evolution of the central CIG galaxy.

The CIG actually samples a variety of environments, from galaxies in interaction with physical satellites to galaxies with no neighbours within 3 Mpc.

A clear segregation appears between early-type CIG galaxies in weak interaction and isolated late-type CIG galaxies. Isolated galaxies are in general bluer, with likely younger stellar populations and a rather high star formation rate with respect to older, redder interacting CIG galaxies. Reciprocally, the satellites are redder and with older stellar populations around massive early-type CIG galaxies, while they have a younger stellar content around massive late-type CIG galaxies. This suggests that the CIG is composed of a heterogeneous population of galaxies, sampling from old systems of galaxies to more recent, dynamical systems of galaxies. Interacting CIG galaxies might have a mild tendency (0.3-0.4 dex) to be more massive, which may indicate a higher frequency of having suffered a merger in the past.

In light of the above findings, the construction of catalogues of galaxies in relation to their environments should take into account the redshift information to distinguish small, faint, interacting satellites from a background projected galaxy population, and reach a more comprehensive 3-dimensional picture of the surroundings. Therefore, in the last part of the thesis work, we present new catalogues of isolated galaxies, isolated pairs, and isolated triplets in the local Universe ($z \leq 0.080$), homogeneously selected using the 3-dimensional information contained in the SDSS-DR9. We provide catalogues of 4,191 isolated galaxies, 1,270 isolated pairs, and 300 isolated triplets and characterise their relation to the LSS using the projected number density and the tidal strength. The physical companions in the pair and triplet samples usually account for more than 98% of the total tidal strength affecting the central galaxy. We find no difference in their relation with the LSS, which may suggest that these isolated systems have a common origin in their formation and evolution. Most of the isolated galaxies, isolated pairs, and isolated triplets, belong to the outer parts of filaments, walls, and clusters, and generally differ from the void population of galaxies. The three catalogues are publicly available to the scientific community. For galaxies in the catalogues, we provide their positions, redshifts, and degrees of relation with their physical and LSS environments.

Thesis outline

From here we present the work developed during this PhD. In Chapter 1 we present an introduction to the thesis work with an overview on the cosmological scenario, the distribution of galaxies in the Universe, and isolated galaxies. We also present the AMIGA project which is the framework where the thesis study was carried on, as well the definition of the Catalogue of Isolated Galaxies, its refinements, and the multiwavelength studies.

The thesis presented here aims to answer open questions related with the role of the environment on galaxy evolution: Are isolated galaxies a special class or are they simply the most isolated galaxies in the large scale structure? What is the effect of satellites or minor companions on primary galaxies? What are the advantages and main results of the study of the 3-dimensional environment versus previous 2-dimensional studies? In order to answer these and other questions, the PhD work is divided into three main parts:

- revision of the CIG isolation criterion and quantification of the environment for CIG galaxies in Chapter 2,
- identification of physical companions and quantification of their effects on CIG galaxies in Chapter 3,
- and compilation of three catalogues of isolated galaxies, isolated pairs, and isolated triplets in Chapter 4.

Finally, we present the main final conclusions of the thesis in Chapter 5.

In addition, the interactive 3D visualisation software developed is introduced in Appendix A, and the published collaborations during the PhD are presented in Appendix B. Some of the queries to the SDSS CasJobs tool are compiled in Appendix C. A summary table of Chapter 2 and the final table compiled in Chapter 3 are included in Appendix D.

Chapter 1

Introduction

Contents

1.1	Introduction to the thesis work	18
1.1.1	Cosmological scenario	18
1.1.2	The distribution of galaxies in the Universe	19
1.1.3	Isolated galaxies	22
1.2	The AMIGA project	22
1.2.1	The AMIGA project	22
1.2.2	The AMIGA data revision	23
1.2.3	Optical characterisation of the AMIGA sample	25
1.2.4	Previous revision of the environment	27

1.1 Introduction to the thesis work

1.1.1 Cosmological scenario

Current observations ([Planck Collaboration et al. 2013a,b](#)) allow reasonably precise estimation of the cosmological parameters that describe our Universe. The results are consistent with a Λ CDM Universe, called the Standard Model of modern cosmology. According to the model, our Universe is governed by Einstein's General Relativity with zero curvature and two main components: dark energy and cold dark matter. Dark energy is responsible for the acceleration of the Universe. Dark matter, on the contrary, is the major contributor to the gravitational attraction between the galaxies, and drives the formation of discrete objects (i.e. galaxies). Matter as it is usually understood, baryonic matter (protons, neutrons and electrons), contributes only $\sim 4\%$. Meanwhile, dark energy and cold dark matter contribute $\sim 3/4$ and $\sim 1/4$ respectively. Other particles (e.g. neutrinos and photons) make negligible contribution.

These component quantities are usually given in terms of the density parameter. The amount of dark energy is $\Omega_\Lambda = 0.725 \pm 0.016$ and dark matter $\Omega_m = 0.274 \pm 0.012$ ([Komatsu et al. 2011](#)). The density parameter of a given component is the ratio between the density of this component and the critical density, $\Omega = \rho/\rho_c$, where the critical density is defined as $\rho_c = 3H_0^2/8\pi G$, where H_0 is the value of the Hubble constant and G the gravitational constant.

The overall expansion of the Universe is referred to as the Hubble flow, described locally by a first approximation of the Hubble law ([Hubble 1929](#)): $v_H \simeq cz = H_0 d$, where v_H is the recession velocity of a galaxy, c is the velocity of light, and d is the galaxy distance from us. In an expanding Universe a photon emitted by a galaxy with wavelength λ_e is observed with wavelength λ , this displacement $z = \frac{\lambda - \lambda_e}{\lambda_e}$ is called redshift.

The redshift z is directly related to the expansion. For a given cosmological model the distance is a function of z . The redshift is affected by peculiar velocities, i.e. movements produced by gravitational interactions between a galaxy and its neighbours (binaries, groups, clusters): $v = v_H + v_p$. In rich clusters these velocities can exceed 10^3 km s^{-1} . Peculiar velocities can change the value of z from the value expected assuming a smooth Hubble flow, so the estimated distances to nearby galaxies are especially affected unless standard candles like Cepheids can be employed.

In this study we assume a cosmology with $\Omega_\Lambda = 0.7$, $\Omega_m = 0.3$ and $H_0 = 70 \text{ km s}^{-1} \text{ Mpc}^{-1}$.

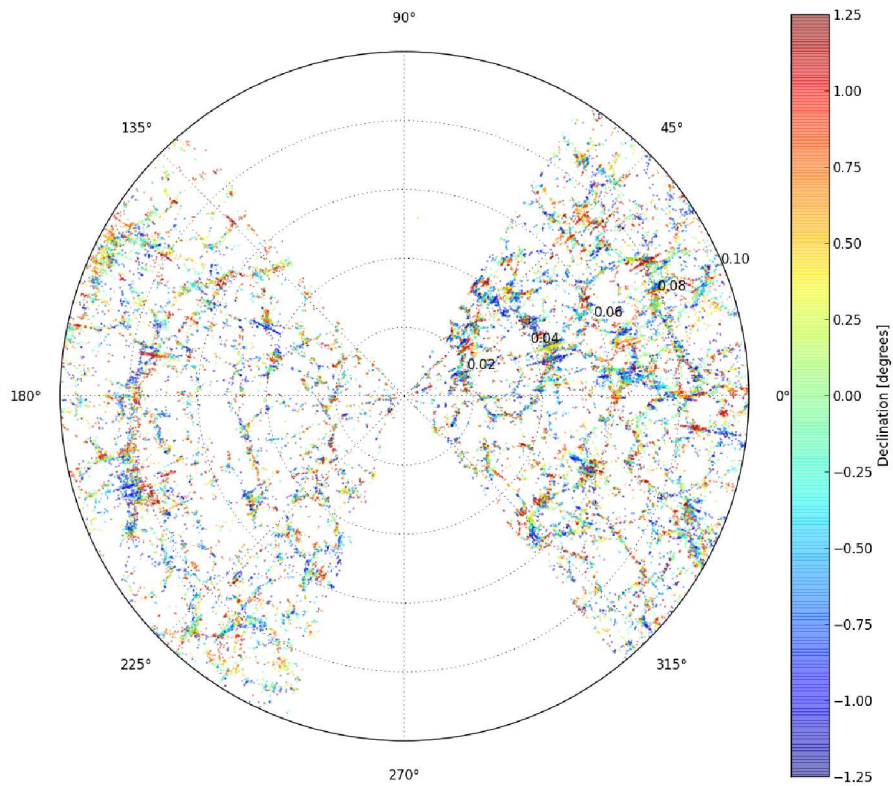


Figure 1.1: SDSS galaxy map. Slices through the SDSS-DR9 3D map of the galaxy distribution. Both slices contain 34274 galaxies within -1.25 and 1.25 degrees in declination. The galaxies are located towards the northern (left part) and southern (right part) Galactic caps (above and below the plane of the galaxy). The region between the wedges was not mapped by SDSS because of dust obscuration in our own Galaxy. Galaxies are coloured according to their declination.

1.1.2 The distribution of galaxies in the Universe

By combining redshift with angular position data, galaxy redshift surveys are essential to provide a 3-Dimensional (3D) map of the galaxy distribution. Recent galaxy surveys like the 2dF Galaxy Redshift Survey (Colless et al. 2001), the Sloan Digital Sky Survey (Abazajian et al. 2003), and the 2MASS Redshift Survey (Huchra et al. 2012), have confirmed that the distribution of galaxies in the Universe is non-uniform, showing a hierarchical structure of filaments and walls, with galaxy clusters at the intersection of the filaments, and large embedded voids with diameters of a few dozens Mpc (see Figs. 1.1 and 1.2). Galaxies in denser structures tend to further cluster in

even larger scale superclusters, representing the largest aggregates in the Universe.

In the local Universe ($z \lesssim 0.1$), the Virgo cluster, approximately 20 Mpc distant, is the largest aggregate of the Local supercluster of galaxies. The Local Group and the Virgo cluster are parts of the Local (Virgo) Supercluster (Courtois et al. 2013). Many luminous galaxies are found in pairs including the Milky Way and Andromeda in the Local Group. Our galaxy itself is surrounded by up to a hundred small satellites at distances $\lesssim 2$ Mpc (Koposov et al. 2008; Tollerud et al. 2008; Wang et al. 2012).

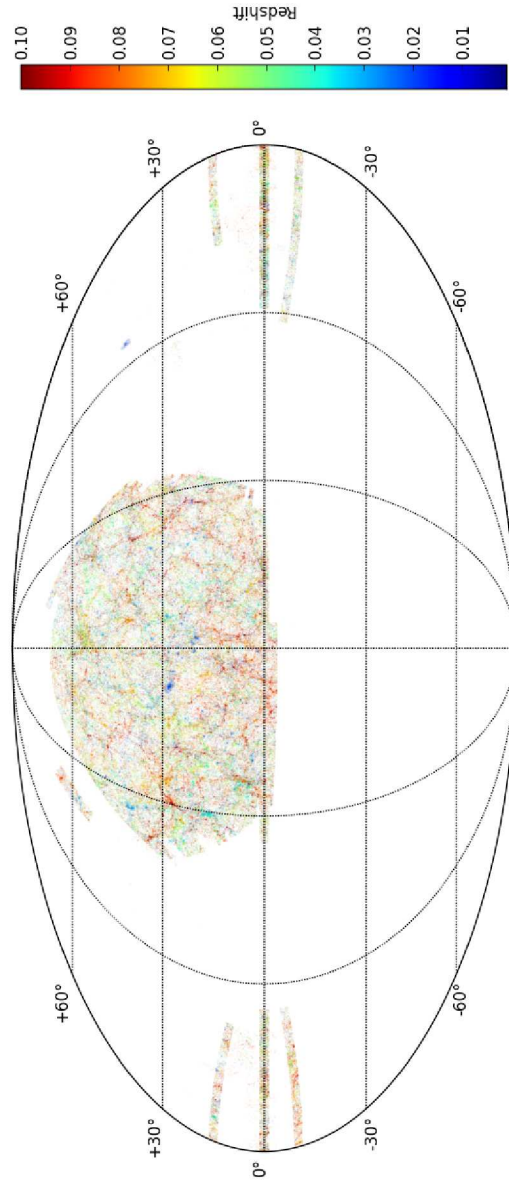


Figure 1.2: Mollweide projection of the Large Scale Structures in the local Universe (North is up, East is to the left). The SDSS-DR9 357358 galaxies are colour coded according to their spectroscopic redshift. The blue cluster at $z \approx 0.023$ and located at (195, 28) corresponds to Coma cluster.

1.1.3 Isolated galaxies

About 54% of galaxies in the local Universe are concentrated in groups and clusters, 20% in regions around them, and the remaining galaxies (referred to as the general field) are distributed along filaments bordering voids (Karachentsev et al. 2011; Makarov & Karachentsev 2011; Elyiv et al. 2013). About 10% of these field galaxies are found in loose pairs and compact groups. Samples of the most isolated galaxies can be extracted from this general field population. Estimation of the fraction of "extremely isolated" galaxies is a topic of growing interest. Studies of isolated galaxies can be argued to begin with the publication of the Catalogue of Isolated Galaxies (CIG, Karachentseva 1973).

The most isolated galaxies in the local Universe will be located in regions of below average density on Mpc scales and will not be subject to significant influence from close neighbours for significant time periods. A significant population of isolated galaxies is of great interest for testing different scenarios of the origin and evolution of galaxies. In this sense, dynamically isolated galaxies are an ideal reference sample for studying the effects of environment on different galaxy properties. Ideal because such a sample represents the most nurture-free galaxy population that exists.

Isolated galaxies have seen an uncertain history with many denying the existence of any significant isolated galaxy population. Does a true population of isolated galaxies exist (i.e. a true field) or are "isolated galaxies" simply the least clustered galaxies in the Universe? Regardless of the answer it is assumed that over the past several billion years the evolution of these objects has been largely driven by internal processes. It is possible to suggest that many or most of these galaxies have spent the majority of their lives in relative isolation.

1.2 The AMIGA project

1.2.1 The AMIGA project

While it is widely accepted that galaxy evolution is affected, or even driven, by the influence of nearby galaxies (nurture) a well defined baseline for quantifying this influence is lacking. The AMIGA project (Analysis of the interstellar Medium of Isolated GALaxies¹) was initiated in 2002 at Instituto de Astrofísica de Andalucía (IAA-CSIC) to provide such a baseline by quantifying the properties of a well defined sample of "nature-dominated" galaxies. The AMIGA project adopts the CIG as a starting point, and proceeds to extract a refined sample of the historically most significant sample of isolated galaxies in the local Universe. Naturally this does not address the isolation properties of low luminosity dwarfs because: a) they were not included in the CIG and 2) redshift incompleteness would make reliable isolation assessment impossible.

The main goals of AMIGA are:

1. To compare and quantify properties of different phases of the interstellar medium (ISM) in the galaxies – especially the level of star formation and nuclear activity.

¹<http://amiga.iaa.es>

2. To quantify the role of nature versus nurture by distinguishing between effects of environmental density and one-on-one interactions.
3. To use the isolated galaxy sample as a control or template for studies of star formation and galaxy evolution in denser environments.
4. To use the AMIGA sample to redefine fundamental correlations between measured galaxy properties without the scatter induced by effects of nurture that are present in almost all samples.

All CIG galaxies are found in the Catalogue of Galaxies and Clusters of Galaxies (CGCG; Zwicky & Kowal 1968) with apparent photographic magnitudes $m_{pg} < 15.7$ mag. These systems represent $\sim 3\%$ of the CGCG.

The CIG isolation criteria (Eqs. 1.1 and 1.2) consider a primary galaxy of angular diameter D_P as isolated if there is no neighbour i with an angular diameter D_i between 0.25 and $4 \times D_P$ lying within a projected distance 20 times the diameter of the neighbour:

$$\frac{1}{4} D_P \leq D_i \leq 4 D_P \quad ; \quad (1.1)$$

$$R_{iP} \geq 20 D_i \quad . \quad (1.2)$$

The AMIGA project refines the pioneering CIG in several ways, including: a revision of all galaxy positions (Leon & Verdes-Montenegro 2003); an optical study, including sample re-definition, magnitude correction, and full-sample analysis of the optical luminosity function (Verdes-Montenegro et al. 2005); a morphological revision and type-specific optical luminosity function analysis (Sulentic et al. 2006); a study on $H\alpha$ morphology (Verley et al. 2007a); and a re-evaluation of the degree of isolation of the CIG (Verley et al. 2007b,c). The original CIG contains 1051 elements, but one of the compiled objects is a globular cluster (CIG 781; Verdes-Montenegro et al. 2005) so the size of the sample considered in the rest of this study is $N = 1050$.

The AMIGA project also starts several multiwavelength studies for galaxies in the CIG: characterisation of the B -band luminosity function (Sulentic et al. 2006); Fourier photometric decomposition, optical asymmetry, and photometric clumpiness and concentration (Durbala et al. 2008, 2009); characterisation of the FIR luminosity function (Lisenfeld et al. 2007), radio-continuum (Leon et al. 2008), molecular gas (Lisenfeld et al. 2012), and atomic gas (Espada et al. 2011); characterisation of nuclear activity (Sabater et al. 2008, 2012); optical colours (Fernández Lorenzo et al. 2012); and optical study of the stellar mass-size relation (Fernández Lorenzo et al. 2013).

1.2.2 The AMIGA data revision

Significant number of new data are available since the project started. Several improvements to the CIG have been performed, being among the most relevant the reevaluation of redshifts and distances (Sec. 1.2.2), morphologies (Sec. 1.2.2) and isolation degree (Sec. 1.2.4). Recently, Fernández Lorenzo et al. (2012) revised apparent magnitudes, morphological types, distances and

optical luminosities for the CIG with respect to the ones used in [Verdes-Montenegro et al. \(2005\)](#) and [Lisenfeld et al. \(2007\)](#). In the frame of the Wf4Ever project², this revision of the properties of the CIG has been partially automated by the implementation of scientific workflows.

Redshifts and distances

*Main papers: [Verdes-Montenegro et al. \(2005\)](#)
and [Fernández Lorenzo et al. \(2012\)](#)*

Initially, [Xu & Sulentic \(1991\)](#) reported distances for 476 galaxies in the CIG. Later [Verdes-Montenegro et al. \(2005\)](#) retrieved distances for 574 galaxies collected from 41 references as well as from new observations including ten new redshifts from HI observations. 62 CIG galaxies remain without redshifts.

[Fernández Lorenzo et al. \(2012\)](#) report new redshift and distances for CIG galaxies with heliocentric velocities (v_{Hel}) larger than 1000 km s^{-1} . The value of v_{Hel} for a galaxy with available redshift data has been updated when the errors quoted in the recent bibliography were smaller than in the previous compilation. The new public release of the AMIGA database shows only 40 CIG galaxies without redshift data in the bibliography, hence 1010 out of 1050 CIG galaxies currently have redshift measures. Recently we have found redshift information for seven more CIG galaxies: one from the SDSS and six from the CfA Redshift Survey³.

The mean recession velocity of the CIG is $v = 6624 \text{ km s}^{-1}$ ($z \sim 0.022$), hence the CIG samples the local Universe (see Fig. 1.3). The peaks at redshift near 1500 and 5000 km s^{-1} correspond respectively to galaxies in the Local supercluster and those in more distant large-scale components (particularly Perseus-Pisces).

Morphologies

*Main papers: [Sulentic et al. \(2006\)](#)
and [Fernández Lorenzo et al. \(2012\)](#)*

[Sulentic et al. \(2006\)](#) provide morphological classifications for 80% of CIG galaxies from images of the Palomar Observatory Sky Survey 2 (POSS-II) and new CCD images taken mainly at the 1.5m Observatorio de Sierra Nevada (OSN) for the remaining 20% of the sample. Fig. 1.4 shows some examples of the images used for the classification.

In addition to velocities and distances, [Fernández Lorenzo et al. \(2012\)](#) revised morphologies for all CIG galaxies with $v_{hel} > 1000 \text{ km s}^{-1}$ from CCD images available either from the SDSS or existing data in the AMIGA database ($N = 843$). For CIG galaxies with $v_{hel} < 1000 \text{ km s}^{-1}$ ($N = 57$), morphological types were compiled from the bibliography. For $N = 134$ galaxies with only POSS-II data available, a second revision has been performed, with minor modifications to the values assigned in [Sulentic et al. \(2006\)](#). For the remaining galaxies for which they were unable to perform any classification, [Fernández Lorenzo et al. \(2012\)](#) used data found in NED and HyperLeda databases. Globally there is a shift in the morphologies with respect to [Sulentic](#)

²<http://www.wf4ever-project.org>

³<https://www.cfa.harvard.edu/~dfabricant/huchra/zcat/>

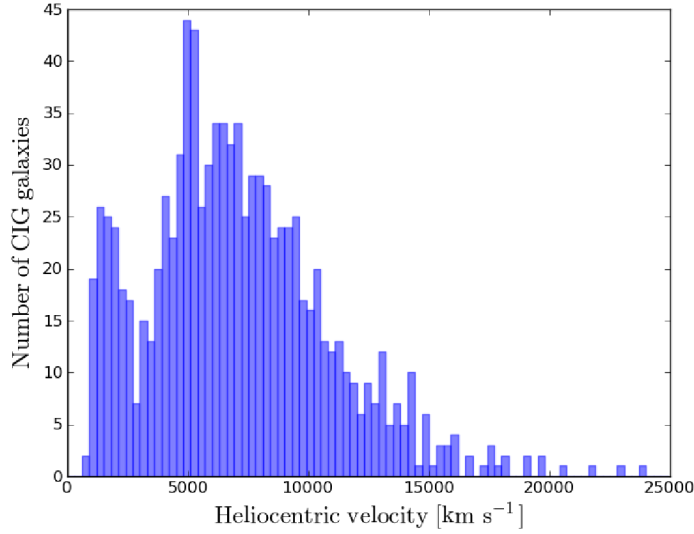


Figure 1.3: Histogram of the optical heliocentric velocities for 1010 CIG galaxies, out of 1050 galaxies in the CIG, currently with redshift measures from [Fernández Lorenzo et al. \(2012\)](#).

[et al. \(2006\)](#) towards later types by $\Delta T = 0.2$, that they interpret as due to the higher resolution provided by CCD images revealing smaller bulges.

All morphological types are found in the CIG and the sample is large enough to permit discrimination on the basis of galaxy type. The sample is dominated by two populations: 1) 82% spirals (Sa-Sd) with the bulk being luminous systems with small bulges (63% between types Sb–Sc) and 2) a significant population of early-type E-S0 galaxies (14%), following the well known morphology-density relation ([Dressler 1980](#)). A considerable number of galaxies in the catalogue ($n = 193$) are flagged for the presence of nearby projected companions or signs of distortion likely due to interaction.

1.2.3 Optical characterisation of the AMIGA sample

The basic properties of galaxies can be affected by both nature (internal processes) or nurture (effects of environment). Disentangling the two effects is becoming an important matter in astrophysics. Observed properties of a sample of isolated galaxies should be mainly the result of internal (natural) evolution. It follows that nurture-induced galaxy evolution can only be understood through a comparative study of galaxies in different environments. In order to study the properties of the different components of the ISM, the star formation and the nuclear activity in isolated galaxies, the AMIGA team have observed or compiled multiwavelength information for the CIG sample: optical, far-infrared, H α line and radio continuum data for the whole sample and H α and CO line for a velocity limited sample. The data are publicly available in the web page of the project via the AMIGA VO compliant interface.

Since the present study is developed using optical digital photometric (CCD) data, we sum-

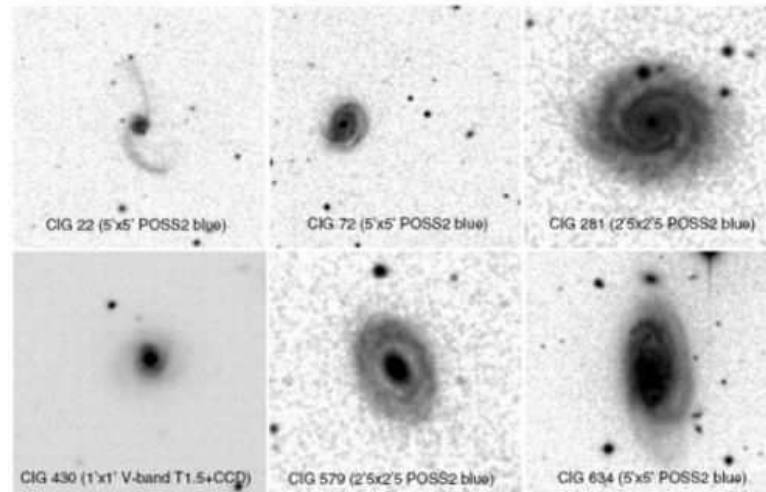


Figure 1.4: Optical images of some AMIGA galaxies, from POSS-II and OSN, used by [Sulentic et al. \(2006\)](#) to perform the morphological classification. Source: [Sulentic et al. \(2006\)](#).

marise here the latest results according to the optical characterisation of the CIG.

a) Optical colours

Main paper: [Fernández Lorenzo et al. \(2012\)](#)

The optical colours of galaxies reflect their stellar populations and these colours correlate with morphology and environment. The distribution of galaxy colours in the $(g - r)$ versus $(u - g)$ plane ([Strateva et al. 2001](#)) shows a strong bimodality with clear separation into red and blue sequences. These two colour peaks correspond roughly to early- (E, S0, and Sa) and late-type (Sb, Sc, and Irr) galaxies, as expected from the respective dominance of old and young stellar populations. Environment is also thought to play a role in the mix of morphological types, which is reflected by the morphology-density relation ([Dressler 1980](#), see also Sec. 1.2.2): in dense environments luminous red early-type galaxies predominate while in the lowest density environment blue late-type spirals are the defining population.

[Fernández Lorenzo et al. \(2012\)](#) take a first look at SDSS $(g - r)$ colours of galaxies in the CIG, finding a weak tendency for spiral galaxies to be redder than objects in close pairs. In comparison with galaxies in denser environments, there is not a clear difference (see Fig. 1.5), however the $(g - r)$ colour of isolated galaxies shows a Gaussian distribution, as might be expected assuming nurture-free evolution. The redder colours of spirals and lower colour dispersions for CIG galaxy subtypes, in comparison with pairs of galaxies, are likely caused by a more passive star formation in isolated galaxies.

b) Optical characterisation of nuclear activity

Main paper: [Sabater et al. \(2012\)](#)

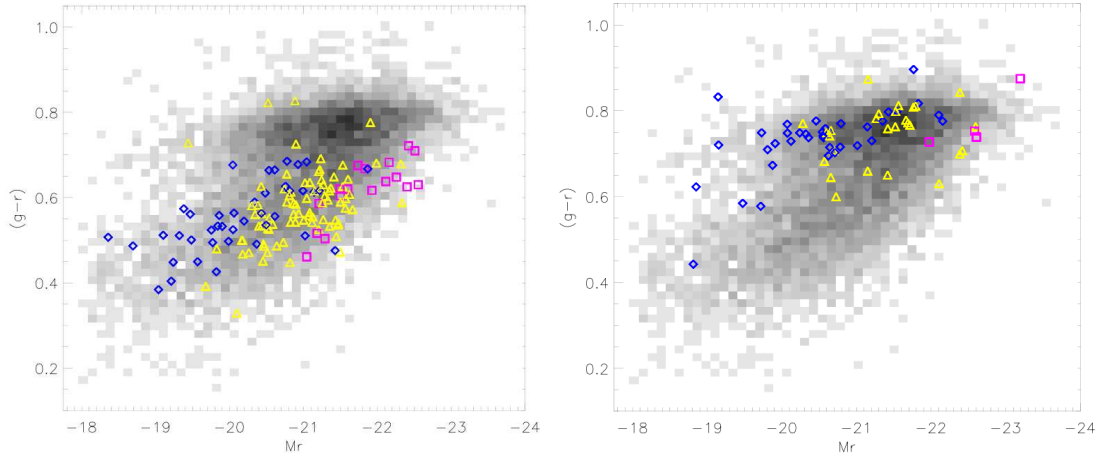


Figure 1.5: $(g-r)$ colour–magnitude diagram for Sc (left panel) and E/S0 (right panel) galaxies in the CIG. The blue diamonds are objects at $z < 0.02$, the yellow triangles are galaxies at redshift $0.02 < z < 0.04$, and the pink squares are objects at $z > 0.04$. The gray scale represents the density diagram obtained from the [Nair & Abraham \(2010\)](#) sample at $0.01 < z < 0.05$, using the data from the SDSS-DR8. Source: [Fernández Lorenzo et al. \(2012\)](#).

Galaxy interactions are thought to induce nuclear activity by removing angular momentum from the gas and, in this way, feeding the central black hole. Hence, a higher rate of active galactic nuclei (AGN) is expected among interacting galaxies. However, different studies have yielded contradictory results: some studies find a higher local density of companions near galaxies hosting an AGN or a higher prevalence of AGN in interacting galaxies, while others find no excess, or only a marginal excess. The use of different classification criteria to evaluate whether the nuclear emission is powered by star formation (SF) or by an AGN also complicates the direct comparison of results found in different studies.

[Sabater et al. \(2012\)](#) present a catalogue of nuclear properties (spectroscopic data, stellar populations, emission lines and classification of optical nuclear activity) for CIG galaxies obtained from optical spectra provided by the SDSS in its 6th Data Release. The prevalence of optical AGN in CIG galaxies is 20.4%, or 36.7% including transition objects (see Fig. 1.6). The fraction of AGN increases steeply towards earlier morphological types and higher luminosities. In comparison with galaxies in Hickson Compact Groups (isolated compact groups of galaxies; HCG, [Hickson 1982](#)), there is no evidence for a difference in the prevalence of AGN between isolated and compact group galaxies. They find that a major interaction is not a necessary condition for the triggering of optical nuclear activity.

1.2.4 Previous revision of the environment

*Main papers: [Verley et al. \(2007c\)](#)
and [Verley et al. \(2007b\)](#)*

One of the AMIGA improvements of the CIG involves the revision and quantification of the

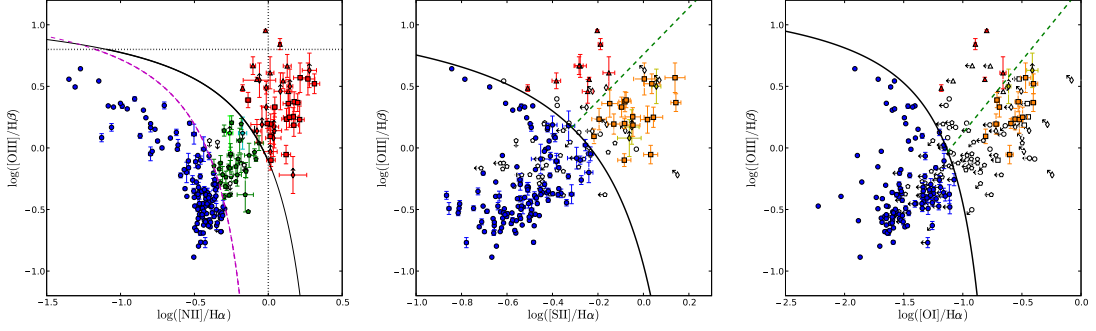


Figure 1.6: *Left panel: $[\text{N}_1\text{I}]$ diagnostic diagram. Middle panel: $[\text{S}_1\text{I}]$ diagnostic diagram. Right panel: $[\text{O}_1\text{I}]$ diagnostic diagram. Source: Sabater et al. (2012).*

isolation criterion. This study supposes the basis reference of the present PhD work.

Verley et al. (2007c) used DPOSS-I and DPOSS-II images for the first revision. The digitised images from photographic plates enabled them to revise the environmental characterisation for all 950 CIG galaxies having radial velocities larger than 1500 km s^{-1} for neighbours within a minimum physical radius of 0.5 Mpc. All candidate neighbours brighter than $m_B = 17.5 \text{ mag}$ were identified in each field using the LMORPHO software (Odehahn 1995; Odehahn et al. 1996, 2002). A catalogue of approximately 54,000 neighbours was created with redshifts available for only $\sim 30\%$ of the sample. Six hundred sixty-six galaxies passed and two hundred eighty-four failed the original CIG isolation criterion based on POSS1.

Fig. 1.7 shows comparison of the magnitude difference distributions for neighbour galaxies considered by the CIG isolation criteria and for the remaining neighbours. With this comparison it was possible to test whether a criterion of isolation based on the difference in magnitudes between the candidate CIG galaxy and its neighbours was, or was not, equivalent to the CIG isolation criteria as claimed by other authors. The overlap between the two distributions shows that a cut in magnitude at 3 is a rather good approximation because it loses only 10% of the neighbours selected by (Karachentseva 1973) on the basis of the linear size factor of 4.

Verley et al. (2007b) used two complementary parameters in order to quantify the isolation degree of each CIG galaxy. The local number density of neighbour galaxies η_k , and the tidal strength Q of the local neighbours on the central galaxy. The local number density η_k is defined as follows:

$$\eta_k \propto \log\left(\frac{k-1}{V(r_k)}\right) \quad (1.3)$$

where $V(r_k) = \frac{4}{3} \pi r_k^3$ and r_k is the projected distance to the k^{th} nearest neighbour, with k equal to 5, or less if there are not enough neighbours in the field. And the tidal strength exerted by one companion is defined as:

$$Q_{iP} \equiv \frac{F_{\text{tidal}}}{F_{\text{bind}}} \propto \frac{M_i}{M_P} \left(\frac{D_P}{R_{iP}}\right)^3 \quad (1.4)$$

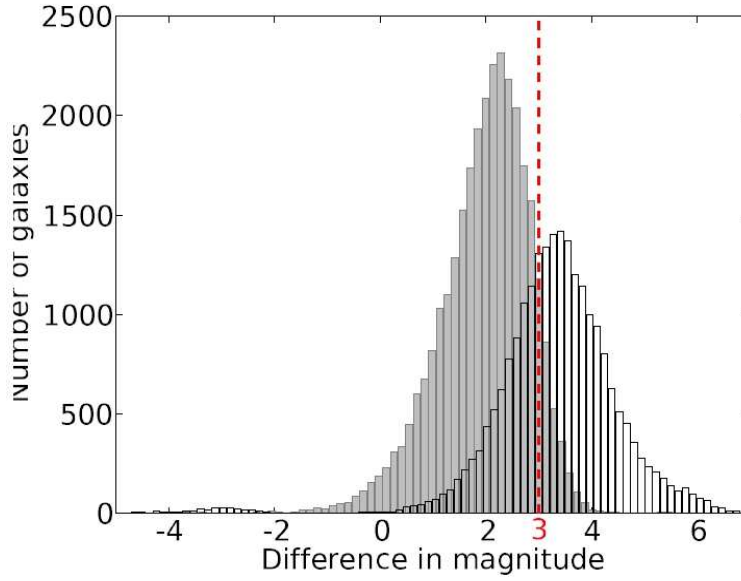


Figure 1.7: Comparison of the magnitude difference distributions for the neighbour galaxies considered by the first CIG isolation criterion (factor 4 in size with respect to their associated CIG galaxy, grey histogram) and for the remaining neighbours (outside the factor 4 in size, unfilled histogram). Source: Verley et al. (2007c).

where M_i and M_P are the mass of the neighbour and the primary galaxy respectively, D_P the apparent diameter of the primary galaxy, and R_{iP} the projected distance between the neighbour and primary galaxy. Using the apparent diameter as an approximation for galaxy mass:

$$Q_{iP} \equiv \frac{F_{\text{tidal}}}{F_{\text{bind}}} \propto \left(\frac{\sqrt{D_P D_i}}{R_{iP}} \right)^3 \quad (1.5)$$

This approximation is based on the dependence of galaxy mass M on size: $M \propto D^\gamma$, with $\gamma = 1.5$ (Dahari 1984; Trujillo et al. 2004). The final tidal parameter considered is a dimensionless estimation of the gravitational interaction strength, calculated from the logarithm of the sum of the tidal strengths created by all the neighbours in the field, $Q = \log(\sum Q_{iP})$.

Fig. 1.8 shows the two isolation parameters for galaxies in the AMIGA sample as well as other samples of galaxies in denser environments: galaxy triplets (KTG; Karachentseva et al. 1979), galaxies in compact groups (HCG; Hickson 1982); and galaxies in Abell clusters (ACO; Abell 1958; Abell et al. 1989). The mean tidal strength estimator increases from CIG galaxies to galaxies in triplets and compact groups. The tidal strength and the local number density estimations are complementary parameters, and it is important to use both of them in order to have an accurate picture of the effect of neighbouring galaxies on the primary galaxy. The CIG galaxies show a continuous spectrum of isolation, as quantified by the two parameters, from very isolated to interacting. The fraction of CIG galaxies whose properties are expected to be little influenced by the environment is 791 (out of 950 galaxies considered in the study). The revised CIG was considered as a reference in further AMIGA works.

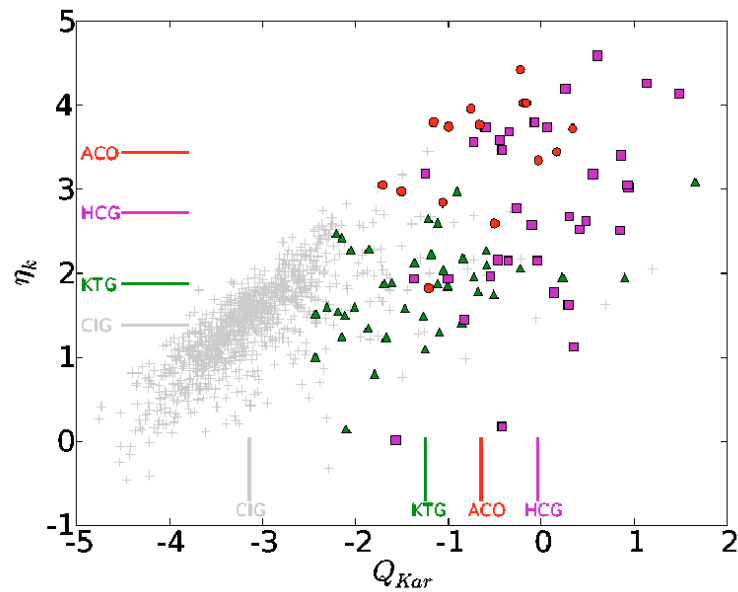


Figure 1.8: Quantification of the environment from [Verley et al. \(2007b\)](#). The y-axis represents the "k-density estimator" and the x-axis the "Tidal forces estimator". CIG galaxies are represented as grey crosses, green triangles are galaxies in triplets, red circles are galaxies of Abell clusters and magenta squares are galaxies in Hickson Compact Groups. The mean value for each sample are indicated as vertical and horizontal lines with the same colour code. Source: [Verley et al. \(2007b\)](#).

Chapter 2

Revision of the isolation degree for galaxies in the Catalogue of Isolated Galaxies

Contents

2.1 Introduction	32
2.2 Data and methodology	33
2.2.1 CIG galaxies in the SDSS	34
2.2.2 Catalogues of neighbours	34
2.2.3 Estimation of apparent diameters from the SDSS	36
2.3 Quantification of the isolation	38
2.3.1 Isolation parameters	38
2.3.2 Comparison with denser environments	39
2.4 Results	40
2.4.1 Photometric study	40
2.4.2 Spectroscopic study	43
2.5 Discussion	46
2.5.1 Photometric study	46
2.5.2 Spectroscopic study	51
2.5.3 Photometric versus spectroscopic studies	52
2.6 Summary and conclusions	55

2.1 Introduction

During the past forty years it has become clear that galaxy properties and evolution can be driven as much by environment as by initial conditions, even if the details of environmental influence are not yet well quantified. Some observed properties show a strong dependence on the environment, for instance, on the optical and ultraviolet luminosity and atomic gas mass function (Blanton & Moustakas 2009), on the infrared luminosity function (Xu & Sulentic 1991) or the associated stellar mass function (Balogh et al. 2001), on the morphology-mass relation (Calvi et al. 2011), and on the galaxy colours (Hogg et al. 2004; Baldry et al. 2006).

Isolated galaxies are located in environments of such low density that they have not been appreciably affected by their closest neighbours during a past crossing time $t_{cc} = 3$ Gyr (Verdes-Montenegro et al. 2005). The observed physical properties of these systems are expected to be mainly determined by initial formation conditions and secular evolutionary processes. A representative sample of isolated galaxies is therefore needed to test models of galaxy formation and evolution. It may also serve as a reference sample in studies of galaxies in pairs, triplets, groups, and clusters. This will aid our understanding of the effects of the environment on fundamental galaxy properties.

Statistical studies of isolated galaxies require a large and morphologically diverse sample. Few good samples of isolated galaxies exist, one of the largest being the Catalogue of Isolated Galaxies (CIG; Karachentseva 1973). The original visual systematic search for isolated galaxies using the First Palomar Observatory Sky Survey (POSS-I) employs a visual projected isolation criterion. Since the redshift distances of only a few galaxies were known at that time, isolation in the third dimension could not be directly estimated. Instead, any galaxy with nearby similar-size neighbours was rejected. The resulting CIG includes 1050 galaxies (plus CIG 781, a globular cluster mistakenly included in the original list).

Despite the importance of analysing pure 'nature' samples, not many additional studies of isolated galaxies were carried out in the following three decades (Huchra & Thuan 1977; Adams et al. 1980; Arakelian & Magtesian 1981; Brosch & Shaviv 1982; Varela et al. 2004). This led many scientists to assume that no real isolated galaxy population exists. It is natural therefore that the AMIGA (Analysis of the interstellar Medium of Isolated GALaxies¹) project (Verdes-Montenegro et al. 2005) is based upon a re-evaluation of the CIG. It is a first step in trying to identify and better understand isolated galaxies in the local Universe. Durbala et al. (2008) used a subsample of 100 typical CIG galaxies (Sb, Sbc, and Sc) and found that most of them have a bulge-to-total luminosity ratio $B/T < 0.1$. If B/T is a measure of environmental dynamical processing (MacArthur et al. 2010), galaxies in the CIG sample appear to be very little affected by it. The late-type population that dominates the AMIGA sample (Sulentic et al. 2006) may indicate that they have been alone for most of their lives.

Verley et al. (2007b,c) calculated two isolation parameters (the local number density and the tidal strength) for 950 galaxies in the CIG sample using an automated search for neighbours on the first and second digitised POSS (DPOSS-I and II) based on photographic plates. They provided an exhaustive list of $\sim 54,000$ possible satellites that were used to identify several CIG galaxies failing the CIG isolation criteria.

¹<http://amiga.iaa.es>

The first data release of the Sloan Digital Sky Survey (SDSS-DR1; Abazajian et al. 2003) has rekindled the interest on isolated galaxy studies in the past decade (Allam et al. 2005). In this context, new and available photometric data from the SDSS motivated us to perform a fully digital revision of the isolation degree for the CIG galaxies. The SDSS-III (Eisenstein et al. 2011) maps one third of the sky using CCD detectors. The SDSS also provides spectra that allow us to estimate galaxy distances, enabling an improved revision of the degree of isolation for 411 CIG galaxies with a fairly complete spectroscopic coverage in the last Data Release (DR9; Ahn et al. 2012) catalogue. Some other recent catalogues of isolated galaxies have been compiled, introducing isolation criteria using the spectroscopic information from earlier SDSS data releases. Elyiv et al. (2009) applied three-dimensional Voronoi tessellation to volume-limited galaxy samples, using spectroscopic data from SDSS-DR5, and identified 2394 isolated galaxies. Vavilova et al. (2009) refined the sample by selecting galaxies with the highest level of isolation, the Qisol sample, composed of 600 galaxies. These two samples suffer from the incompleteness in the SDSS spectroscopic sample, limited at $m_{r,\text{Petrosian}} < 17.77$ mag. To compensate for the SDSS spectroscopic incompleteness, other authors used statistical techniques (Edman et al. 2012), photometric redshifts also provided by the SDSS (Guo et al. 2011), or selected different volume-limited samples (Tollerud et al. 2011). A revision for possible photometric companions is needed out of the volume-limited samples considered (Hernández-Toledo et al. 2010).

Here we perform a photometric and spectroscopic census and quantify the environment of the CIG galaxies covered by the SDSS-DR9. In Sect. 2.2, we describe in detail the data and methodology used to revise the isolation of the CIG galaxies in the SDSS, including a description of our automated pipeline used to produce a catalogue of their potential neighbours. The method to quantify the isolation degree, as well as the selection of the comparison samples used, are explained in Sect. 2.3. Results from the study using the photometric and spectroscopic catalogues of the SDSS are presented in Sect. 2.4. A revision of the CIG is presented in Sect. 2.5 to determine how many galaxies remain isolated based on the recent SDSS-DR9 data from both the photometric and the spectroscopic catalogues. Neighbours considered in each study are then used for the estimation of the isolation degree. We present our conclusions in Sect. 2.6.

2.2 Data and methodology

The SDSS-DR9² (Eisenstein et al. 2011; Ahn et al. 2012) provides images and spectra covering 14,555 square degrees mostly of the northern sky. The SDSS database provides homogeneous and moderately deep photometry in five pass-bands. The 95% completeness limits for the images are $(u, g, r, i, z) = (22.0, 22.2, 22.2, 21.3, 20.5)$, respectively. The images are mostly taken under good/average seeing conditions (the median is about $1''.4$ in r -band) on moonless nights. The photometric catalogue of detected objects was used to identify the targets for spectroscopy: a) the main galaxy sample (Strauss et al. 2002), with a target magnitude limit of $m_{r,\text{Petrosian}} < 17.77$ mag corrected for Galactic dust extinction, and b) the Baryon Oscillation Spectroscopic Survey (BOSS; Dawson et al. 2013), which uses a new spectrograph (Smee et al.

²<http://www.sdss3.org/>

2012) to obtain spectra of galaxies with $0.15 < z < 0.8$ and quasars with $2.15 < z < 3.5$, which is useful to reject background objects in our study. The data are processed using automatic pipelines (Blanton et al. 2011).

2.2.1 CIG galaxies in the SDSS

The scheme of the pipeline we followed is presented in Fig. 2.1. We found $N = 799$ CIG galaxies included in the SDSS photometric catalogue, of which ten were removed because the photometric data were unreliable (due to a nearby bright star or because the galaxy is too close to an edge of the field): CIG 13, 95, 388, 402, 573, 713, 736, 781, 802, and 810. We used recession velocities from the AMIGA database³ (Fernández Lorenzo et al. 2012) for CIG galaxies. We chose a projected physical radius of 1 Mpc ($H_0 = 75 \text{ km s}^{-1} \text{ Mpc}^{-1}$) to evaluate the isolation degree⁴. If we were to assume a typical field velocity dispersion of the order of 190 km s^{-1} (Tonry et al. 2000) it would require about $t_{\text{cc}} \sim 5.2 \text{ Gyr}$ for a companion to cross this distance, guaranteeing that the galaxy has been isolated most of its lifetime. We focused our study on CIG galaxies with recession velocities $v \geq 1500 \text{ km s}^{-1}$, which additionally reduced our sample to $N = 693$, to avoid an overwhelming search for potential neighbours (the angular size on the sky for 1 Mpc at a distance of 1500 km s^{-1} is approximately $2^\circ.9$).

The CIG isolation criteria (Eqs. 1.1 and 1.2) require one to examine the isolation in a field as large as 80 times the diameter of each CIG galaxy. For a typical CIG galaxy, with diameter $D_p = 30 \text{ kpc}$, this translates into a projected distance of $R_{iP} = 2.4 \text{ Mpc}$. Even selecting a reasonable and constant search radius, the variable radius resulting from the CIG isolation criteria usually represents a very large field, and 1 Mpc often corresponds to a part of it. Therefore, we cannot verify the isolation for the entire field used by Karachentseva (1973), but we are able to determine if neighbour galaxies close to the primary CIG galaxy are violating the CIG isolation criteria.

Model magnitudes in r -band (the deepest images) were used in our study. We used r_{90} , the Petrosian radius containing 90 % of the total flux of the galaxy in the r -band⁵, as explained in Sect. 2.2.3.

Our final sample is composed of $N = 636$ CIG galaxies, and 1 Mpc radius fields are completely covered in the photometric SDSS-DR9 catalogue.

2.2.2 Catalogues of neighbours

We used the CasJobs⁶ tool to search for neighbour galaxies within a 1 Mpc radius around each of the 636 CIG galaxies⁷ (see right column in Fig. 2.1). Neighbour galaxies were selected with the following criteria to extract a sample as clean as possible: 1) galaxies with $11.0 \leq m_r \leq 21.0$

³<http://amiga.iaa.es/p/139-amiga-public-data.htm>

⁴Note that the search radius is larger than in Verley et al. (2007c), who used a minimum physical radius of 0.5 Mpc due to technical limitations.

⁵<http://www.sdss3.org/dr9/algorithms/magnitudes.php>

⁶<http://skyservice.pha.jhu.edu/CasJobs/>

⁷To allow the reproducibility of this work, initial tables are available at <http://amiga.iaa.es>, CDS, and SDSS-DR9 websites and requests on demand.

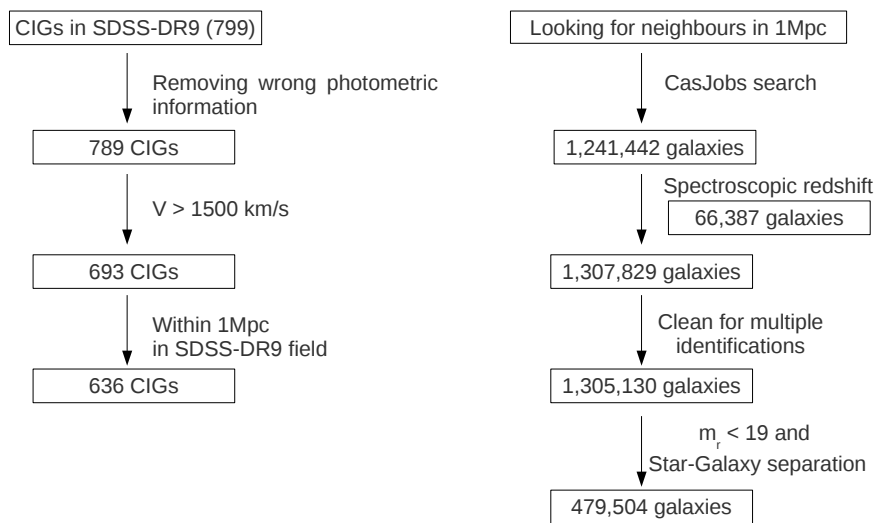


Figure 2.1: Diagram of the methodology. The scheme used to select primary galaxies is shown in the left column, and the selection for the neighbours is shown in the right column.

without flags on size measures, 2) removal of suspicious detections, checking that the object has pixels detected in the first pass and has a valid radial profile, and 3) flagged as a non-saturated source.

A first sample of 1,241,442 candidate neighbour galaxies was compiled using these conditions. Without imposing the condition for non-saturated objects, we find a contamination of nearly 50% by saturated stars with magnitudes brighter than $m_r \sim 17$ mag. Galaxies with a very bright nucleus can also be flagged as saturated sources in the SDSS, which makes it necessary to complete our sample by adding saturated galaxies from the spectroscopic catalogue (66,387 galaxies). Our final sample contains 1,307,829 neighbour galaxies selected by an automated method from the SDSS.

We found a contamination of multiple object identifications for nearby and extended galaxies. A clean sample of 1,305,130 galaxies was obtained selecting the brightest (typically also the largest) object in these cases.

We also improved the star-galaxy separation provided by the SDSS from an empirical selection of objects using a size/magnitude diagram (see Fig. 2.2). Objects situated in the horizontal bottom part are mostly stars misclassified as galaxies. Bright objects in the upper part of the diagram are saturated stars, fainter objects in the upper part (and below $\log[\text{Area}] = 1.1$) are spurious detections. Objects fainter than $m_r = 19$ mag were removed, since the star-galaxy separation becomes difficult and inaccurate. Our final photometric sample of neighbour galaxies is composed of a total of 479,504 neighbour galaxies around 636 CIG galaxies.

2.2.3 Estimation of apparent diameters from the SDSS

The CIG isolation criteria defined by Karachentseva (1973) are based on apparent diameters of galaxies, which makes these measurements critical in our study. SDSS gives different radius measurements (for the five photometric bands): 1) de Vaucouleurs and exponential radii, which depend directly on the galaxy intensity profile, and 2) Petrosian radii $r_{\text{Petrosian}}$, using a modification of the Petrosian (1976) system. Petrosian values measure galaxy fluxes within a circular aperture and define the radius using the shape of the azimuthally averaged light profile. Petrosian radii containing 90% (r_{90}) and 50% (r_{50}) of the total flux are provided by the SDSS. We adopted Petrosian values for this study because they do not depend on model fits (Bernardi et al. 2010). However, after a visual inspection of SDSS three-colour images for CIG galaxies, Petrosian diameters do not recover the total galaxy major axis, and are generally smaller than the projected major axis of a galaxy at the 25 mag/arcsec² isophotal level (D_{25}) originally used by Karachentseva (values measured in the B -band), even though a new approach for background subtraction was applied in the last two data releases of the SDSS (Blanton et al. 2011).

To transform Petrosian sizes into more accurate optical measurements equivalent to the original D_{25} used by Karachentseva, we compared Petrosian diameters from the SDSS ($D_{\text{SDSS}} = 2r_{90}$) with apparent optical diameters given in ancillary databases. We performed a linear regression analysis for CIG galaxies using measures from 1) HyperLeda⁸; 2) $isoA_r$ (isophotal major axis at the 25 mag/arcsec² isophote in r -band) from SDSS-DR7 (Abazajian et al. 2009) because we visually verified that in general it covers the total galaxy; 3) the major axis from the

⁸<http://leda.univ-lyon1.fr/>

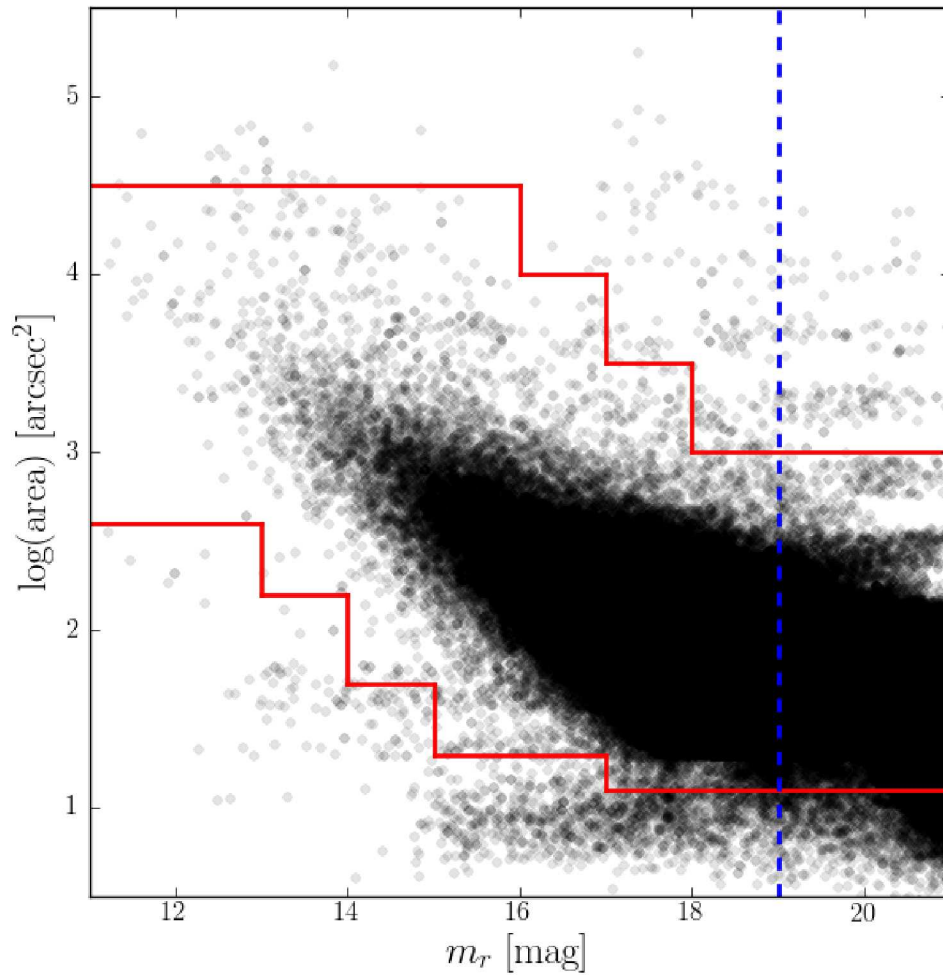


Figure 2.2: Star-galaxy separation. Considering the object area from the Petrosian radius r_{90} , we carried out an empirical inspection, performing a selection in apparent magnitude and size. Resolved objects within the red contour are very likely galaxies. The dashed blue line corresponds to the selected cut at $m_r = 19$ mag.

Table 2.1: Estimation of apparent diameters from the SDSS using different comparison samples. Col. 1: Galaxy samples considered for the estimation. Col. 2: Apparent diameter measure used for the estimation. Col. 3: Apparent diameter source. Col. 4: Number of objects used. Col. 5: Correction factor for each estimation $D_{25} \simeq \text{factor} \times D_{\text{SDSS}}$.

Objects	Apparent diameter	Database	# of matches	Factor
CIGs	D_{25}	HyperLeda	636	1.58
CIGs	$isoA_r$	SDSS-DR7	560	1.41
CIGs	Major axis	NED	567	1.83
CIGs	Kron radius	SDSS-DR9	719	2.17
Neighbours	D_{25}	Verley+07c	28,209	1.41
Neighbours	D_{25}	HyperLeda	13,972	1.23
Neighbours	Kron radius	SDSS-DR9	27,719	1.43

NASA/IPAC Extragalactic Database (NED⁹); and 4) the Kron radii, running SExtractor (Bertin & Arnouts 1996) on i -band images of CIG galaxies from the SDSS-DR9, which, after visually examining on the fits images, is the measurement that better recovers the total size of the CIG galaxy.

But CIG galaxies are not representative of the size of the galaxies that we are interested in: neighbour galaxies are typically smaller than CIG galaxies. To avoid bias, we focused the size correction on neighbour galaxies. We performed a cross-match with the catalogue of neighbours compiled by Verley et al. (2007c), based on D_{25} and SExtractor diameters. Since this correlation is made from digitised photographic measurements, other correlations were calculated: based on D_{25} from HyperLeda for galaxies in the neighbour sample brighter than $m_{r,\text{model}} = 16$ mag and with $r_{90} > 5$ arcsec; and based on the SExtractor Kron radii from SDSS-DR9 images in the i -band for four CIG fields at different recession velocities.

Correction factors for SDSS diameters as a function of the above measurements are shown in Table 2.1, including the corresponding number of galaxies used. In the rest of this study, we use a corrected apparent diameter $D_{\text{SDSS,corr}} = 1.43 D_{\text{SDSS}}$ (see also Sabater et al. 2013) both for neighbours and for CIG galaxies. This factor was obtained as the median of the values in Table 2.1 to approximate the original D_{25} used by Karachentseva (1973).

2.3 Quantification of the isolation

2.3.1 Isolation parameters

We used modified isolation parameters from Sect. 1.2 to quantify the isolation degree throughout.

An estimate of η_k was calculated taking into account the distance of the k^{th} nearest neighbour to the CIG galaxy. We calculated this parameter according to Eq. 1.3, choosing k equal to 5 or

⁹<http://ned.ipac.caltech.edu/>

lower when there were not enough neighbours in the field. The farther the k^{th} nearest neighbour, the smaller the local number density η_k .

We calculated a second independent parameter involving a cumulative measure of the tidal strength produced by neighbour galaxies. To improve the quantification of the isolation degree, we adopted a modified version of the Q parameter (Eq. 1.4), where apparent magnitudes from the SDSS-DR9 were used to estimate galaxy masses. This methodology therefore minimises the effect of the correction factor used for estimating apparent diameters. Assuming that the stellar mass is proportional to the r -band flux, that is a linear mass-luminosity relation (Bell et al. 2003, 2006), we considered $Flux_r \propto Mass$ at a fixed distance, with $m_r = -2.5 \log(Flux_r)$.

Then, for one companion from Eq. 1.4:

$$\log Q_{iP} \propto 0.4 (m_r^P - m_r^i) + 3 \log \left(\frac{D_P}{R_{iP}} \right) , \quad (2.1)$$

where m_r^P and m_r^i are the apparent magnitudes in r -band of the primary CIG galaxy and the i^{th} neighbour, respectively. The total tidal strength created by all the neighbours is then defined as

$$Q = \log \left(\sum_i Q_{iP} \right) . \quad (2.2)$$

The higher the value of Q , the more affected from external influence the galaxy, and vice-versa.

Given that the CIG is assembled with the requirement that no similar size neighbours are found close to the CIG galaxy, companion galaxies are expected to be faint (mostly dwarf companions). Therefore, no companion galaxies with similar brightness are expected close to the CIG galaxy.

2.3.2 Comparison with denser environments

We selected other samples of galaxies from denser environments to make a comparison with the isolation degree of galaxies in the CIG sample: 1) isolated pairs of galaxies (KPG; Karachentsev 1972), 2) galaxy triplets (KTG; Karachentseva et al. 1979), 3) galaxies in compact groups (HCG; Hickson 1982), and 4) galaxies in Abell clusters (ACO; Abell 1958; Abell et al. 1989).

The KPG sample allowed us to separate effects of galaxy environment density from effects of one-on-one interactions, while the KTG, HCG, and ACO galaxy samples show the effects of increasingly richer environments. The KPG, KTG, and HCG catalogues were visually compiled using visual isolation criteria as well, accordingly, they complement the CIG sample nicely.

The KTG, HCG, and ACO samples were adopted from Verley et al. (2007b) because they were selected to sample a volume of space roughly equivalent to the one covered by the CIG, and to avoid possible biases. For consistency, we also followed the same selection criterion as for CIG galaxies, keeping galaxies with recession velocities $v \geq 1500 \text{ km s}^{-1}$.

The final comparison sample is composed of 360 KPGs out of 603 pairs listed by Karachentsev (1972), 30 KTGs out of 84 triplets listed by Karachentseva et al. (1979), 24 HCGs out of 100 compact groups compiled by Hickson (1982), and 12 ACOs out of more than 2,700 galaxy clusters listed by Abell (1958) and Abell et al. (1989).

2.4 Results

We performed a photometric and, for the first time, spectroscopic revision of the CIG isolation criteria around each CIG galaxy within a projected radius of 1 Mpc. The available redshift information allowed us to identify possible physical companions down to the SDSS spectroscopic completeness. Neighbour galaxies were used to estimate the isolation degree for the CIG galaxies.

2.4.1 Photometric study

Photometric revision of the CIG isolation criteria

We applied both of the CIG isolation criteria to the neighbours around each CIG galaxy within a projected field radius of 1 Mpc. First of all, we identified neighbour galaxies with an apparent diameter in the range defined by Eq. 1.1. They represent the galaxies considered as potential perturbers by Karachentseva (1973). The second step was to determine which of these objects were projected at a distance lower than the one defined in Eq. 1.2. When a galaxy was found to have no neighbour violating Eqs. 1.1 and 1.2, that galaxy was considered isolated according to the CIG isolation criteria.

In Sect. 2.2.2 we have compiled an automatic selected sample of 479,504 neighbours; of these, 2,109 are potential companions according to the CIG isolation criteria (Eqs. 1.1 and 1.2) within 1 Mpc. After an additional visual inspection we found that 89 candidates fail our aim of obtaining a sample of neighbour galaxies without contamination by saturated stars.

The revision of the CIG isolation criteria was performed for 636 CIG galaxies using 479,415 neighbour galaxies within 1 Mpc radius around each CIG galaxy. Of these, 121,872 neighbour galaxies violate Eq. 1.1 within 1 Mpc, and a small number, 3,433 neighbour galaxies, violate Eq. 1.2 within 1 Mpc. The total number of potential companions violating Eqs. 1.1 and 1.2 within 1 Mpc is very small, 2,020 galaxies.

We found 86 CIG galaxies without a neighbour, 117 CIG galaxies with one possible companion, and 433 CIG galaxies with more than one possible companion after applying the CIG isolation criteria within 1 Mpc. There are 13 CIG galaxies with more than ten possible companions. CIG 589 has the largest number of companions (14 possible companions).

The search radius of 1 Mpc for each of the 636 CIG galaxies considered in the photometric study (Sect. 2.4.1), covers the area defined by Karachentseva (1973) for 59 fields only; of these, four CIG galaxies are isolated (CIG 50, 299, 651, and 1032) according to the CIG isolation criteria.

The results of this revision are listed in columns 2, 3, and 4 of Table 2.2.

Photometric isolation parameters

The isolation parameters local number density $\eta_{k,p}$ (Eq. 1.3) and tidal strength $Q_{\text{Kar},p}$ (Eq. 2.2) were calculated using the photometric data. Only galaxies within a factor 4 in apparent diameter with respect to the CIG galaxy were considered (Eq. 1.1) to minimise the contamination of background/foreground galaxies, following Karachentseva (1973). We calculated R_{iP} using

Table 2.2: Revision of the isolation degree using photometric data.

(1)	(2)	(3)	(4)	(5)	(6)
CIG	$r_{1\text{Mpc}}$	$\frac{r_{1\text{Mpc}}}{r_{80D_p}}$	isol	$Q_{\text{Kar,p}}$	$\eta_{k,p}$
1	35.32	0.31	0	-3.35	2.03
2	36.92	0.49	1	-3.19	1.70
4	111.58	0.65	0	-2.78	1.92
5	32.78	0.62	0	-1.60	3.02
6	56.94	0.71	0	-2.84	2.34
7	20.22	0.26	1	-3.37	2.11
8	40.65	0.49	0	-1.83	2.65
...

Notes. The full table is available in electronic form at <http://amiga.iaa.es> and in CDS. The columns correspond to (1) the galaxy identification according to the CIG, (2) the projected angular radius, in arcmin, equal to the adopted distance at 1 Mpc, and (3) the ratio between projected angular radius at 1 Mpc (in arcmin) over the original field radius used in the CIG isolation criteria. When the ratio is greater than or equal to 1, the fixed physical radius of 1 Mpc covers the entire original area. (4) Result of the CIG isolation criteria: "1" if the galaxy passes, "0" if it fails. (5) $Q_{\text{Kar,p}}$, tidal strength estimate of similar-size neighbours. (6) $\eta_{k,p}$, local number density of similar-size neighbours.

Table 2.3: Means and standard deviations of the isolation parameters for the CIG and for the comparison samples.

	CIG	KPG	KTG	HCG	ACO
N	636	360	30	24	12
mean($Q_{\text{Kar,p}}$)	-2.51	-0.95	-1.11	-0.32	-0.75
std($Q_{\text{Kar,p}}$)	0.68	1.11	0.79	0.89	0.70
mean($\eta_{k,p}$)	2.39	2.85	3.09	3.49	3.51
std($\eta_{k,p}$)	0.45	0.56	0.46	0.57	0.59

projected angular distances on the sky. For the local number density, the projected distance to the k^{th} nearest neighbour, r_k , was calculated as the angular separation in arcmin normalised by the apparent diameter of the central CIG galaxy. The values of the isolation parameters are listed in Table 2.2 and are plotted in Fig. 2.3a.

The tidal strength $Q_{\text{Kar,p}}$ and the local number density $\eta_{k,p}$, were also calculated for the comparison samples KPG, KTG, HCG, and ACO (see Fig. 2.3b). Means and standard deviations are shown in Table 2.3. As expected, the trend of the mean values, from isolated to denser environments, shows that isolation parameters are sensitive enough to the effects of the environment.

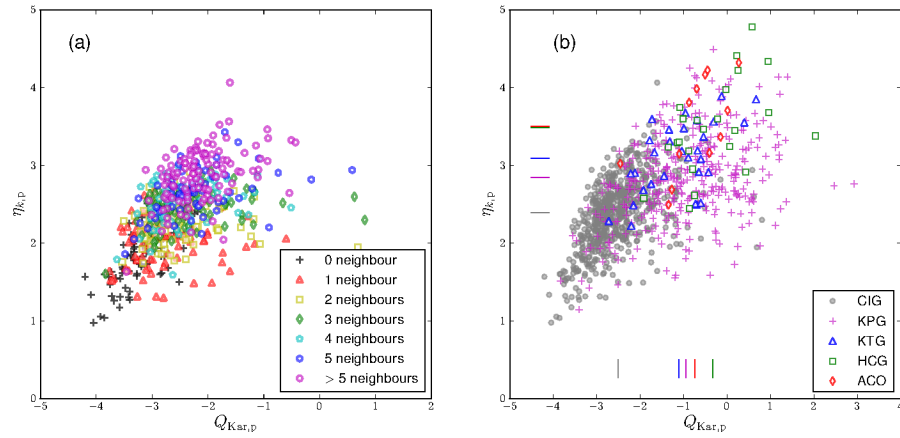


Figure 2.3: Photometric isolation parameters. (a): Calculated isolation parameters (local number density $\eta_{k,p}$ and tidal strength $Q_{Kar,p}$) for similar-size neighbour galaxies using the photometric data. Symbols and colours in the legend correspond to the number of neighbours that violate the CIG isolation criteria. (b): Comparison between isolation parameters (local number density $\eta_{k,p}$ and tidal strength $Q_{Kar,p}$) for the CIG and the comparison samples using photometric data. Pairs (KPG) are depicted by violet pluses, triplets (KTG) by blue triangles, compact groups (HCG) by green rectangles, and Abell clusters (ACO) by red diamonds. The mean values of each sample are indicated following the same colour code.

2.4.2 Spectroscopic study

Spectroscopic revision of the CIG isolation criteria

Owing to the relatively new availability of large spectroscopic surveys, most of the environment has long been estimated only with photometric analysis for any type of samples (isolated, pairs, triplets, groups, and clusters). Only during the past decade and despite the inhomogeneity and incompleteness of the spectroscopic surveys at very low and high redshifts, some spectroscopic studies were performed (Elyiv et al. 2009; Vavilova et al. 2009).

In this section we performed a spectroscopic revision and an improvement of the CIG isolation criteria. Eqs. 1.1 and 1.2 within 1 Mpc were applied to identify the CIG galaxies that appear to be physically isolated using the spectroscopic sample of the SDSS.

For this study, we selected fields with a redshift completeness greater than 80% with respect to the photometric sample at $m_r \leq 17.7$ mag (the percentage of extended neighbours down to $m_r < 17.7$ mag lying within a 1 Mpc projected separation from the CIG galaxy that have a measured redshift), which is, approximately, the redshift completeness limit of the SDSS spectroscopic main galaxy sample (Strauss et al. 2002). Four hundred and eleven CIG fields fulfil this requirement, surrounded by 70,169 cleaned neighbour galaxies with spectroscopic information.

To evaluate the physical association of the projected neighbours, we introduce a third condition based on the velocity difference between neighbour galaxies with respect to each CIG galaxy $|\Delta v| = v_i - v_p$.

Surprisingly, the velocity difference distribution shows a peak close to $|\Delta v| = 0 \text{ km s}^{-1}$ (see Fig. 2.4). From the figure, we are able to separate a flat continuum distribution of foreground/background neighbours, considered as the fraction of galaxies that are probably not linked to the central galaxy, from physically linked satellites. More than one third of the neighbours within $|\Delta v| \leq 3,000 \text{ km s}^{-1}$ have a velocity difference $|\Delta v| \leq 250 \text{ km s}^{-1}$ (36%, see Fig. 2.4). To recover all of these probable physical companions, we considered from the figure and adopting a conservative enough velocity difference selection, that a CIG galaxy fulfils the CIG isolation criteria if it has no neighbour violating Eqs. 1.1 and 1.2 within 1 Mpc and $|\Delta v| \leq 500 \text{ km s}^{-1}$ (see also Elyiv et al. 2009; Karachentseva et al. 2010a, 2011).

The results of the revision of the CIG isolation criteria, using spectroscopic data, are listed in column 2 of Table 2.4.

The number of galaxies that appear as isolated increases when the third condition is introduced, because they have spectroscopic neighbours with discordant redshifts and violating Eqs. 1.1 and 1.2 within 1 Mpc. We found that 347 CIG galaxies appear to be isolated according to the CIG isolation criteria and have no companion within 1 Mpc and $|\Delta v| \leq 500 \text{ km s}^{-1}$. The search radius of 1 Mpc covers the area defined by Karachentseva (1973) for 35 fields only. Of these, 32 CIG galaxies pass, while 3 fail the CIG isolation criteria within 1 Mpc and $|\Delta v| \leq 500 \text{ km s}^{-1}$ (CIG 264, 480, and 637).

A total of 30,222 neighbour galaxies of the 70,169 galaxies with available redshift within the spectroscopic magnitude limit violate Eq. 1.1 within 1 Mpc, and a very small number, 643 neighbours, also violate Eq. 1.2 within 1 Mpc, 75 of them also fulfil the third condition, that is $|\Delta v| \leq 500 \text{ km s}^{-1}$ within 1 Mpc.

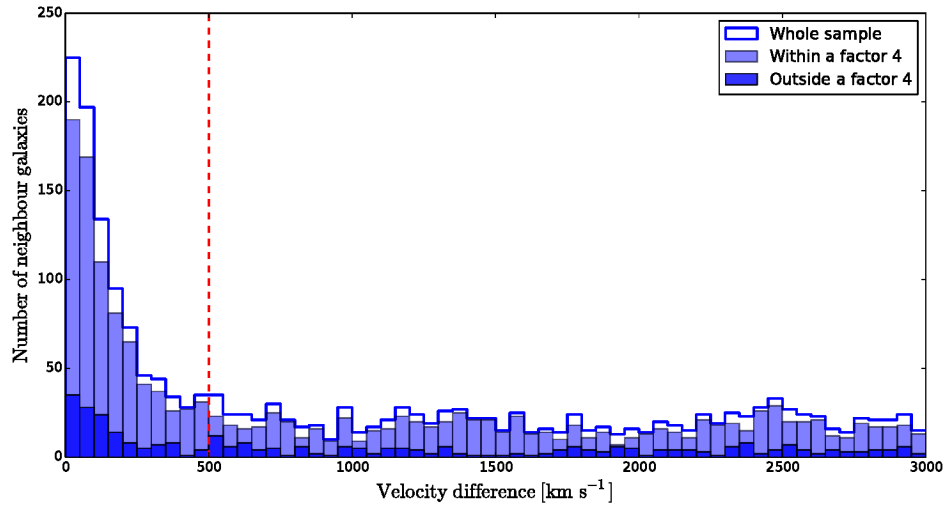


Figure 2.4: Comparison of the velocity difference distributions $|\Delta v|$ for neighbour galaxies with respect to the central CIG galaxy (411 fields): for the neighbour galaxies violating Eq. 1.1 (i.e., a factor 4 in apparent diameter with respect to their associated CIG galaxy); for the remaining neighbours (outside the factor 4 in apparent diameter); and for the whole sample of neighbours (sum of the previous two samples). The vertical line corresponds to the selected value of reference at $|\Delta v| = 500 \text{ km s}^{-1}$.

Table 2.4: Revision of the isolation degree using spectroscopic data.

(1)	(2)	(3)	(4)	(5)	(6)	(7)	(8)	(9)	(10)	(11)	(12)	(13)
CIG	isol	k_{500}	Q_{500}	$f_{Q_{500}}$	$\eta_{k,500}$	$f_{\eta_{k,500}}$	$z_{\text{comp}} [\%]$	$k_{500,\text{ul}}$	$Q_{500,\text{ul}}$	$f_{Q_{500,\text{ul}}}$	$\eta_{k,500,\text{ul}}$	$f_{\eta_{k,500,\text{ul}}}$
11	1	0	NULL	2	NULL	2	87.16	1	-6.11	0	NULL	1
33	1	1	-5.41	0	NULL	1	98.78	1	-5.41	0	NULL	1
56	1	5	-4.12	0	0.02	0	94.31	5	-4.12	0	0.02	0
60	1	5	-4.94	0	0.32	0	98.16	5	-4.94	0	0.32	0
187	1	0	NULL	2	NULL	2	87.72	0	NULL	2	NULL	2
198	0	2	-2.92	0	0.15	0	93.94	2	-2.92	0	0.15	0
199	0	4	-3.78	0	-0.12	0	86.21	4	-3.78	0	-0.12	0
...

Notes. The full table is available in electronic form at <http://amiga.iaa.es> and in CDS. The columns correspond to (1) the galaxy identification according to the CIG; (2) the result of the CIG isolation criteria for neighbours within 1 Mpc and $|\Delta v| \leq 500 \text{ km s}^{-1}$; "1" if the galaxy passes, "0" if it fails; (3) k_{500} , number of neighbours within 1 Mpc and $|\Delta v| \leq 500 \text{ km s}^{-1}$; (4) Q_{500} , tidal strength estimation using neighbours within 1 Mpc and $|\Delta v| \leq 500 \text{ km s}^{-1}$; (5) $f_{Q_{500}}$, flag in Q_{500} : "0" if $k_{500} \geq 1$, "2" if $k_{500} = 0$; (6) $\eta_{k,500}$, local number density using neighbours within 1 Mpc and $|\Delta v| \leq 500 \text{ km s}^{-1}$; (7) $f_{\eta_{k,500}}$, flag in $\eta_{k,500}$: "0" if $k_{500} \geq 2$, "1" if $k_{500} = 1$, "2" if $k_{500} = 0$; (8) z_{comp} , redshift completeness in the field; (9) $k_{500,\text{ul}}$, number of neighbours within 1 Mpc and $|\Delta v| \leq 500 \text{ km s}^{-1}$ using upper limits; (10) $Q_{500,\text{ul}}$, tidal strength upper limit estimation using neighbours within 1 Mpc and $|\Delta v| \leq 500 \text{ km s}^{-1}$; (11) $f_{Q_{500,\text{ul}}}$, flag in $Q_{500,\text{ul}}$: "0" if $k_{500,\text{ul}} \geq 1$, "2" if $k_{500,\text{ul}} = 0$; (12) $\eta_{k,500,\text{ul}}$, local number density using neighbours within 1 Mpc and $|\Delta v| \leq 500 \text{ km s}^{-1}$; (13) $f_{\eta_{k,500,\text{ul}}}$, flag in $\eta_{k,500,\text{ul}}$: "0" if $k_{500,\text{ul}} \geq 2$, "1" if $k_{500,\text{ul}} = 1$, "2" if $k_{500,\text{ul}} = 0$.

Spectroscopic isolation parameters

The available redshift data allowed us to calculate the two isolation parameters, the local number density and tidal strength, using physical size and physical projected distance.

We estimated the isolation parameters $\eta_{k,500}$ and Q_{500} , from Eqs. 1.3 and 2.2 respectively, taking into account all the neighbour galaxies within 1 Mpc and $|\Delta v| \leq 500 \text{ km s}^{-1}$ with respect to the central CIG galaxy. To compare this with the photometric estimate, we also calculated $Q_{\text{Kar},s}$ and $\eta_{k,s}$ only including similar-size galaxies with spectroscopy within a factor 4 in apparent diameter in 1 Mpc.

We calculated the isolation parameters for the 411 CIG fields considered in the spectroscopic revision, with more than 80% completeness in redshift. If they were incomplete, we estimated upper limits using photometric redshifts also available in the SDSS.

The values of the isolation parameters are listed in Table 2.4.

2.5 Discussion

2.5.1 Photometric study

Photometric revision of the CIG isolation criteria

As mentioned in Sect. 2.4.1, we performed a photometric revision of the CIG isolation criteria around each CIG galaxy within a projected radius of 1 Mpc, finding that 2,020 neighbour galaxies are potential companions that violate Eqs. 1.1 and 1.2. The left panel in Fig. 2.5 shows that these potential neighbours tend to be smaller than their corresponding CIG galaxy and tend to concentrate at larger distances to the central galaxy. This means that small neighbours ($\frac{D_i}{D_p} < 0.25$) can be located at closer distances to the CIG since their effect on the evolution of the central galaxy is almost negligible by the CIG isolation criteria. In contrast, larger neighbours could be located at gradually larger distances. That is the reason why we need to estimate the isolation degree, to quantify the effect of the missing neighbours on the evolution of the central CIG galaxy. The 2,020 potential companions are distributed around 550 CIG fields, of which 55 cover the original search area used by Karachentseva (1973). The right panel in Fig. 2.5 clearly shows that about 90% of the CIG fields do not cover the original search area ($\frac{r_{1\text{Mpc}}}{r_{80D_p}} < 1$).

Verley et al. (2007c) estimated that about 1/3 of the AMIGA sample (284 out of 950) fails the CIG isolation criteria within a minimum physical distance of 0.5 Mpc. Although we were unable to search for companions within the original area used by Karachentseva (1973), we can assess that about 1/6 of the sample fails the CIG isolation criteria within a fixed area of field radius of 1 Mpc.

The sample of neighbour galaxies inspected originally by Karachentseva (1973) in the construction of the CIG is not available. Nevertheless, we can compare our results with the catalogue of neighbours compiled by Verley et al. (2007c), who revised the CIG on the same original material (Palomar Observatory Sky Survey, POSS). Compared with Verley et al. (2007c), we found a much larger number of neighbours around each CIG galaxy. Indeed, Verley et al. (2007c) extracted neighbour galaxies brighter than $B = 17.5$ mag. In the c and d panels of Fig. 2.6, we show that the SDSS identification of neighbours goes deeper than the POSS and also detected

smaller neighbours. We also found that the 2,020 potential companions according to the CIG isolation criteria within 1 Mpc are mostly faint, with $\Delta m_r \geq 3$ mag, which suggests that they are nearby and low-luminosity galaxies missed by the CIG isolation criteria. The POSS search for companions misses the faintest and smaller galaxies, with respect to the magnitudes of the primary CIG galaxies. In fact, the mean magnitude difference Δm_r and size ratio $\frac{D_p}{D_i}$ between neighbour and the central CIG galaxy is 1.58 dex fainter and 0.18 dex lower in the SDSS than in the POSS. The presence of faint galaxies does not violate the CIG isolation criteria because these systems are smaller than $1/4 \times D_p$. The SDSS also has a redshift incompleteness at lower magnitudes $m_{r,\text{Petrosian}} < 14.5$ mag (Strauss et al. 2002). After a visual inspection of the neighbours in common with Verley et al. (2007c) that were missed by the SDSS search, we estimate that at apparent magnitudes $m_r < 15$ mag, we missed, approximately one galaxy per field. These missing neighbours are usually projected close to saturated stars, which were not considered in our selection of neighbours in the SDSS.

Other studies about isolated galaxies claim that an equivalent CIG isolation criteria could be obtained by selecting neighbours within a magnitude range. Prada et al. (2003) modified Eq. 1.1 by selecting a magnitude difference of $\Delta m = 2$, Hernández-Toledo et al. (2010) and Toribio et al. (2011) considered neighbours within a magnitude difference of $\Delta m = 2.5$, which translates into a factor 10 in brightness, and Allam et al. (2005), the most restrictive, selected neighbours within a magnitude difference of $\Delta m = 3$, which is about a factor of 16 in brightness. If we replace in Eq. 1.1 the approximate factor 4 in size with a factor 3 in magnitude, we find that 231 CIG galaxies appear to be isolated instead of 86 galaxies (see Sect. 2.4.1). The CIG isolation criteria are thus more restrictive and consider very faint galaxies as possible minor companions. Although the two definitions in the search for neighbours are not fully equivalent (see Verley et al. 2007c), we found that 65% of neighbour galaxies that violate Eq. 1.1 within 1 Mpc have $\Delta m_r \geq 3$, hence are low-mass objects; this means that we are able to observe faint associated satellite galaxies. This result justifies the need to quantify the isolation degree using the isolation parameters. The quantification of the tidal strength takes into account the size of the neighbour, and the effect of a satellite can be different from the effect of a similar-size neighbour galaxy.

Photometric isolation parameters

The isolation parameters, local number density ($\eta_{k,p}$), and tidal strength that affect the CIG galaxy ($Q_{\text{Kar},p}$) were estimated using photometric data (see Sect. 2.4.1).

These two parameters are complementary in quantifying the isolation degree and give consistent results, as shown in Fig. 2.3a. When a galaxy presents low values for both the local number density and the tidal strength estimate, the galaxy is well isolated from any sort of external influence. In contrast, when the two values are high, the evolution of the galaxy can be perturbed by the environment, and this galaxy is not suitable to represent the normal features of isolated galaxies. Galaxies in denser environments, such as isolated pairs or triplets (see Fig. 2.3b), typically present relatively low values for the local number density, but high tidal strength. Studies that only use a density estimator can misclassify interacting galaxies as isolated because they do not take into account the mass of the neighbour galaxy, therefore another complementary parameter (the tidal strength) is needed. On the other hand, if the local number density is high and the tidal strength low, the environment of the galaxy is composed of nearby

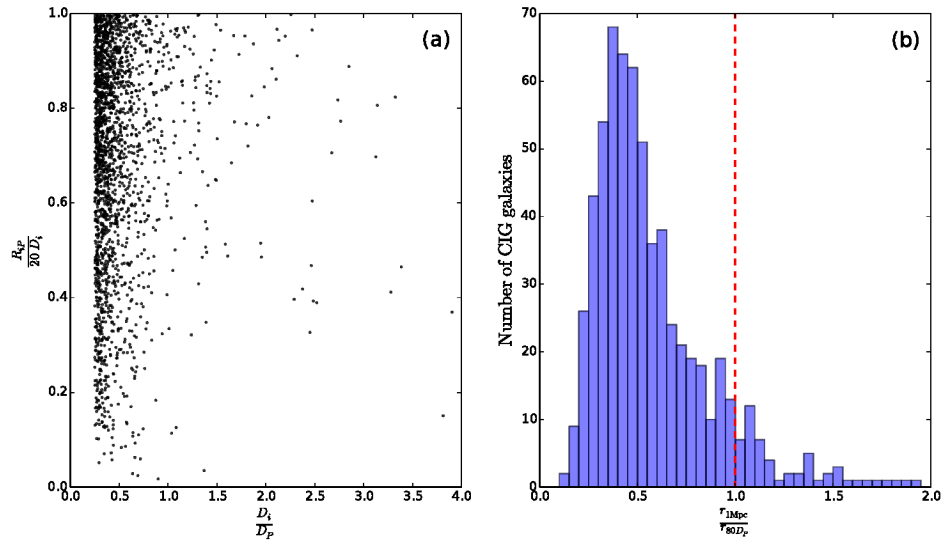


Figure 2.5: (a): Characterisation of the 2,020 potential companions violating Eqs. 1.1 and 1.2 within 1 Mpc. (b): Distribution of the ratio between a projected angular radius at 1 Mpc (in arcmin) across the original field radius used by Karachentseva (1973) ($\frac{r_{1\text{Mpc}}}{r_{80D_p}}$). The vertical line corresponds to the reference value at $r_{1\text{Mpc}} = r_{80D_p}$, i.e. the search area of 1 Mpc radius is equal to the original search area used in the construction of the CIG.

small neighbours.

The CIG isolation criteria are also represented in Fig. 2.3a. The most isolated CIG galaxies, without a neighbour and depicted by black pluses, show the lowest values for both parameters. With a growing number of neighbours, CIG galaxies move to the upper right in the diagram. However, a galaxy apparently not isolated might appear in the lower left part if its k^{th} nearest neighbour is far away from the CIG and if it does not have many similar-size neighbours. CIG galaxies that fail Eqs. 1.1 and 1.2 within 1 Mpc and have a higher number of potential neighbours represent a population more that strongly interacts with their environment.

According to numerical simulations, the evolution of a galaxy may be affected by external influence when the corresponding tidal force amounts to 1% of the internal binding force (Athanasoula 1984; Byrd & Howard 1992), that is, $\frac{F_{\text{tidal}}}{F_{\text{bind}}} = 0.01$, which corresponds to a tidal strength of $Q = -2$. For the local number density, this approximately translates into a value of $\eta_{k,p} = 2.7$ (see Fig. 2.3a). Note that the limit value for the local number density differs from previous AMIGA works ($\eta_k = 2.4$ in Verley et al. 2007b). This theoretical value allows us to separate the interactions that might affect the evolution of the primary galaxy. Figure 2.3a shows that the whole subsample of 86 CIG galaxies isolated according to the CIG isolation criteria within 1 Mpc (represented by black pluses) satisfies the threshold $Q_{\text{Kar,p}} < -2$.

Of the 550 CIG galaxies that violate the CIG isolation criteria within 1 Mpc, 433 CIG galaxies have $Q_{\text{Kar,p}} < -2$, and 340 CIG galaxies also have a relatively low number density environment ($\eta_{k,p} < 2.7$), therefore they can be considered to be mildly affected by their environment. Hence, from the photometric study, 426 CIG galaxies are suitable to represent a reference sample of isolated galaxies (67% of the sample of CIG galaxies found in the photometric catalogue of the SDSS), since their evolution is dominated by internal processes.

Figure 2.3 b shows the comparison of the local number density and tidal strength estimate for the CIG and for galaxies in denser environments: KPG, KTG, HCG, and ACO. Both estimates of the parameters increase from isolated galaxies to denser environments.

These results show that the isolation parameters, even for photometric studies suffering projection effects, are sensitive enough to distinguish between environments dominated by different numbers of similar size galaxies. Quantitatively, it is important to note that the mean values of the tidal strength for denser environment are, at least, one dex higher than $Q = -2$, which means that their evolution is clearly affected by their environment.

To compare the quantification of the isolation in this study with that of Verley et al. (2007b), we performed another calculation of the isolation parameters, restricting our fields to 0.5 Mpc (which is the minimum physical radius used in the previous AMIGA work). When comparing tidal strengths calculated using Eqs. 1.5 and 2.1, we found a good correlation (with a systematic shift of nearly 0.5 dex) with a large scatter. This scatter is directly related to the differences found between neighbours of the databases used, explained in Sect. 2.5.1. Verley et al. (2007b) provided a final catalogue of 791 isolated galaxies, based on an estimate of the best limits for selecting the sample ($Q < -2$ and $\eta_k < 2.4$), of which 620 galaxies are in common with the present study. Of these, 486 also fulfil the new selection criteria defined in this study, hence, despite the poor correlation between the isolation parameters, only 22% of these galaxies fail the new selection criteria defined here.

In general, the galaxies in the samples studied here appear to be less isolated according to

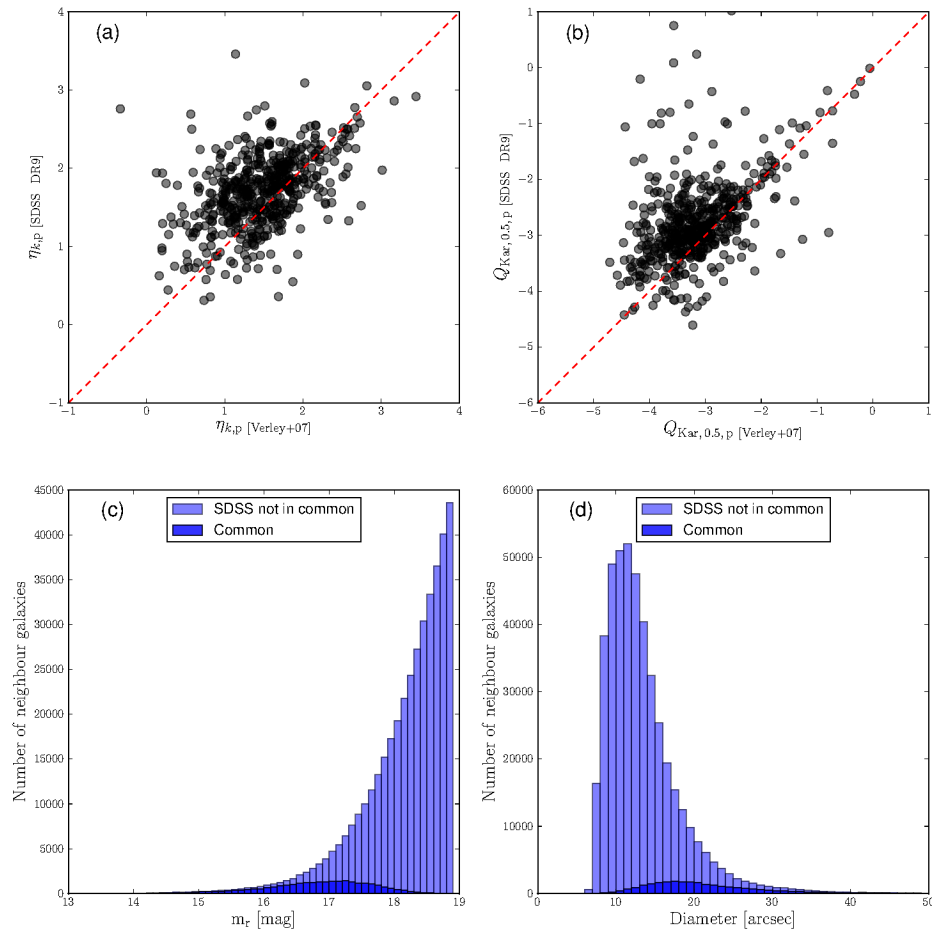


Figure 2.6: Isolation parameter differences between this study and Verley et al. (2007b). (a): Difference in $\eta_{k,p}$ isolation parameter for neighbour galaxies within a factor 4 in size. (b): Difference in $Q_{0.5,Kar,p}$ isolation parameter for neighbour galaxies within a factor 4 in size. (c): Apparent magnitude distribution for neighbour galaxies in common with Verley et al. (2007c) and galaxies in this study. (d): Apparent diameter distribution for neighbour galaxies in common with Verley et al. (2007c) and SDSS galaxies in this study.

the new method and data. Mean values of the isolation parameters for galaxies in the CIG, KTG, HCG, and ACO, are higher (except for the tidal strength for HCG and ACO) than in previous AMIGA works (see Table 8 in Verley et al. 2007b, compared with Table 2.3), which means fewer isolated galaxies. This result is directly related to the number of neighbours found in the SDSS compared with the POSS. We consider our modification for the tidal strength as a better estimate because it is based on the less scattered mass-luminosity relation. The SDSS provides linear photometric data (CCD), higher sensitivity, and better resolution than digitised photographic plates.

2.5.2 Spectroscopic study

Spectroscopic revision of the CIG isolation criteria

As obtained in Sect. 2.4.2 of 347 CIG galaxies, out of 411 fields with redshift completeness higher than 80% fulfil the CIG isolation criteria within 1 Mpc and $|\Delta v| \leq 500 \text{ km s}^{-1}$ when the redshift is taken into account.

The first isolation criterion of the CIG proposed by Karachentseva (1973) to remove foreground and background galaxies (Eq. 1.1), is not fully efficient. About 50% of the neighbours, considered as potential companions using Eq. 1.1 within 1 Mpc, have very high recession velocities with respect to the central CIG galaxy, so the first isolation criterion of the CIG is too restrictive and could consider galaxies as not isolated that are mildly affected by their environment (see Fig. 2.4). On the other hand, the first isolation criterion of the CIG which requires similar apparent diameter companions, accounts for most of the physical neighbours. But we also found that about 92% of the neighbour galaxies with recession velocities similar to the corresponding CIG galaxy are not considered as potential companions by the CIG isolation criteria.

We considered a different isolation criterion using the spectroscopic data, taking into account only neighbour galaxies within 1 Mpc and $|\Delta v| \leq 500 \text{ km s}^{-1}$ with respect to the velocity of the central galaxy, that is, without imposing any difference in size. We found that 105 CIG galaxies have no physical companions instead of 347 when considering the CIG isolation criteria within 1 Mpc and $|\Delta v| \leq 500 \text{ km s}^{-1}$ (see Sect. 2.4.2). In this case we were indeed too restrictive. According to Fig. 2.4, we can consider that only neighbours in the peak of the distribution are physical companions of their corresponding CIG galaxy. In this case, nearly a third of the CIG sample (126 galaxies) have no physical companions (within 1 Mpc and $|\Delta v| \leq 250 \text{ km s}^{-1}$). This means that nearby dwarf galaxies linked to the corresponding CIG galaxy were not taken into account by the CIG isolation criteria. But also part of the similar redshift neighbours might be background galaxies that do not affect the central CIG galaxy. We were able to recover the brightest dwarfs in the spectroscopic study, down to the $m_r = 17.77$ magnitude limit for SDSS spectra. A more extended study will be performed in a future work, taking into account nearby and similar redshift companions to identify physical satellites that affect the evolution of the central CIG galaxy and, by consequence, a more physical estimate of the isolation degree of the CIG.

Spectroscopic isolation parameters

The isolation parameters local number density ($\eta_{k,500}$) and tidal strength (Q_{500}) were estimated for the 411 fields considered in the spectroscopic study with a redshift completeness higher than 80% at $m_r = 17.7$ mag within 1 Mpc (see Sect. 2.4.2).

Redshift information is necessary to reject fore- and background galaxies, which reduces projection effects.

There is no correlation between the photometric and spectroscopic estimates (see Fig. 2.7). In general, we were unable to predict the spectroscopic parameters from the photometric estimate. Overall, the values of the isolation parameters are in general much lower in the spectroscopic estimate, showing that the projection effects lower the number of isolated candidates in the photometric study.

The upper-limit estimates of the isolation parameters were calculated considering photometric redshifts, as explained in Sect. 2.4.2. When the added neighbour is small and close to the CIG, the local number density changes, but the tidal strength remains almost the same. But if the neighbour is similar in size, there are marked increments in both parameters.

The displacement due to the upper limits, represented by solid grey lines in Fig. 2.8, is independent of the redshift completeness. Only ten CIG galaxies show changes in the parameters, the highest for CIG 492 with an increase of 0.07 dex in the tidal strength and 0.12 dex in the local number density. This change is due to the addition of one close ($R_{ip} \approx 470$ kpc) and faint ($\Delta m_r \geq -3.3$) companion with $|\Delta v| \approx 500$ km s⁻¹. CIG 254 and CIG 418 show an increase in the tidal strength of 0.53 dex and 0.47 dex, respectively. The local number density in these cases changes from being flagged as -99 to $\eta_{k,500} = 0.21$ and $\eta_{k,500} = -0.46$, respectively, due to the addition of a first nearest neighbour. We conclude that even if the redshift completeness of the SDSS is limited to $m_{r,\text{Petrosian}} < 17.77$ mag, the spectroscopic estimate of the isolation parameters is more realistic than the photometric estimate, from which the uncleaned objects are difficult to remove with an automated pipeline.

2.5.3 Photometric versus spectroscopic studies

We assessed the validity of some assumptions that were used during the construction of the CIG and, in light of the SDSS-DR9 spectroscopic information, considered and systematically quantified the differences between the photometric and spectroscopic studies. For the first time, we thus highlighted the quantified differences, strengths, and weaknesses of the two approaches and applied them to one common sample.

Clearly the spectroscopic information provides a better physical view of the environment of the galaxies. Nevertheless, there is still not complete full spectroscopic coverage for the neighbour galaxies of the CIG, therefore a pure photometric estimation is still needed to obtain a lower limit of the isolation parameters that is homogeneously defined and consistent for the whole CIG in the SDSS footprint. In addition, since the original materials were very different between Verley et al. (2007c), that is, digitised photographic POSS I - II plates, and our work, it has been necessary to repeat the photometric estimation of the isolation parameters. From this we were able to perform a fair comparison between photometric and spectroscopic isolation parameters, without being biased by the discrepancies in the constructed databases (star-galaxy

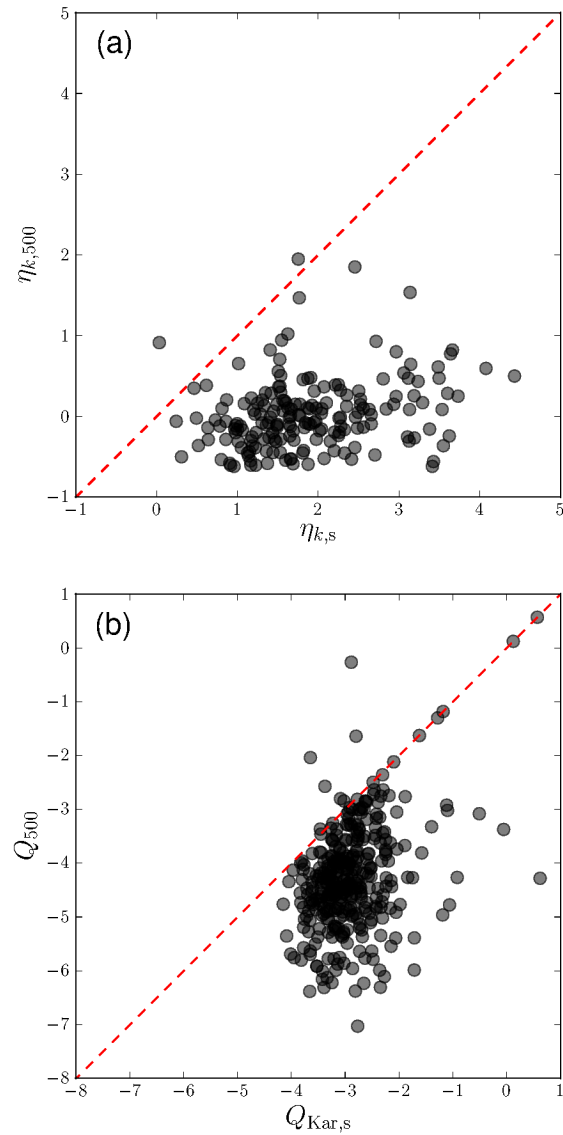


Figure 2.7: Photometric vs. spectroscopic estimates of the isolation parameters when using the velocity differences to reject fore- and background galaxies (vertical axis) instead of galaxies within a factor 4 in size (horizontal axis). (a): Difference in the local number density estimate. (b): Difference in the tidal strength estimate.

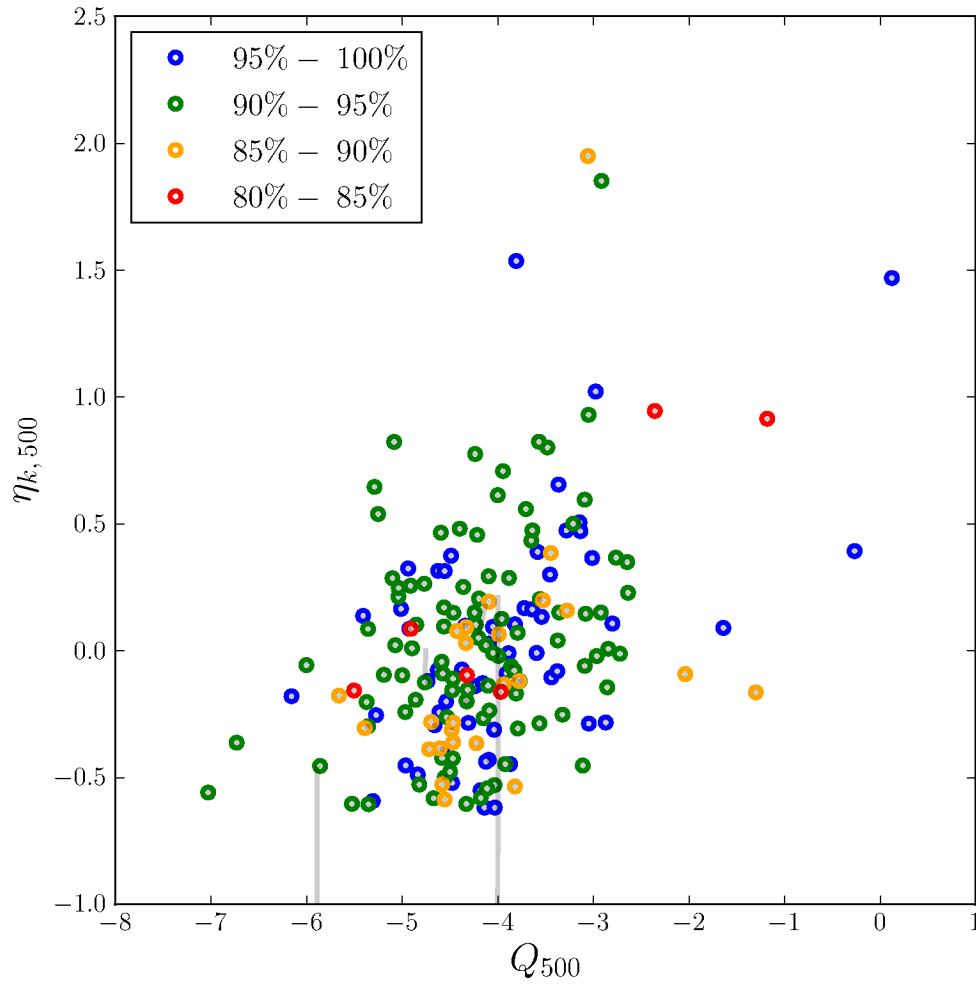


Figure 2.8: Estimate of the isolation parameters, local number density $\eta_{k,500}$ and tidal strength Q_{500} , for 306 CIG galaxies with at least one neighbour within 1 Mpc and $|\Delta v| \leq 500 \text{ km s}^{-1}$ using the spectroscopic data. Upper-limit estimates are depicted by solid grey lines. Colours, according to the legend, correspond to the redshift completeness of each CIG field (the percentage of extended neighbours, down to $m_r < 17.7$ mag lying within a projected separation of 1 Mpc from the CIG galaxy with a measured redshift).

separation, magnitudes, completeness limits, sizes, etc).

We found that of the 411 CIG galaxies with more than 80% redshift completeness (i.e., the percentage of extended neighbours down to $m_r < 17.7$ mag that lie within a projected separation of 1 Mpc from the CIG galaxy with a measured redshift), 54 CIG galaxies previously identified as isolated according to the CIG isolation criteria within 1 Mpc actually have similar redshift companions (i.e., neighbours with $|\Delta v| \leq 500 \text{ km s}^{-1}$ within 1 Mpc). When considering only neighbours with $|\Delta v| \leq 500 \text{ km s}^{-1}$ within 1 Mpc, we find that 105 CIG galaxies of 411 show no similar redshift neighbours. There are only nine CIG galaxies isolated according to these two modifications of the CIG isolation criteria (CIG 314, 451, 473, 541, 545, 608, 613, 655, and 668).

2.6 Summary and conclusions

We used the SDSS-DR9 photometric and spectroscopic databases to re-evaluate the degree of isolation of 636 galaxies in the Catalogue of Isolated Galaxies (CIG; [Karachentseva 1973](#)). This re-evaluation using CCD images and spectra continues and improves the work of [Verley et al. \(2007b,c\)](#) which was based upon the digitised photographic plates from POSS-1 and POSS-2. We used the SDSS-DR9 to search for neighbour galaxies within a projected physical radius of 1 Mpc, which doubles the radius used in previous AMIGA works. We first applied the CIG isolation criteria within 1 Mpc to the SDSS photometric database. Using the SDSS spectroscopic database, we then refined the study for 411 fields, of which more than 80% of the extended neighbours down to $m_r < 17.7$ mag lying within a projected separation of 1 Mpc from the CIG galaxy have a measured redshift. The isolation degree was quantified using two different and complementary parameters: the local number density η_k and the tidal strength Q , which affect the central CIG galaxy.

A summary of the different samples used in the photometric and spectroscopic studies is shown in [Table D.1](#).

Our conclusions are the following:

1. Of the 636 CIG galaxies considered in the photometric study, 426 galaxies appear to be isolated in projection: 86 CIG galaxies are isolated according to the CIG isolation criteria within a projected field radius of 1 Mpc; 340 appear to be mildly affected by their environment.
2. The use of the SDSS database permits one to identify faint companions that were not found in previous AMIGA papers ([Verley et al. 2007c](#)). The SDSS provides linear photometry, improved sensitivity, and better spatial resolution than digitised photographic plates. Consequently, the isolation parameters of the revised AMIGA sample are improved, which reduces the sample by about 20%.
3. On average, galaxies in the AMIGA sample show lower values in the local number density and the tidal strength parameters than galaxies in denser environments such as pairs, triplets, compact groups, and clusters. In general, galaxies in the studied samples show higher values of the isolation parameters than those reported by [Verley et al. \(2007b\)](#).

4. Of the 411 fields considered in the spectroscopic study with more than 80% redshift completeness, 347 galaxies are isolated according to the CIG isolation criteria within a radius of 1 Mpc and $|\Delta v| \leq 500 \text{ km s}^{-1}$ with respect to the central CIG galaxy.
5. The upper-limit estimates of the isolation parameters were calculated considering photometric redshifts: 103 CIG galaxies have no neighbours within 1 Mpc within the specified apparent diameter range and $|\Delta v| \leq 500 \text{ km s}^{-1}$.
6. The spectroscopic local number density and the tidal strength were calculated for 308 CIG galaxies with at least one neighbour within 1 Mpc and $|\Delta v| \leq 500 \text{ km s}^{-1}$. This estimate improves the quantification of the isolation degree with respect to the photometric study, which is only a rough first approximation.
7. The availability of the spectroscopic data allowed us to check the validity of the CIG isolation criteria within a field radius of 1 Mpc, which is not fully efficient. About 50% of the neighbours considered as potential companions in the photometric study are in fact background objects. On the other hand, we also found that about 92% of neighbour galaxies that show recession velocities similar to the corresponding CIG galaxy are not considered by the CIG isolation criteria as potential companions. These neighbours are most likely dwarf systems, with $D_i < 0.25 D_p$, which may have a considerable influence on the evolution of the central CIG galaxy.

Chapter 3

Effects of the environment on galaxies in the Catalogue of Isolated Galaxies: physical satellites and Large Scale Structure

Contents

3.1 Introduction	58
3.2 The sample and the data	59
3.3 Identification of physical companions	60
3.3.1 Escape speed	60
3.3.2 Gaussian distribution of physical satellites	61
3.4 Quantification of the environment	61
3.4.1 Tidal strength parameter	61
3.4.2 Projected number density parameter	64
3.5 Results	64
3.5.1 Spectroscopic identification of physical satellites around galaxies in the CIG	64
3.5.2 Large Scale Structure	65
3.5.3 Local environment versus large scale environment	65
3.5.4 Correction for the redshift incompleteness	68
3.6 Discussion	68
3.6.1 The construction of the CIG	68
3.6.2 Identification of satellites	70
3.6.3 Local and large scale environments around CIG galaxies	71
3.6.4 Influence of the environment on the evolution of the primary galaxies	72
3.7 Summary and conclusions	74

3.1 Introduction

Isolated galaxies are located, by definition, in low-density regions of the Universe, and should not be significantly influenced by their neighbours. Does a separate population of isolated galaxies exist, or are isolated galaxies simply the least clustered galaxies of the Large Scale Structure (LSS)? It is assumed that over the past several billion years the evolution of these objects has largely been driven by internal processes. A significant population of isolated galaxies is of great interest for testing different scenarios of the origin and evolution of galaxies. In this sense, isolated galaxies are an ideal sample of reference for studying the effects of environment on different galaxy properties. Such a sample would represent the most nurture-free galaxy population.

Studies of isolated galaxies can be argued to begin with the publication of the Catalogue of Isolated Galaxies (CIG; [Karachentseva 1973](#)). The AMIGA (ANalysis of the interstellar MEdium of Isolated GALaxies¹) project ([Verdes-Montenegro et al. 2005](#)) is based upon a re-evaluation of the CIG. It is a first step in trying to identify and better characterise isolated galaxies in the local Universe. [Verdes-Montenegro et al. \(2005\)](#) argued that 50% or more galaxies in the CIG show a homogeneous redshift distribution. [Sulentic et al. \(2006\)](#), and more recently [Fernández Lorenzo et al. \(2012\)](#), found that 2/3 of the CIG are Sb-Sc late-type galaxies, and 14% are early-type. This implies an extremely high late-type fraction and extremely low early-type population. At intermediate redshift, [Cooper et al. \(2012\)](#) found that early-type systems in higher density regions tend to be more extended than their counterparts in low density environments. Taking into account the effect of the local environment, [Fernández Lorenzo et al. \(2013\)](#) show that the number of satellites around a galaxy affects its size. Galaxies in the [Nair & Abraham \(2010\)](#) sample with zero or one satellite have larger sizes than galaxies in the CIG having two or more satellites.

The distribution of satellites (faint companions) around isolated primary galaxies provides important information about galaxy formation, as well as a critical test of the Λ CDM model on small scales ([Einasto & Einasto 1987](#); [Choi et al. 2007a](#); [Agustsson & Brainerd 2010](#); [Ferrero et al. 2012](#); [Anderhalden et al. 2013](#); [Bozek et al. 2013](#)). This explains the growing interest for studying the satellite distribution ([Prada et al. 2003](#); [Sales & Lambas 2005](#); [Guo et al. 2012](#)), and for exploring the link between galaxy properties and the satellite population ([Park et al. 2007](#); [Guo et al. 2011](#); [Karachentseva et al. 2011](#); [Edman et al. 2012](#); [González et al. 2013](#)).

According to a previous study ([Argudo-Fernández et al. 2013a](#), submitted), the criterion proposed by [Karachentseva \(1973\)](#) to remove fore- and background galaxies is not fully efficient. About 50% of the neighbours, considered as potential companions, have very high recession velocities with respect to the central CIG galaxy: the condition is too restrictive, and may consider as not isolated galaxies slightly affected by their environment. On the other hand, the CIG isolation criterion require similar apparent diameter companions, which account for most of the physical neighbours.

In fact, about 92% of neighbour galaxies showing recession velocities similar to the corresponding CIG galaxy are not considered as potential companions by the CIG isolation criterion, and may have a non negligible influence on the evolution of the central CIG galaxy. This mo-

¹<http://amiga.iaa.es>

tivates us to extend the study, taking into account nearby and similar redshift companions to identify physical satellites affecting the evolution of the central CIG galaxy, so as to provide a more physical estimation of the isolation degree of the CIG. About 60% of the CIG galaxies have no major (similar-size) companion in the SDSS, according to the CIG (purely photometric) isolation criterion. Nevertheless, considering the third dimension, only 1/3 of the sample has no similar redshift neighbours (Argudo-Fernández et al. 2013a, submitted).

In this context the CIG represents an excellent sample to study the relation of galaxy properties on both local and large-scale environments.

In the present work, we aim to identify and quantify the effects of the satellite distribution around a sample of CIG galaxies, as well as the effects of the Large Scale Structure. This study is organised as follows: in Sect. 3.2, the sample and the data used are presented. The method to identify the potential satellite galaxies is described in Sect. 3.3. In Sect. 3.4, we describe the parameters used to quantify the environment. We present our results in Sect. 3.5 and the associated discussion in Sect. 3.6. Finally a summary and the main conclusions of the study are presented in Sect. 3.7. Throughout the study, a cosmology with $\Omega_{\Lambda 0} = 0.7$, $\Omega_{m0} = 0.3$, and $H_0 = 70 \text{ km s}^{-1} \text{ Mpc}^{-1}$ is assumed.

3.2 The sample and the data

The CIG (Karachentseva 1973) has been assembled with the requirement that no similar size galaxy i with angular diameter D_i between 1/4 and 4 times the apparent diameter D_P of the primary CIG galaxy lies within $20 D_i$ (Eqs. 3.1 and 3.2):

$$\frac{1}{4} D_P \leq D_i \leq 4 D_P \quad ; \quad (3.1)$$

$$R_{iP} \geq 20 D_i \quad . \quad (3.2)$$

Until recently, most of the identifications and evaluations of large samples of isolated galaxies have been carried out using photometric data. The advent of the Sloan Digital Sky Survey (SDSS; York et al. 2000; Eisenstein et al. 2011) has opened up the possibility to develop a detailed spectroscopic study of the environment of galaxies in the CIG.

Our starting sample is based on the CIG galaxies found in the ninth data release (DR9; Ahn et al. 2012) of the SDSS. We focus our study on CIG galaxies with recession velocities $v \geq 1500 \text{ km s}^{-1}$ (Verley et al. 2007c) so as to avoid an overwhelmed search for potential neighbours (the angular size on the sky for 1 Mpc at a distance of 1500 km s^{-1} is approximately 2.9°). We then add the requirement that more than 80% of the neighbours within a projected radius of 1 Mpc possess a spectroscopic redshift in either the main galaxy sample (Strauss et al. 2002), with magnitudes between $14.5 < m_{r,\text{Petrosian}} < 17.77$, or in the Baryon Oscillation Spectroscopic Survey (BOSS; Dawson et al. 2013) which uses a new spectrograph (Smee et al. 2012) to obtain spectra of galaxies with $0.15 < z < 0.8$ and quasars with $2.15 < z < 3.5$, thus useful to reject background objects in our study. The SDSS data are processed using automatic pipelines (Blanton et al. 2011).

In order to evaluate the effects of the large scale environment, we follow a methodology similar to Argudo-Fernández et al. (2013a, submitted), searching for neighbours around 386 CIG fields completely covered by the SDSS within a physical projected radius of 3 Mpc.

Model magnitudes in the r -band (the deepest images) are used in our study. Sizes are estimated from r_{90} , the Petrosian radius containing 90% of the total flux of the galaxy in the r -band², as explained in Argudo-Fernández et al. 2013a (submitted).

3.3 Identification of physical companions

To recover the physical satellites around the CIG galaxies, we first focus on the satellites which are within the escape speed of each CIG galaxy (Sect. 3.3.1). We also propose a more conservative method using the stacked Gaussian distribution of the velocity difference of the neighbours, with respect to the corresponding CIG galaxy, which gives an upper limit for the influence of the local environment (Sect. 3.3.2).

3.3.1 Escape speed

To identify the physical satellites which may have had a secular influence on the central CIG galaxy, we use the escape speed in order to select the physically bound satellite galaxies. The escape speed at a given distance reads:

$$v_{\text{esc}} = \sqrt{\frac{2GM_P}{R_{iP}}} \quad , \quad (3.3)$$

where G is the universal gravitational constant, M_P is the dynamical mass of the central CIG galaxy, and R_{iP} is the distance between the neighbour i and the primary galaxy P .

In the upper panel of Fig. 3.1, the histogram of the stellar masses (Fernández Lorenzo et al. 2013) of the CIG galaxies is presented. Stellar masses in Fernández Lorenzo et al. (2013) are calculated by fitting the spectral energy distribution using the routine kcorrect (Blanton & Roweis 2007). K_s -band photometry from 2MASS (Skrutskie et al. 2006) are also used when available. The logarithm of the stellar mass spans 8.4–11.2 M_\odot , with a peak towards 10.3 M_\odot . The dynamical masses of the CIG galaxies are estimated from their stellar masses, to which we add a typical value of 90% of dark matter.

Several levels of the escape speed are shown in the middle panel of Fig. 3.1, as a function of the projected distance, up to 0.3 Mpc. The levels are calculated for a typical stellar mass of $10^{10.3} M_\odot$, translating into a dynamical mass of $10^{11.3} M_\odot$. In the lower panel, we show the characteristic trumpet shape (caustic) (Kaiser 1987; Strauss & Willick 1995; Diaferio & Geller 1997) under which the satellite galaxies would be captured. Above the caustic, the neighbour galaxies possess a velocity sufficient to evade the gravitational attraction of the primary galaxy and are not captured, although fly-by interactions may influence the structure and evolution of the primary galaxy.

²<http://www.sdss3.org/dr9/algorithms/magnitudes.php>

The satellite galaxies considered by the escape speed are all neighbour galaxies with $|\Delta v| \leq \sqrt{\frac{2GM_P}{R_{iP}}}$ km s⁻¹ and lying at a distance lower than 0.3 Mpc.

3.3.2 Gaussian distribution of physical satellites

Some galaxies may pass nearby a primary CIG galaxy, but with a velocity so high that they interact once with the CIG galaxy and then leave. To take into account the potential effect of fly-by encounters, we develop a more conservative method to recover most of the galaxies which have interacted with the CIG galaxies. We do so by stacking all the primaries and their satellites in order to obtain statistically robust results.

In the upper panel of Fig. 3.2, we show the distribution of the absolute values of the radial velocity difference between the projected neighbour galaxies and the central CIG galaxies ($\Delta v = v_{\text{neigh}} - v_{\text{CIG}}$). Two components appear clearly in the figure. The first component is a flat continuum distribution of foreground/background neighbours, extending to Mpc scales, and related to the LSS distribution of galaxies. The second component is the over-abundance of neighbour galaxies peaking at $|\Delta v| = 0$ km s⁻¹; most of those would be dynamically related to the central CIG galaxies. In order to estimate the standard deviation, σ , of the distribution, we first estimate the median level of the background between 300 and 1000 km s⁻¹, and remove it. A Gaussian distribution appears for velocity differences minor than 300 km s⁻¹. We vary σ between 70 and 300 km s⁻¹ and use a χ^2 fitting minimisation to obtain the standard deviation of the satellite distribution: $\sigma = 105$ km s⁻¹. Consequently, the 3σ limit is at 315 km s⁻¹. The neighbour galaxies with $|\Delta v| \leq 315$ km s⁻¹ show a substantial liability to gather in the inner 0.3 Mpc around the CIG galaxies (see the lower panel of Fig. 3.2). This dynamical link is also confirmed by the constancy of the standard deviation for radii lower than 0.3 Mpc (see the upper panel of Fig. 3.5, and the associated analysis in Sect. 3.5.3). To be very conservative and recover 99.7% of the physically linked companions, we consider that all neighbours within $|\Delta v| \leq 3\sigma$ may be interacting with their corresponding CIG galaxy.

Hence, the satellite galaxies selected by the Gaussian distribution are all neighbour galaxies with $|\Delta v| \leq 315$ km s⁻¹ and lying at a distance lower than 0.3 Mpc. This method provides an upper limit on the quantification of the local environment, since more galaxies will be considered as satellites with respect to those selected following the escape speed method.

3.4 Quantification of the environment

In order to quantify the isolation degree of the CIG galaxies, we use two complementary parameters: the tidal strength Q that the neighbours produce on the central galaxy, and the projected density η_k (Eqs. 3.6 and 3.7) of neighbour galaxies considered in this study.

3.4.1 Tidal strength parameter

The tidal strength parameter is defined as:

$$Q_{iP} \equiv \frac{F_{\text{tidal}}}{F_{\text{bind}}} \propto \frac{M_i}{M_P} \left(\frac{D_P}{R_{iP}} \right)^3, \quad (3.4)$$

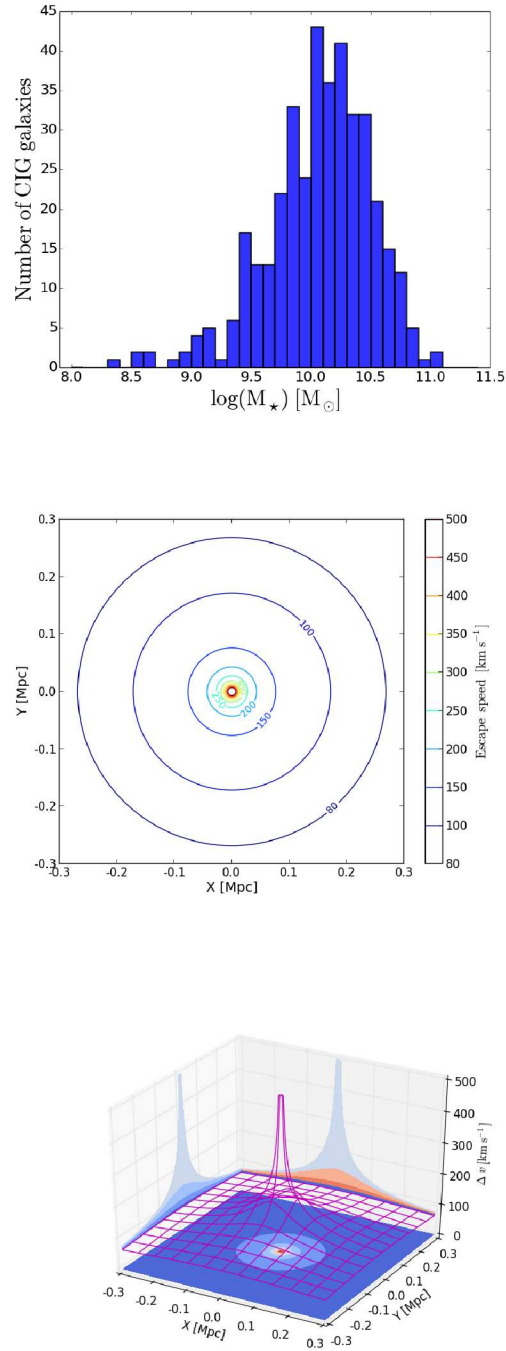


Figure 3.1: (*upper panel*): Histogram of the stellar masses of the CIG galaxies. (*middle panel*): 2-Dimensional escape speed schema in celestial coordinates space. The physically linked associations correspond to neighbour galaxies at distance to the central CIG galaxy and $|\Delta v|$ less than the corresponding value according to circle lines. (*lower panel*): 3-Dimensional escape velocity schema in a redshift-space diagram (line-of-sight velocity versus projected distance). The physically linked associations correspond to neighbour galaxies under the 'trumpet' surface.

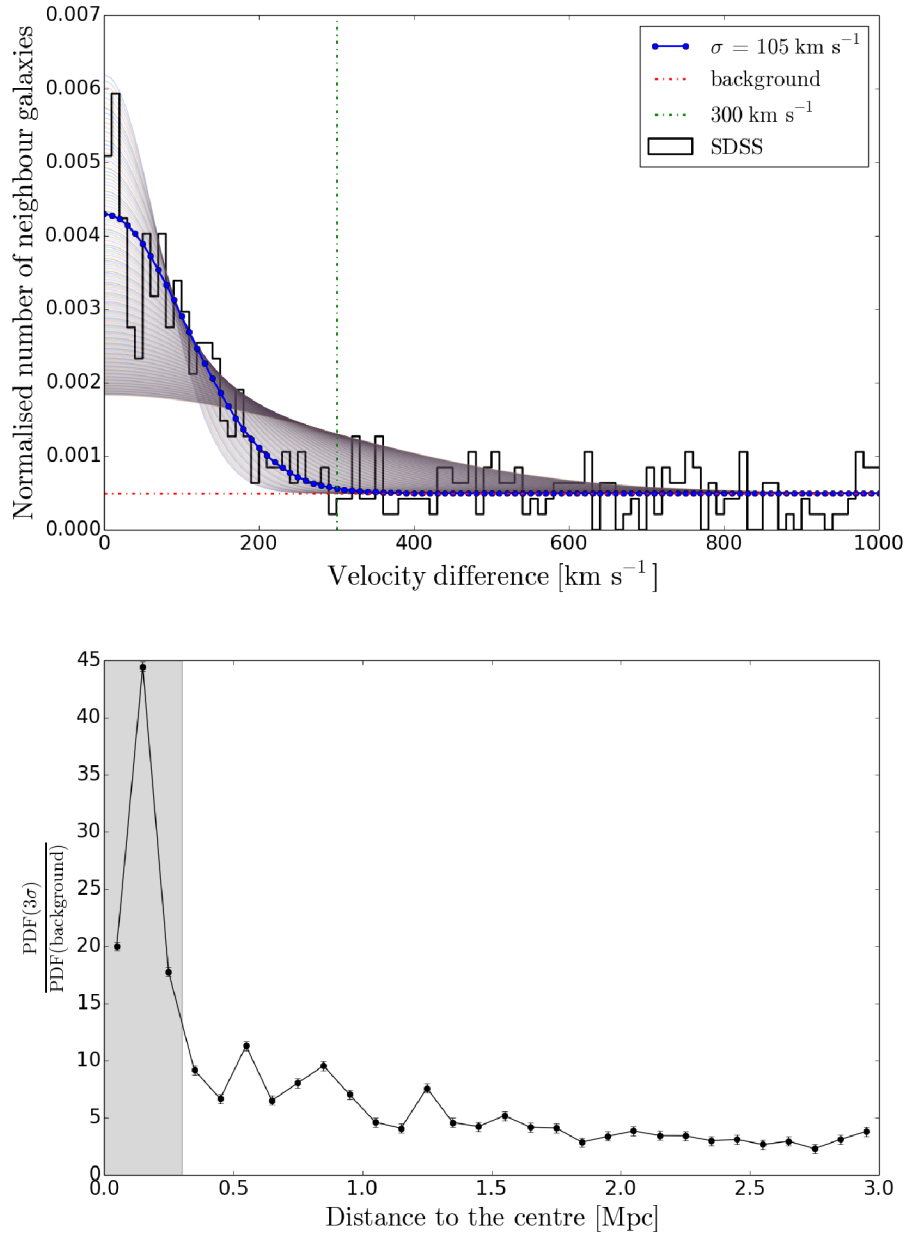


Figure 3.2: (*upper panel*): Absolute values of the line-of-sight velocity difference between neighbours and the central CIG galaxy: $|\Delta v|$ distribution obtained by stacking 411 CIG fields within 1 Mpc field radius (black histogram), and corresponding Gaussian distribution fits for σ between 70 and 300 km s⁻¹ (grey curves) with the best fit (blue curve). The Gaussian fit has been done within $|\Delta v| = 300 \text{ km s}^{-1}$ (vertical line) and considering as a zero point the flat continuum distribution of background neighbours (horizontal line). (*lower panel*): Probability Density Function (PDF) for neighbour galaxies peaking at $|\Delta v| = 0 \text{ km s}^{-1}$ over PDF for the background flat population selected in the interval $1000 < |\Delta v| < 3000 \text{ km s}^{-1}$, as a function of the distance to the central CIG galaxy. The inner 0.3 Mpc are shaded.

where M_i and M_P are the masses of the neighbour and the principal galaxy respectively, D_P the apparent diameter of the principal galaxy, and R_{iP} the projected physical distance between the neighbour and principal galaxy. Absolute magnitudes, M_r , derived from the SDSS-DR9, are used to approximate galaxy masses. Assuming that stellar mass is proportional to r -band flux, i.e. a linear Mass-Luminosity relation (Bell et al. 2003, 2006), we consider $Flux_r \propto mass$. Then:

$$\log Q_{iP} \propto 0.4 (M_r^P - M_r^i) + 3 \log \left(\frac{D_P}{R_{iP}} \right) \quad , \quad (3.5)$$

where M_r^P and M_r^i are the magnitudes of the principal CIG galaxy and the neighbour, respectively, and $D_P = 2 r_{90}$ scaled by a factor 1.43 (see Argudo-Fernández et al. 2013, submitted) to match the definition of diameter used in the literature (projected major axis of a galaxy at the 25 mag arcsec⁻² isophotal level or D_{25} , Verley et al. 2007b). The total tidal strength is then defined as:

$$Q = \log \left(\sum_i Q_{iP} \right) \quad . \quad (3.6)$$

The logarithm of the sum of the tidal strength created by all the neighbours in the field is a dimensionless estimation of the gravitational interaction strength (Verley et al. 2007b). The greater the value of Q , the less isolated from external influence the galaxy, and vice-versa.

3.4.2 Projected number density parameter

To characterise the LSS around the CIG galaxies, we also define the projected number density parameter (Verley et al. 2007b, Argudo-Fernández et al. 2013a, submitted), as follows:

$$\eta_{k,LSS} \propto \log \left(\frac{k-1}{V(r_k)} \right) \quad , \quad (3.7)$$

where $V(r_k) = \frac{4}{3} \pi r_k^3$ and r_k is the projected physical distance to the k^{th} nearest neighbour, with k equal to 5, or less if there were not enough neighbours in the field. The farther the k^{th} nearest neighbour, the smaller the projected number density $\eta_{k,LSS}$.

3.5 Results

3.5.1 Spectroscopic identification of physical satellites around galaxies in the CIG

Out of the 386 CIG galaxies considered in this study, 349 have no physically linked satellites, which represents 90% of the sample. Among the 37 CIG galaxies with at least one physical companion within its escape speed boundary, 30 have one satellite, six have two satellites, and one has three satellites (CIG 771). There is no CIG galaxy with more than three physically linked satellites. The values of the tidal forces exerted by these satellites on the CIG galaxies are listed in columns 2, 3, 4, and 5 of Table D.2.

Following the more conservative Gaussian distribution of physical satellites around the CIG galaxies leads to upper limits. Out of the 386 CIG galaxies, 327 (85% of the sample) have

no physical companion within a projected distance of 0.3 Mpc. Out of the remaining 59 CIG galaxies (15%), 46, 11, and 2 CIG galaxies (CIG 237 and CIG 771) are in interaction with one, two, and three physical companions, respectively.

Examples of the environment for three CIG galaxies are shown in Fig. 3.3. CIG 203 has no physically bound companions. On the other hand, CIG 401 and CIG 771 are interacting locally with companions that are caught under their gravitational influence.

3.5.2 Large Scale Structure

To quantify the large scale environment around the CIG galaxies, we use the two isolation parameters defined in Sect. 3.4. The parameter Q_{LSS} takes into account all companions within 3 Mpc and $|\Delta v| < 315 \text{ km s}^{-1}$ to provide the sum of the tidal strengths exerted on the CIG galaxies. The parameter $\eta_{k,\text{LSS}}$ accounts for the number density of companions within $|\Delta v| < 315 \text{ km s}^{-1}$ and projected at the distance of the 5th nearest neighbour with respect to the CIG galaxy. Only 10 CIG galaxies (less than 3% of the sample) are farther away than 3 Mpc from any other galaxy with a SDSS measured spectrum.

In Fig. 3.4, the projected number density is shown versus the tidal strength parameter. Due to the logarithmic definition of the parameters, the figures appear to span several orders in magnitude (3 dex for $\eta_{k,\text{LSS}}$ and 7 dex for Q_{LSS}) showing the large scatter in the environments found around the CIG galaxies. The results of the quantifications of the environment are listed in columns 6, 7, and 8 of Table D.2.

The large scale environment is graphically exemplified around three CIG galaxies in the right column of Fig. 3.3. There is a sparse population of galaxies in the LSS around CIG 203, while CIG 401 and CIG 771 show a much more crowded LSS within 3 Mpc.

3.5.3 Local environment versus large scale environment

To evaluate the role of the physically bound satellites with respect to the large scale environment, we compare the magnitudes of the sum of the tidal forces produced by the physical companions to the sum of the tidal forces engendered by all the galaxies in the LSS. When at least one physical companion is present near a CIG galaxy, its effect largely dominates (usually more than 90%) over the tidal forces generated by the LSS. This effect is clearly visible in Fig. 3.4. The ratios $Q_{\text{sat}}/Q_{\text{LSS}}$ and $Q_{\text{sat,sup}}/Q_{\text{LSS}}$ are tabulated in columns 9 and 10 of Table D.2, respectively.

It seems that there is a natural distinction between the physically bound satellites and the LSS. This dichotomy appears for instance if we plot the standard deviation of a Gaussian fitting as a function of the projected distance (see the upper panel of Fig. 3.5). Up to ~ 0.3 Mpc, most of the galaxies are linked to their host. If the systems have been in interaction long enough, they are relaxed and the velocity differences are virialised. This appears as a plateau in the inner ~ 0.3 Mpc, with a constant standard deviation $\sigma \approx 105 \text{ km s}^{-1}$. At larger distances, the standard deviation monotonically increases due to the rising fraction of the LSS galaxies enclosed.

The physically captured satellite galaxies are typically 1.5 dex fainter than the magnitude of galaxies lying farther away (see the middle panel of Fig. 3.5). In average, the galaxies in the inner ~ 0.3 Mpc are also smaller (about $0.4 \times D_P$) compared to galaxies which are not satellites ($\sim 0.7 \times D_P$).

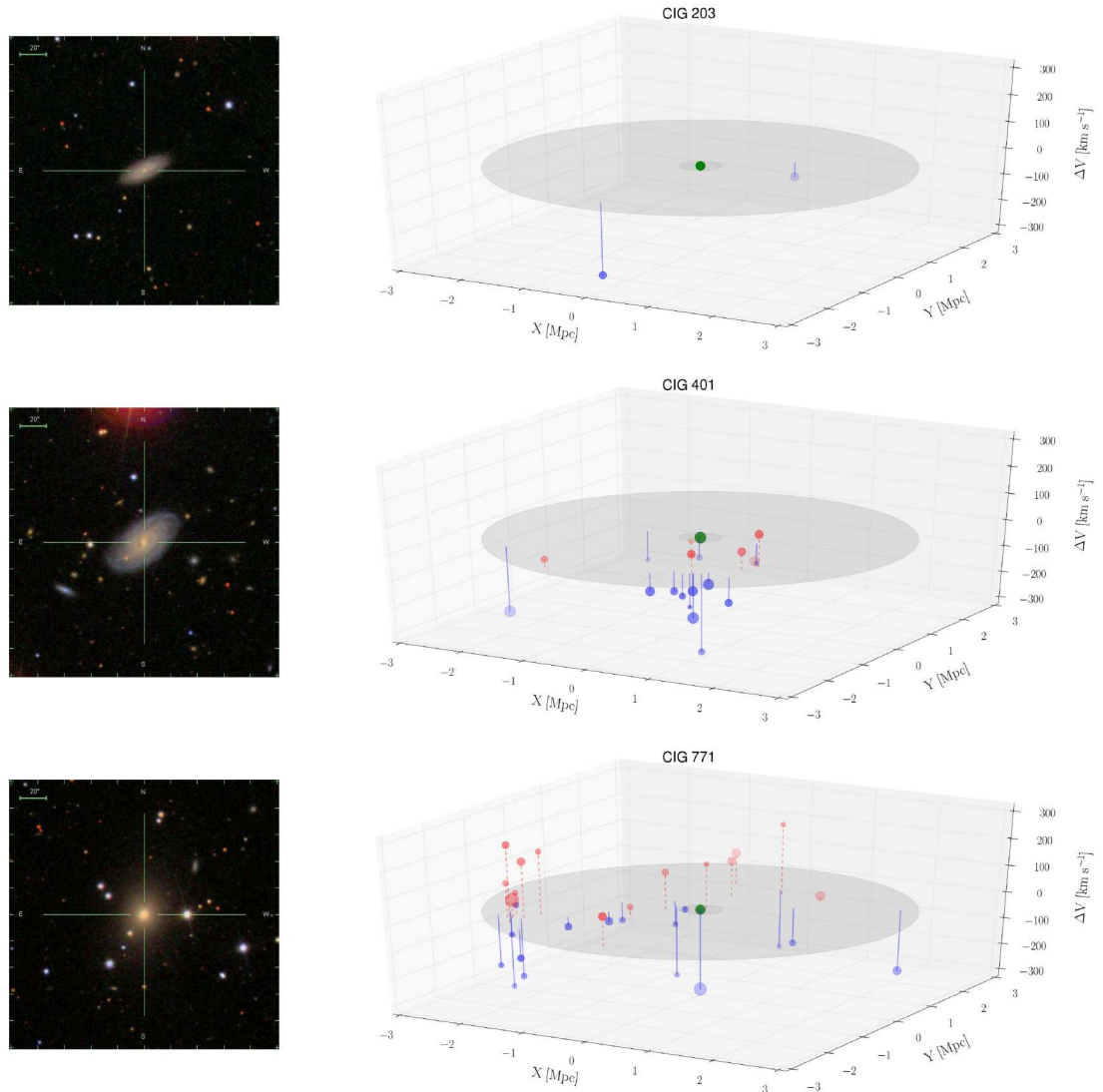


Figure 3.3: SDSS three-colour images (left, with a field of view of 3'3, North is up, East is to the left) and representation in 3D (right) of the environment of the galaxies CIG 203 (upper panel), CIG 401 (middle panel), and CIG 771 (lower panel). The central green spheres correspond to the locations of the primary CIG galaxies. Grey disks at 0.3 and 3 Mpc boundaries represent the areas to study the local environment and the LSS, respectively. The sizes of the symbols are proportional to the diameters of the neighbours (not at scale), in red or blue according to blueshift or redshift of the neighbours. Vertical lines indicate the projection of the neighbours in the 2-Dimensional plane.

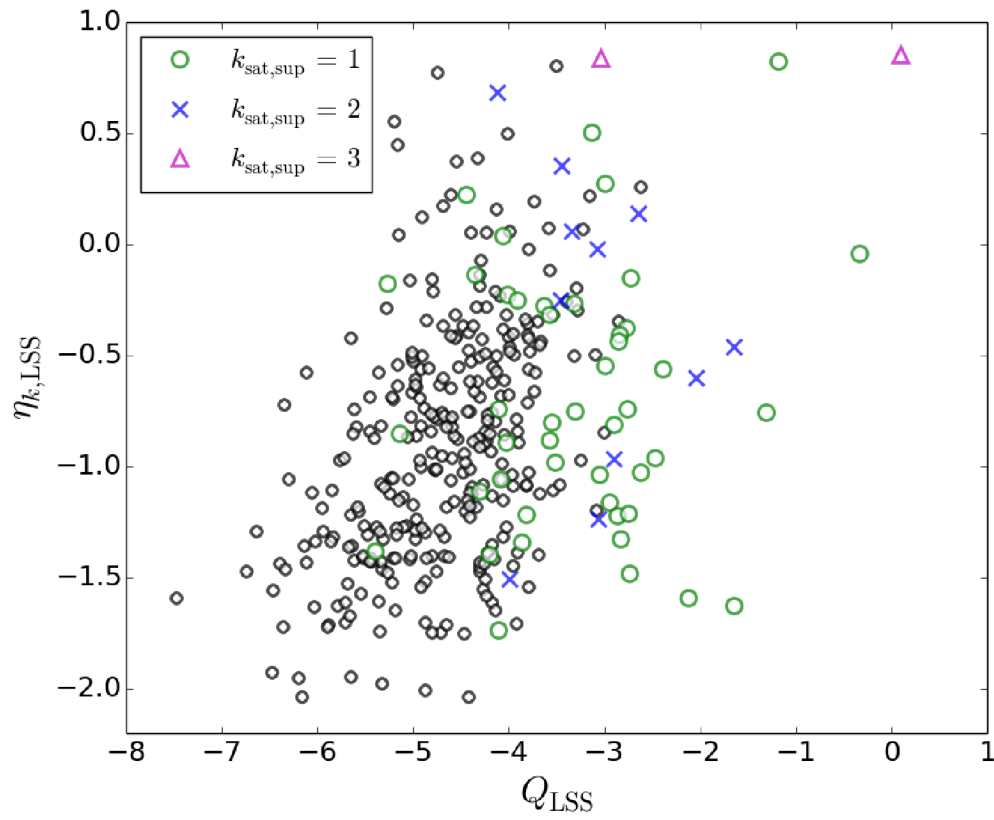


Figure 3.4: Projected number density $\eta_{k,\text{LSS}}$ versus tidal strength Q_{LSS} diagram for the LSS. CIG galaxies with one, two, and three dynamically linked satellites are depicted by green circles, blue crosses, and magenta triangles, respectively.

The connection between the CIG and the LSS is revealed by comparing the apparent magnitudes and sizes of the galaxies with $|\Delta v| < 315 \text{ km s}^{-1}$ to the ones of the galaxies outside this limit (see middle and lower panels of Fig. 3.5, respectively). Galaxies with similar velocities have magnitudes and sizes closer to the ones of CIG galaxies, compared to background and foreground galaxies (defined by galaxies with recession velocities in the range $315 < |\Delta v| < 3000 \text{ km s}^{-1}$), disclosing the association between the CIG galaxies and their surrounding LSS.

3.5.4 Correction for the redshift incompleteness

As mentioned in Sect. 3.2, the sample used in this study was selected for CIG fields with at least 80% redshift completeness (the mean completeness of the sample is 92.5%). In order to correct the estimation of the local environment for the remaining neighbours up to 20% of incompleteness, we use the photometric redshift z_p provided by the SDSS (z of the schema Photoz, for galaxies at magnitudes $m_r < 17.77$ according to Sabater et al. 2013). After a first rejection of neighbours with $z_p > 0.1$ as background galaxies, we select as potential companions neighbour galaxies with $|z_{\text{CIG}} - z_p| < 2.5 z_{p,\text{Err}}$ (Guo et al. 2011), where z_{CIG} is the spectroscopic redshift of the CIG galaxy and $z_{p,\text{Err}}$ is the photometric redshift error. The upper limit on the local tidal strength is then calculated considering these potential companions at the same distance as their corresponding CIG galaxy, i.e., the least favourable case for the isolation.

This correction is applied to the already conservative Gaussian distribution selection of physical satellites, introducing no change for 356 CIG galaxies (92% of the sample). Out of the remaining 30 CIG galaxies, 22 CIG galaxies without satellite acquire one, six CIG galaxies pass from one to two satellites, and one CIG galaxy passes from two to three satellites. Only one CIG galaxy, CIG 626, gains more than one possible satellite, passing from none to three possible satellites.

The inclusion of one missing redshift galaxy as a potential companion increases the tidal strength by a mean value of 13%, with respect to the tidal strength generated by the spectroscopic satellites, the most unfavourable cases being for CIG 278 and CIG 495 where the effect of the missing galaxy amounts to 64% and 83%, respectively.

3.6 Discussion

3.6.1 The construction of the CIG

As shown in Sect. 3.5.1, 10% (and up to 15%) of the CIG galaxies are directly interacting with satellites. To seek why these systems are included in the CIG, it is worth to recall that the CIG has been constructed visually, on photographic material (Karachentseva 1973). Unfortunately, the sample of neighbour galaxies inspected originally is not available. Nevertheless, a revision has been carried out by Verley et al. (2007c) on the same original material (Palomar Observatory Sky Survey, POSS), providing a catalogue of approximately 54,000 neighbours. By comparing the physically bound satellites found in the SDSS to this POSS-based catalogue, we should be able to point out some drawbacks due to the use of photographic plates and the nearly total lack of redshift availability, forty years ago.

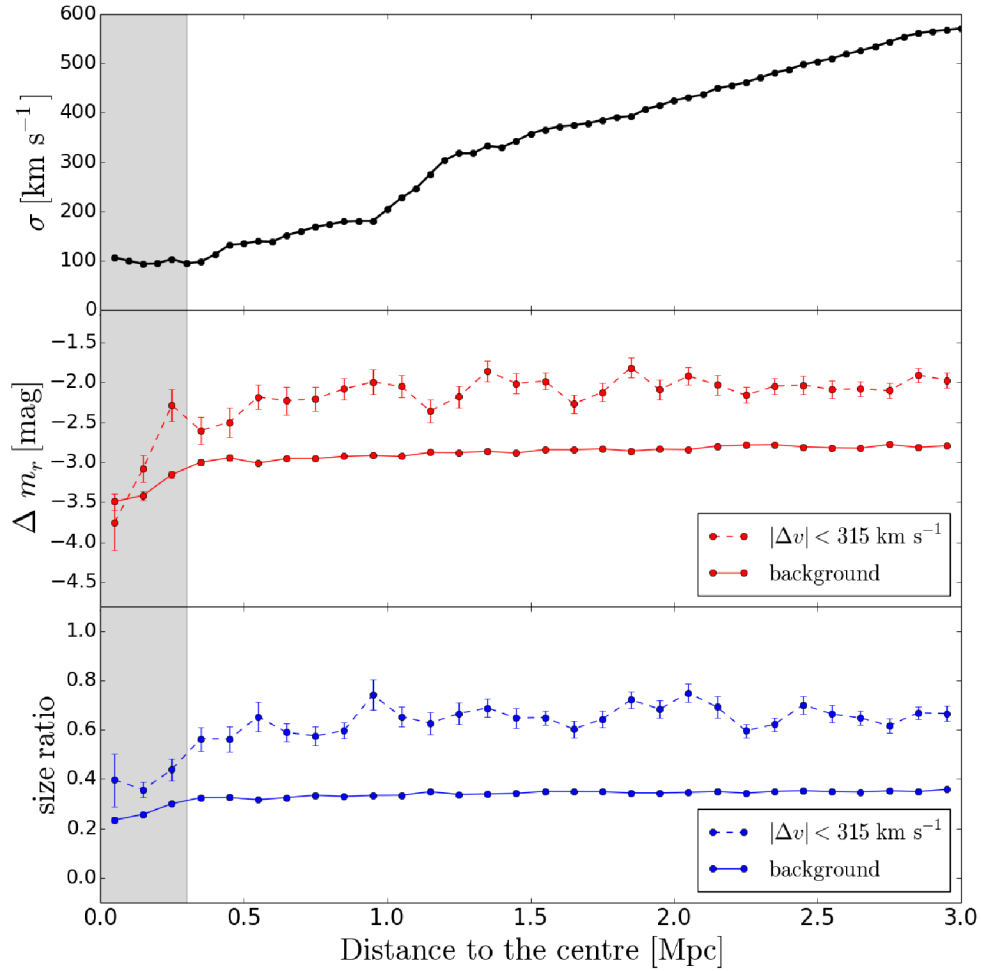


Figure 3.5: (*upper panel*): Standard deviation σ of the Gaussian distribution fitting for $|\Delta v|$ as a function of the distance to the central galaxy. (*middle panel*): Magnitude difference Δm_r for satellites ($|\Delta v| \leq 315 \text{ km s}^{-1}$, red dashed line) and for background galaxies ($315 < |\Delta v| < 3000 \text{ km s}^{-1}$, red solid line) as a function of the distance to the central CIG galaxy. (*lower panel*): Size ratio ($\frac{D_i}{D_p}$ between neighbour i and its corresponding primary CIG galaxy P) for satellites ($|\Delta v| \leq 315 \text{ km s}^{-1}$, blue dashed line) and for the background population ($315 < |\Delta v| < 3000 \text{ km s}^{-1}$, blue solid line) as a function of the distance to the central CIG galaxy. The inner 0.3 Mpc are shaded in the three panels.

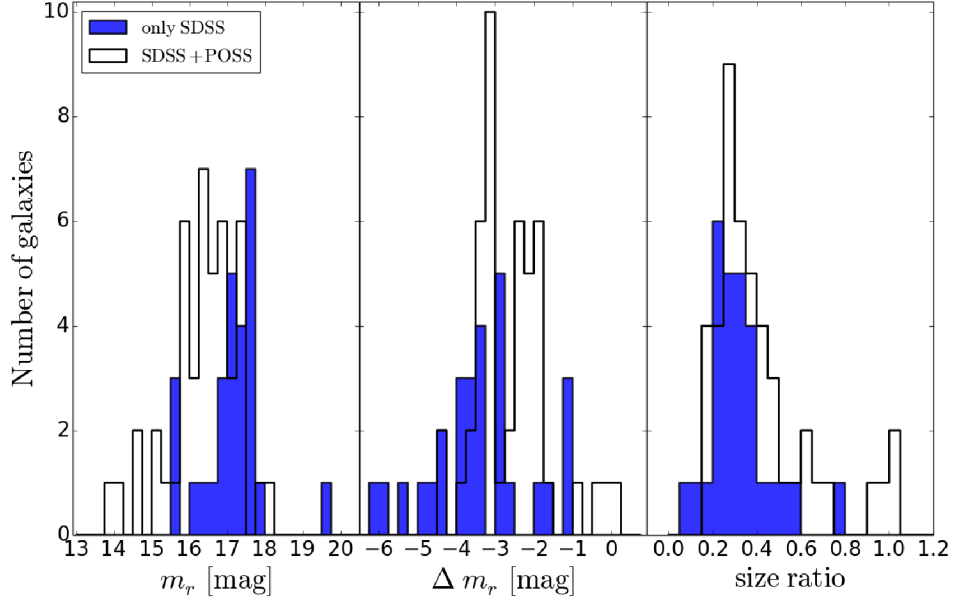


Figure 3.6: Distribution of apparent magnitude (left panel), apparent magnitude difference (central panel), and size ratio (right panel) for physical linked satellites. Distributions for satellites which were not identified in the POSS (Verley et al. 2007c) are represented by blue histograms.

In the left panel of Fig. 3.6, we show that the SDSS identification of satellites goes, in general, deeper than the POSS. Indeed, Verley et al. (2007c) recover neighbour galaxies brighter than $B = 17.5$. The slight overlap of magnitudes between the two distributions is due to the non-linearity of the photographic material, as well as the varying zero-point from field to field in the POSS calibration (Verley et al. 2007c). Equally, in the central panel of Fig. 3.6, we see that the POSS search for companions misses the faintest galaxies, with respect to the magnitudes of the primary CIG galaxies.

Nonetheless, Karachentseva (1973) did not use any magnitude criterion to search for companions, and used only the apparent diameters of galaxies instead. In the right panel of Fig. 3.6, it is shown that about half of the physical companions missed by the POSS have diameters smaller than one fourth of the diameter of their corresponding CIG galaxy, and were therefore not considered by the CIG isolation criterion. In fact, 23% of the missing physical companions are dwarf galaxies discarded by the original study. Redshift surveys are mandatory in order to distinguish small, faint, interacting satellites from a background projected galaxy population.

3.6.2 Identification of satellites

Due to the spectroscopic redshift limit of the SDSS, analysing the satellite population around isolated galaxies is a challenge. We have some limitations to take into account. We are only

able to detect bright neighbours (M 31 or M 33 like galaxies) and the brightest dwarfs (Large Magellanic Cloud and Small Magellanic Cloud like satellites) around most central galaxies. Nevertheless, the spectroscopic catalogue of the SDSS is complete to $m_r < 17.77$ mag, so we are always able to detect neighbours within $\Delta m_r \leq 2$ mag, even for the faintest CIG galaxy.

The spatial location of satellites with respect to their primary galaxies is uncertain due to redshift space distortions and projection effects. We follow a very conservative approach and use the projected separation between the neighbour and the CIG galaxy, providing a lower limit on the 3D distance between the two galaxies, which increases the number of potentially linked satellites taken into account by the escape speed and Gaussian distribution selections. This will translate on conservative higher limits for the isolation parameters.

In addition, the redshifts only account for the radial (line of sight) component of the peculiar velocities of the galaxies. Consequently, the velocity difference Δv supplies also a lower limit and exaggerates the number of physically related companions, in particular for the escape speed selection method. Nevertheless, the escape velocity method selects satellites minimising the effect of background objects, although there is an uncertainty about the total dynamical mass of the primary galaxy.

On the other hand, the Gaussian distribution method selects as satellites all neighbours within $|\Delta v| \leq 3\sigma$ and at projected physical distances to the central galaxy $d \leq 0.3$ Mpc. The 3σ cut ensures that we recover more than 99.7% of the physically associated satellites. This method includes also a fraction of fly-by encounters that may have an influence on the evolution of the primary galaxies. However, this is a compromise because, at the same time, it incorporates galaxies which are more likely located at 4.5 Mpc from the primary galaxy rather than at the same distance and with a velocity difference $\Delta v = 315 \text{ km s}^{-1}$ (following the lineal approximation of the Hubble law $v = H_0 D$). This explains why the Gaussian distribution provides an upper limit to the escape speed selection.

3.6.3 Local and large scale environments around CIG galaxies

Although only up to 15% of the CIG galaxies in the sample are in interaction with a physically bound satellite, almost all galaxies (97%) can be directly related to a LSS. The very large scatter in the quantification of the LSS (see the values spanned by $\eta_{k,\text{LSS}}$ and Q_{LSS} in Fig. 3.4) shows that the CIG includes both galaxies dominated by their immediate environment as well as galaxies almost free from any external influence. In particular ten CIG galaxies are not associated to a LSS, at least within 3 Mpc: CIG 229, 245, 284, 318, 331, 541, 542, 546, 674, and 702 (see their three-colour images in Fig. 3.7).

The continuous distributions of the $\eta_{k,\text{LSS}}$ and Q_{LSS} isolation parameters show that the CIG spans all the variety of environments between these two extreme cases. The connection of the CIG galaxies with the LSS is obvious due to the excess of similar redshift galaxies between 0.3 and 3 Mpc, as can be seen in the lower panel of Fig. 3.2. According to the middle and lower panels of Fig. 3.5, the large scale association is also noticeable due to higher number of brighter and bigger galaxies at redshift similar to those of the CIG galaxies, with respect to fainter, smaller background objects. Hence, the CIG galaxies are distributed following the LSS of the local Universe, although presenting a large heterogeneity in their degree of connection with it.

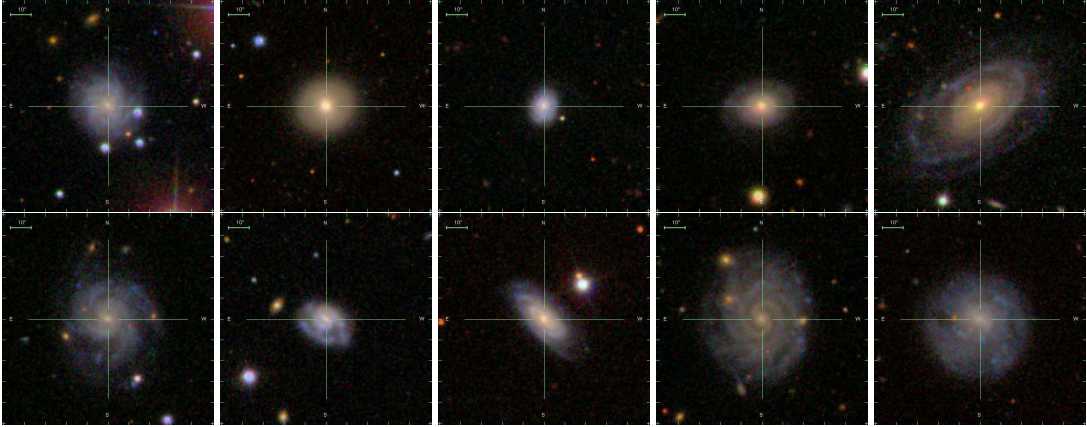


Figure 3.7: SDSS three-colour images (field of view of $1'.7$, North is up, East is to the left) of the ten most isolated CIG galaxies in the SDSS-DR9 footprint. From upper left to lower right: CIG 229, 245, 284, 318, 331, 541, 542, 546, 674, and 702.

Some illustrations of the different environments around the CIG galaxies are shown in Fig. 3.3. Due to the large and roughly equivalent number of blue- and redshifted neighbour galaxies within the projected 3 Mpc, the galaxy CIG 771 may reside in the outskirts of a poor cluster. The galaxy CIG 401 seems to be located towards the edge of a LSS, such as a filament or a wall. On the other hand, the galaxy CIG 203 appears only mildly in relation with a LSS since only two LSS neighbours can be found in its environment. Its isolation parameters are very low ($\eta_{k,\text{LSS}} = -1.94$ and $Q_{\text{LSS}} = -5.65$) and its spatial location could be towards a void part of the local Universe. This environment is closer to the one of the ten galaxies for which we find no relation with the LSS within the first 3 Mpc. It is interesting to note that, out of the ten most isolated galaxies studied here, nine are clearly late type spirals showing symmetric morphologies, with no visible signs of interaction (see Fig. 3.7). Some of these galaxies could represent the closest remains of a fossil spiral population.

3.6.4 Influence of the environment on the evolution of the primary galaxies

To delimit the role of the environment on the physical properties of the galaxies we compare, within the CIG, the most isolated galaxies to the interacting ones. The subsample of interacting galaxies encloses galaxies with at least one physically bound companion in their vicinity (k_{sat} or $k_{\text{sat,sup}}$ strictly positive). The subsample containing the most isolated CIG galaxies incorporates the galaxies presenting the lowest values of the projected number density ($\eta_{k,\text{LSS}} < 1.5$) and tidal strength ($Q_{\text{LSS}} < 6$), along with the ten galaxies isolated from both their local and LSS environments (CIG 229, 245, 284, 318, 331, 541, 542, 546, 674, and 702).

In the upper left panel of Fig. 3.8, the distribution of the stellar masses of the interacting and isolated galaxies are shown. Both subsamples extend from $10^{8.5}$ to $10^{11.0} M_{\odot}$, although the interacting galaxies might have a mild tendency (0.3-0.4 dex) to be more massive, which may indicate a higher frequency of having suffered a merger in the past. There is no notable difference

in the distributions of the absolute magnitudes between the two subsamples (upper central panel of Fig. 3.8).

Colours are calculated using $(g - r)$, where $g = m_g$ and $r = m_r$ are g - and r -band Galactic extinction corrected magnitudes using Schlegel et al. (1998) dust maps. The median $(g - r)$ value for the galaxies with physically bound satellites ($k_{\text{sat}} > 0$) is 0.80, while the median value for the galaxies least affected by external tidal forces ($Q_{\text{LSS}} < -6$) drops to 0.61 (upper right panel of Fig. 3.8). This suggests that the CIG galaxies in interaction are in general redder and with older stellar populations with respect to the most isolated galaxies in the CIG which are bluer due to younger stellar populations.

In the lower left panel of Fig. 3.8, the morphological T -types (Fernández Lorenzo et al. 2012) of the most interacting and most isolated galaxies are shown. The fraction of early-type galaxies ($T < 0$) is dominated by interacting galaxies. On the other hand, the most isolated galaxies concentrate around the Sc type ($T = 5$), meaning that they are mainly late-type spiral galaxies. This trend is confirmed by the 10 most isolated galaxies: only one is early-type, while the remaining nine are consistently distributed around the Sc type. The inverse concentration index (ICI) defined as the ratio of the radii containing 50% and 90% of the Petrosian fluxes in the SDSS r -band, $C \equiv r_{p,50}/r_{p,90}$, is also an indicator of the morphological type. Early-type galaxies with a de Vaucouleurs profile will display values of the ICI around 0.3 while morphologies dominated by an exponential disk will show typical ICI values towards 0.43 (Strateva et al. 2001). The ICI histograms in the lower central panel of Fig. 3.8 confirm the trends based on the visual (optical) morphology: a segregation between early-type galaxies in interaction and isolated late-type galaxies. These tendencies can be related to the well known morphology-density relation for field and cluster galaxies (Dressler 1980; Dressler et al. 1997), but it is noteworthy to appreciate it even when the local environment is defined by only one, two, or three faint satellites.

The stellar populations of primary galaxies can be characterised in terms of $(u - r)$ colours (corrected from the Galactic extinction following Schlegel et al. 1998). In the lower right panel of Fig. 3.8, the well known SDSS-discovered bimodality appears, with an optimal separation at $(u - r) = 2.22$ (Strateva et al. 2001). Isolated galaxies mainly distribute in the range $(u - r) < 2.22$, while interacting galaxies spread over the area defined by $(u - r) > 2.22$. This segregation means that isolated galaxies are in general bluer, with a younger stellar population and rather high star formation with respect to older, redder interacting galaxies. These colours, in combination with morphological trends previously noticed and the $(g - r)$ colours, lead to a coherent view where isolated star forming galaxies are separated from older early-type galaxies in interaction.

In Fig. 3.9, we show some mean properties of the physically linked satellites as a function of the stellar masses of the primary CIG galaxies, for two subsamples: physical satellites around early- and late-type CIG galaxies. The distribution of the absolute magnitudes of the satellites is comparable for both subsamples, although the most massive early-type CIG galaxies ($M_{\star} > 10^{10.5} M_{\odot}$) may very marginally attract brighter satellites (see upper panel of Fig. 3.9). A clearer tendency appears for the distribution of the ICI: massive early-type CIG galaxies will preferentially be surrounded by more early-type companions, with respect to late-type CIG galaxies which will present a higher fraction of late-type satellites (see central panel of Fig. 3.9).

This dichotomy is also seen in the $(g-r)$ colours of the satellites: the satellites are redder, likely have older stellar populations, around massive early-type CIG galaxies while they may present a younger stellar content around massive late-type CIG galaxies, as seen in the lower panel of Fig. 3.9.

This means that if the local environment has an influence on the evolution of the CIG galaxies, reciprocally, the satellites around the CIG galaxies may also be affected by the nature of the primary galaxy. This suggests that the CIG is composed by an heterogeneous population of galaxies, sampling old systems of galaxies but also spanning more recent, dynamical systems of galaxies.

3.7 Summary and conclusions

We present a study of the 3-dimensional environment for a sample of 386 galaxies in the Catalogue of Isolated Galaxies (CIG; Karachentseva 1973), using the Ninth Data Release of the Sloan Digital Sky Survey (SDSS-DR9).

We identify and quantify the effects of the satellite distribution around a sample of galaxies in the CIG. To recover the physical satellites around the CIG galaxies, we first focus on the satellites which are within the escape speed of each CIG galaxy. We also propose a more conservative method based on the stacked Gaussian distribution of the velocity difference of the neighbours, which gives an upper limit to the influence of the local environment.

In comparison to a previous study (Argudo-Fernández et al. 2013a, submitted) we can estimate the effect of the physical associations that were not taken into account by the CIG isolation criterion, which could also have a non negligible influence on the evolution of the central CIG galaxy. The tidal strengths affecting the primary galaxy are estimated to quantify the effects of the local and Large Scale Structure (LSS) environments. To characterise the LSS around the CIG galaxies, we define the projected number density parameter at the 5th nearest neighbour.

Our main conclusions are the following:

1. Out of the 386 CIG galaxies considered in this study, 349 (90% of the sample) have no physically linked satellite. Following the more conservative Gaussian distribution method to identify physical satellites around the CIG galaxies leads to upper limits: out of the 386 CIG galaxies, 327 galaxies (85% of the sample) would have no physical companion within a projected distance of 0.3 Mpc.
2. Consequently, 10% (and up to 15%) of the CIG galaxies are directly interacting with physically bound satellites. Interacting CIG galaxies might have a mild tendency (0.3-0.4 dex) to be more massive, which suggests a higher frequency of having suffered a merger in the past. Satellites are in general redder, brighter, and bigger for more massive central CIG galaxies. Also, massive elliptical and lenticular CIG galaxies tend to have satellites with earlier types than similar mass spiral CIG galaxies.
3. Although 15% at most of the CIG galaxies in the sample are in interaction with a physically bound satellite, almost all galaxies (97%) can be directly related to a LSS. The

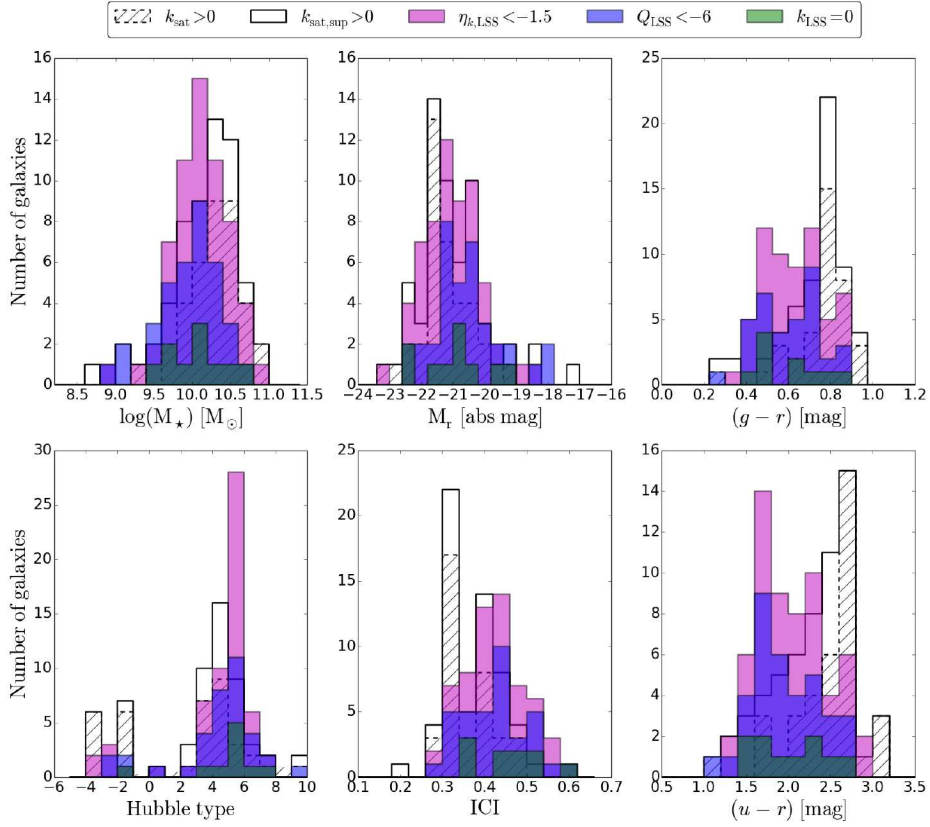


Figure 3.8: Distributions of the stellar mass (upper left panel), r-band absolute magnitude (upper central panel), $(g-r)$ colour (upper right panel), morphological Hubble type (T) according to Fernández Lorenzo et al. (2012) (lower left panel), inverse concentration index (lower central panel), and $(u-r)$ colour (lower right panel) for CIG galaxies. The distributions for the 10 most isolated CIG galaxies are represented by green histograms, and the most isolated CIG galaxies in terms of projected density $\eta_{k,LSS}$ and tidal strength Q_{LSS} are represented by magenta and blue histograms, respectively. On the contrary, distributions for CIG galaxies with satellites are represented by white histograms (hatched histograms for the escape speed selection and plain white histograms in case of upper limit selection of satellites).

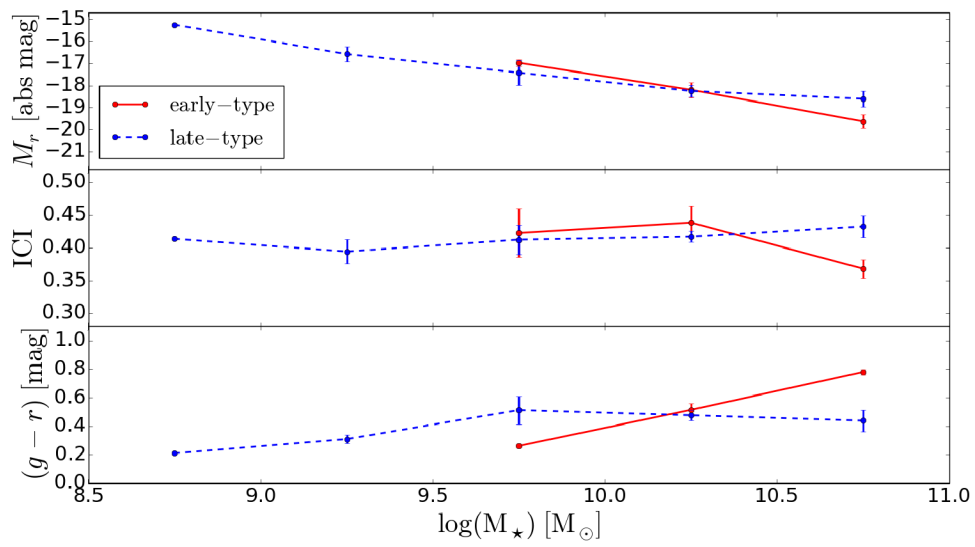


Figure 3.9: Mean r -band absolute magnitude (upper panel), ICI (middle panel), and $(g - r)$ colour (lower panel) for bound physical satellites as a function of CIG galaxy stellar mass. Mean satellite properties for early-type ($T \leq 0$, red solid line) and late-type ($T > 0$, blue dashed line) CIG galaxies are represented. Error bars are given by the standard deviation.

very large scatter in the quantification of the LSS shows that the CIG includes both galaxies dominated by their immediate environment as well as galaxies almost free from any external influence.

4. The continuous distributions of the $\eta_{k,LSS}$ and Q_{LSS} isolation parameters show that the CIG spans a variety of environments. The connection of the CIG galaxies with the LSS is obvious due to the excess of similar redshift galaxies between 0.3 and 3 Mpc. The CIG galaxies are distributed following the LSS of the local universe, although presenting a large heterogeneity in their degrees of connection with it.
5. To evaluate the role of the physically bound satellites with respect to the large scale environment, we compare the magnitudes of the sum of the tidal strengths produced by the physical companions to the sum of the tidal strengths created by all the galaxies in the LSS. When at least one physical companion is present near a CIG galaxy, its effect largely dominates (usually more than 90%) the tidal strengths generated by the LSS.
6. To delimit the role of the environment on the physical properties of the galaxies we compare, within the CIG, the most isolated galaxies to the interacting ones. We find a clear segregation between early-type CIG galaxies in interaction and isolated late-type CIG galaxies. Isolated galaxies are in general bluer, with a younger stellar population and rather high star formation with respect to the older, redder interacting galaxies. These $(u - r)$ colours, in combination with the morphological trends and the $(g - r)$ colours, lead to a coherent view where isolated star forming galaxies are separated from older elliptical galaxies in interaction.
7. Conjointly, we find that the satellites are redder and with older stellar populations around massive early-type CIG galaxies while they have a younger stellar content around massive late-type CIG galaxies. This means that if the local environment has an influence on the evolution of the CIG galaxies, reciprocally, the satellites around the CIG galaxies may also be affected by the nature of the primary galaxy. This suggests that the CIG is composed of a heterogeneous population of galaxies, sampling old systems of galaxies but also spanning more recent, dynamical systems of galaxies.
8. As mentioned, the CIG samples a variety of environments, from galaxies in interaction with physical satellites to galaxies with no neighbours in the first 3 Mpc around them. Hence, in the construction of catalogues of galaxies in relation to their environments (isolated, pairs, and triplets of galaxies), redshift surveys are required in order to distinguish small, faint, interacting satellites from a background projected galaxy population and reach a more comprehensive 3-dimensional picture of the surroundings.

Chapter 4

Catalogues of isolated galaxies, isolated pairs, and isolated triplets in the local Universe

Contents

4.1 Introduction	80
4.2 Data and definition of the samples	81
4.3 Physical definition	82
4.4 Quantification of the environment	83
4.4.1 Tidal strength	83
4.4.2 Projected density	83
4.5 Results	85
4.5.1 The catalogues	85
4.5.2 Relation to the Large Scale Structure	93
4.5.3 Morphology	93
4.6 Discussion	96
4.6.1 The catalogues	96
4.6.2 Relation with the Large Scale Structure	96
4.6.3 Euclidean Minimum Spanning Tree	100
4.6.4 Morphology	100
4.7 Summary and conclusions	103

4.1 Introduction

It has long been known that galaxies are not distributed uniformly through space (Dressler 1980; Dressler et al. 1997; Einasto & Einasto 1987). Recent galaxy surveys like the 2dF Galaxy Redshift Survey (Colless et al. 2001), the Sloan Digital Sky Survey (Abazajian et al. 2003), and the 2MASS Redshift Survey (Huchra et al. 2012), which map the Large Scale Structure of the Universe (LSS), have confirmed that galaxies are distributed in a hierarchical structure of filaments and walls, and large embedded voids (Choi et al. 2007b; Hoyle et al. 2012; Pan et al. 2012). Galaxies in groups and clusters tend to further cluster in even larger scale superclusters, representing the largest aggregates in the Universe.

More than half of the galaxies (54%) in the local Universe ($z \lesssim 0.1$) appear concentrated in the virialised groups and clusters (Courtois et al. 2013). Another 20% of galaxies are located in collapsing regions around groups and clusters (Tully 1987; Crook et al. 2007; Makarov & Karachentsev 2011). The remaining populations of galaxies are referred as the "field", and are distributed mainly along the diffuse filaments bordering cosmic voids. About 10% of these galaxies can be found in loose pairs and compact groups (Xu & Sulentic 1991; Karachentseva et al. 2011).

New photometric and spectroscopic measurements of galaxies from galaxy surveys lead to a better understanding of the relation of galaxy properties with the environment, e.g.: the morphology-density relation (Añorve et al. 2009); optical and ultraviolet luminosity, and atomic gas mass function (Blanton & Moustakas 2009; Dariush et al. 2011); the morphology-mass relation (Calvi et al. 2011); the infrared luminosity and stellar-mass function (Balogh et al. 2001); galaxy colours (Grützbauch et al. 2011, and references therein); the rate of accretion events (Ellison et al. 2010; Adams et al. 2012); and nuclear activity (Kauffmann et al. 2004; Choi et al. 2009; Sabater et al. 2013).

The observed properties of isolated galaxies (galaxies which have not been appreciably affected by their closest neighbours during a past crossing time $t_{cc} = 3$ Gyr Verdes-Montenegro et al. 2005) are likely determined mainly by initial formation conditions and secular evolutionary processes. In this context, isolated galaxies represent the nurture-free zero point for isolating secular processes (Verley et al. 2007c,b). This is the reason why the estimation of the fraction of truly isolated galaxies is a topic of growing interest (Karachentseva 1973; Vettolani et al. 1986; Morgan et al. 1998; Márquez & Moles 1999; Varela et al. 2004; Allam et al. 2005; Elyiv et al. 2009; Karachentsev et al. 2010; Karachentseva et al. 2010b,c,a). Other authors have focused on the study of isolated early-type galaxies (Aars et al. 2001; Colbert et al. 2001; Pisano et al. 2002; Marcum et al. 2004; Niemi et al. 2010; Fuse et al. 2012), and the comparisons of galaxy properties for isolated galaxies and denser environments (Arakelian & Magtesian 1981; Einasto & Einasto 1987; Solomon & Sage 1988; Athanassoula 2003; Coziol et al. 2011; Sabater et al. 2012).

By combining redshift with angular position data, galaxy redshift surveys are essential tools to provide a 3-Dimensional (3D) map of the galaxy distribution. Prada et al. (2003); Melnyk et al. (2009); Hwang & Park (2010); Karachentseva et al. (2011); Tollerud et al. (2011); Edman et al. (2012); Wang & White (2012); Guo et al. (2012, Argudo-Fernández et al. 2013b, submitted) use available spectroscopic data and new 3D techniques in order to identify satellite systems

around isolated galaxies and quantify their effects on galaxy properties.

In a previous work (Argudo-Fernández et al. 2013b, submitted) we describe the 3-dimensional environment for a sample of 386 galaxies from the Catalogue of Isolated Galaxies (CIG, Karachentseva 1973) using the Ninth Data Release of the Sloan Digital Sky Survey (SDSS-DR9). We find that CIG galaxies are distributed following the LSS of the local Universe with a large heterogeneity in their degree of connection with it, from galaxies in interaction with physical satellites to galaxies with no neighbours within 3 Mpc.

Due to the large uncertainty introduced by projection effects in the construction of catalogues of galaxies in relation to their environments, redshift surveys are required for detecting small, faint, interacting satellites from a background projected galaxy population, which leads to a more comprehensive 3D picture of the surroundings. In the present study, we aim to compile and characterise samples of isolated galaxies, isolated pairs, and isolated triplets in the local Universe.

This study is organised as follows: in Sect. 4.2 the data and the isolation criterion used to compile the different samples are presented. The methods to identify the physical systems are described in Sect. 4.3. In Sect. 4.4 we introduce the parameters used to quantify the environment of the galaxies in the catalogues. We present our results in Sect. 4.5 and the associated discussion in Sect. 4.6. Finally a summary and the main conclusions of the study are presented in Sect. 4.7. Throughout the study, a cosmology with $\Omega_{\Lambda 0} = 0.7$, $\Omega_{m0} = 0.3$, and $H_0 = 70 \text{ km s}^{-1} \text{ Mpc}^{-1}$ is assumed.

4.2 Data and definition of the samples

The isolated samples are based on the SDSS-DR9 (Ahn et al. 2012). The primary sample is composed of galaxies from the main spectroscopic sample (Strauss et al. 2002) with model magnitudes in the r -band (the deepest images) $11 \leq m_r \leq 15.7$ (sufficient to develop a homogeneous isolation definition within at least 2 magnitudes fainter, since the redshift completeness of the SDSS is $m_{r,\text{Petrosian}} < 17.77 \text{ mag}$), and with a redshift $0.005 \leq z \leq 0.080$. We discard galaxies with redshift less than 0.005 to avoid an overwhelming search of their neighbourhood, and possible errors in photometry for very extended galaxies. Galaxies with a redshift above 0.080 are also discarded in order to facilitate future studies based on visual morphological classifications.

After compiling a first sample of primary galaxies under these conditions, we proceed to clean the sample following a similar pipeline to previous works (Argudo-Fernández et al. 2013a, b, submitted): (a) we select the galaxies with 1 Mpc radius fields completely encompassed in the photometric SDSS-DR9 footprint, (b) a star-galaxy separation, to reject stars misclassified as galaxies by the automated pipelines of the SDSS, and (c) an automated clean for multiple identifications for the same galaxy.

In order to identify the environment of the primary galaxies, we use the CasJobs¹ tool to search for neighbours, hereafter the neighbour sample, within 1 Mpc around each primary galaxy in the spectroscopic sample of the SDSS, and with redshift between 0.001 and 0.100. A star-galaxy separation and cleaning for multiple identifications are also performed to clean the

¹<http://skyservice.pha.jhu.edu/CasJobs/>

neighbour sample. All galaxies in the primary sample are also found in the neighbour sample.

The SDSS spectroscopic main galaxy sample is supposedly complete in magnitude range $14.5 \lesssim m_r \lesssim 17.7$ (Strauss et al. 2002). To avoid most selection effects related to the redshift incompleteness, we select the primary galaxies where the percentage of extended neighbours (within 1 Mpc in the previously specified magnitude range) with measured redshift is greater than 80%.

The final sample of primary galaxies is composed of 34,127 galaxies, surrounded by 1,599,068 galaxies in the neighbour sample. We use these compiled samples to extract the catalogues of isolated galaxies, isolated pairs and isolated triplets.

We search for galaxies in the primary sample, with zero, one, and two companions in the neighbour sample within radial velocity differences $-500 \leq \Delta v \leq 500 \text{ km s}^{-1}$ and within 1 Mpc from the primary galaxy. Therefore, our isolation criterion is based on a selection in velocity difference-projected distance space.

In order to remove multiple identifications for the same pair and triplet candidates, we choose the unique systems where the brightest galaxy is in the primary sample. This brightest galaxy must have one or two neighbours according to the isolation criteria, if the system is a candidate for isolated pair or isolated triplet, respectively. Under these criteria, we find a total of 4,285 isolated galaxy, 3,892 isolated pair, and 2,692 isolated triplet candidates.

But not all galaxies in the magnitude range $14.5 \lesssim m_r \lesssim 17.7$ are in the SDSS spectroscopic sample. Due to fibre collisions (two fibres of the SDSS spectrograph cannot be placed closer than $55''$, Strauss et al. 2002) close galaxy pairs/mergers cannot be independently identified as two different targets. Therefore, we visually revise the three-colour images of each candidate in the previous samples. We remove 139 isolated galaxy candidates, 95 isolated pair candidates, and 49 isolated triplet candidates.

Out of the 95 pair candidates removed, we identify 45 as isolated galaxy candidates, since the "neighbour" is actually part of the same primary galaxy (i.e., an H II region, or a source missed by our pipeline to clean for multiple identifications, for very extended face-on and edge-on primary galaxies). Similarly, out of the 49 triplet candidates removed, 34 are identified as pair candidates.

The final numbers of isolated system candidates are 4,191 isolated galaxies, 3,831 isolated pairs, and 2,643 isolated triplets.

4.3 Physical definition

By definition, isolated galaxies have not been appreciably affected by their closest neighbours during a past crossing time $t_{\text{cc}} = 3 \text{ Gyr}$ (Verdes-Montenegro et al. 2005). Assuming a typical field velocity dispersion of the order of 190 km s^{-1} (Tonry et al. 2000), it would require about $t_{\text{cc}} \sim 5.2 \text{ Gyr}$ to cross the selected field radius of 1 Mpc. The isolation criterion in this study is more conservative than the original definition. Therefore, the final catalogue of isolated galaxies is composed of the 4,191 entries in the sample of candidates, since we consider that these galaxies have been isolated a large part of their lifetime.

The 2D distribution of Δv and distance d (from the brightest galaxy, hereafter A) for isolated pair and isolated triplet candidates, shows a clear over-density, approximately at $-200 \lesssim \Delta v \lesssim 200 \text{ km s}^{-1}$

and $d \lesssim 500$ kpc (see the upper panel of Fig. 4.1). We consider that neighbour galaxies in these dense regions are more likely connected to their corresponding primary galaxy. The neighbour galaxies at higher Δv and d would be related to the large scale distribution of galaxies.

The middle panel of Fig. 4.1 shows the estimation of the standard deviation σ of the $\Delta v \equiv |v_A - v_N|$ distribution, where v_A and v_N are the line-of-sight velocities of the A galaxy and neighbour N, respectively. The best Gaussian distribution fit gives a value of $\sigma = 85 \text{ km s}^{-1}$. The neighbour galaxies within $\Delta v \leq 2\sigma$ (95.4% of the physically linked companions) show a tendency to be located in the first 450 kpc from the A galaxy (see lower panel of Fig. 4.1). Even in this area, there is another over-density region from 0 to 160 kpc.

We select different Δv and d cut-offs to select the physical isolated systems. Hence, we consider isolated pairs when the faintest galaxy, hereafter B, has $\Delta v \leq 170 \text{ km s}^{-1}$ (2σ) and $d \leq 450$ kpc (shaded outer region in lower panel of Fig. 4.1). In addition, we consider close pairs when the B galaxy has $\Delta v \leq 170 \text{ km s}^{-1}$ (2σ) and $d \leq 160$ kpc (shaded inner region in lower panel of Fig. 4.1). For isolated triplets, we require that the two fainter galaxies, hereafter B and C, should have $\Delta v \leq 170 \text{ km s}^{-1}$ and $d \leq 450$ kpc. Among them, we consider close triplets when both B and C galaxies have $\Delta v \leq 170 \text{ km s}^{-1}$ and $d \leq 160$ kpc.

4.4 Quantification of the environment

We use two parameters to quantify the effect of one-by-one interactions and the large scale environment on galaxy properties: the tidal strength parameter Q (Eq. 4.1) and the projected density η_k (Eq. 4.2).

4.4.1 Tidal strength

The tidal strength parameter Q is an estimation of the gravitational interaction strength that the neighbours produce on the central galaxy with respect to the internal binding forces (Verley et al. 2007b; Sabater et al. 2013, Argudo-Fernández et al. 2013a, in press, Argudo-Fernández et al. 2013b, submitted). The tidal strength on a primary galaxy P created by all the neighbours i in the field is:

$$Q \equiv \log \left(\sum_i \frac{M_i}{M_P} \left(\frac{D_P}{d_i} \right)^3 \right) = \log \left(\sum_i \frac{L_{r_i}}{L_{r_P}} \left(\frac{D_P}{d_i} \right)^3 \right), \quad (4.1)$$

where M is the mass of the galaxy, L_r is the corrected luminosity in the r -band and d_i is the projected physical distance of the i^{th} neighbour to the primary galaxy. $D_P = 2\alpha r_{90}$ is the estimated diameter of the primary galaxy, where r_{90} , the Petrosian radius containing 90% of the total flux of the galaxy in the r -band, is scaled by a factor $\alpha = 1.43$ (Argudo-Fernández et al. 2013a, in press). The greater the value of Q , the less isolated from external influence the primary galaxy.

4.4.2 Projected density

To characterise the LSS around the primary galaxies in our catalogues, we also define the projected number density parameter (Verley et al. 2007b, Argudo-Fernández et al. 2013ab, submit-

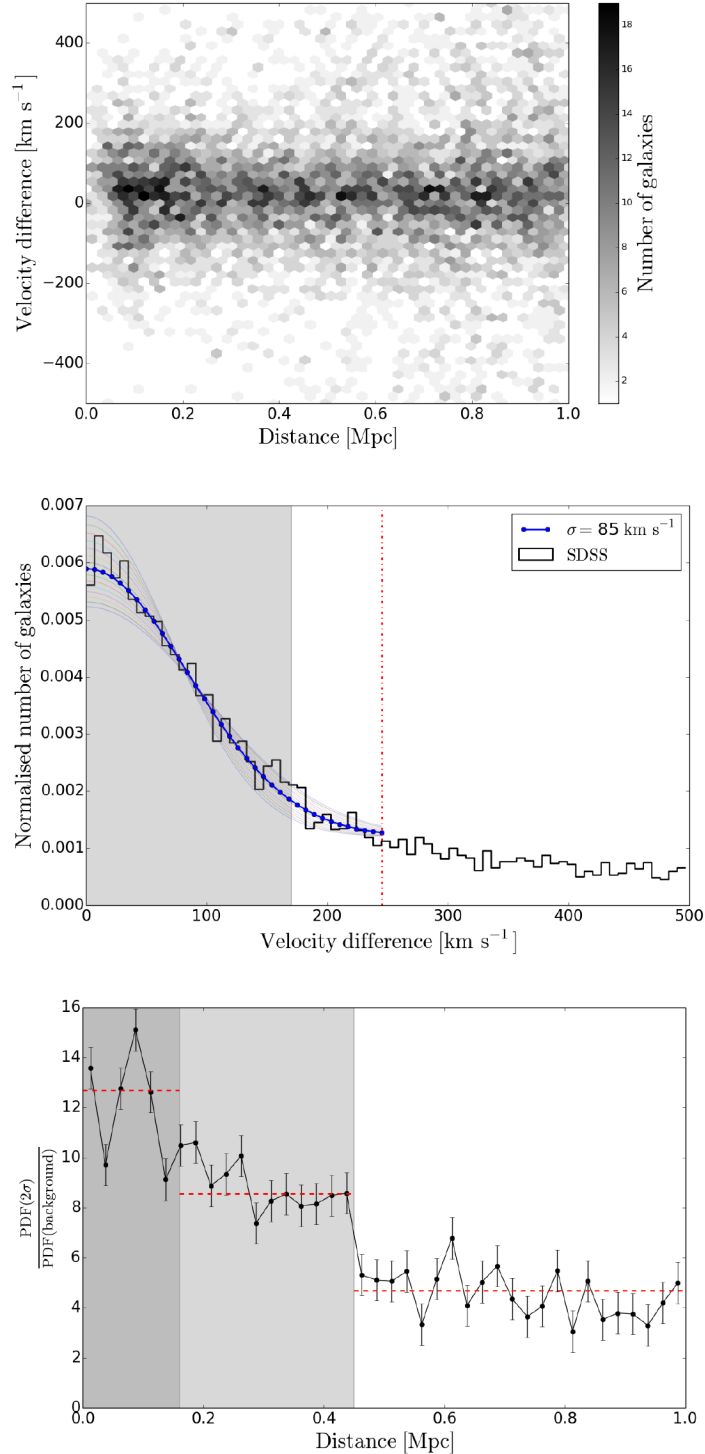


Figure 4.1: Selection of physical pairs and triplets. (*upper panel*): 2D distribution of the line-of-sight velocity difference and projected distance for isolated pair and isolated triplet candidates with respect to the brightest galaxy A. Colours correspond to the galaxy counts according to the colour-bar. (*middle panel*): Absolute values of the line-of-sight velocity difference $\Delta v = |v_A - v_N|$ (black histogram), and the corresponding Gaussian distribution fits for σ between 70 and 100 km s^{-1} (grey curves) with the best fit (blue curve) within the first 250 km s^{-1} (red dashed line). The corresponding 2σ is shaded. (*lower panel*): Probability Density Function (PDF) for neighbour galaxies within 2σ over PDF for the background flat population selected in the interval $300 < \Delta v < 500 \text{ km s}^{-1}$, as a function of the distance to the galaxy A. Red dashed lines correspond to the median values in the different distance intervals. The inner regions up to 160 kpc and 450 kpc are shaded.

ted), as:

$$\eta_{k,\text{LSS}} \equiv \log\left(\frac{k-1}{\text{Vol}(d_k)}\right) = \log\left(\frac{3(k-1)}{4\pi d_k^3}\right), \quad (4.2)$$

where d_k is the projected physical distance to the k^{th} nearest neighbour, with k equal to 5, or less if there were not enough neighbours in the field. The farther the k^{th} nearest neighbour, the smaller the projected number density $\eta_{k,\text{LSS}}$.

4.5 Results

4.5.1 The catalogues

As mentioned in Sect. 4.3, we compile catalogues of isolated galaxies, isolated pairs, and isolated triplets in the local Universe. We identify 4,191 isolated galaxies (see Table 4.1) in the primary catalogue with no neighbours within $\Delta v \leq 500 \text{ km s}^{-1}$ and $d \leq 1 \text{ Mpc}$. This sample represents about 12% of the total number of galaxies in the local Universe ($z \leq 0.080$).

For the final pair and triplet catalogues, we select different Δv and d cut-offs, according to the results shown in Fig. 4.1. The physical isolated systems are selected when $\Delta v \leq 170 \text{ km s}^{-1}$ (2σ) and $d \leq 450 \text{ kpc}$. The close isolated systems are identified when $\Delta v \leq 170 \text{ km s}^{-1}$ (2σ) and $d \leq 160 \text{ kpc}$. We find 1,270 isolated pairs (see Table 4.2), out of them 494 are identified as close pairs; and 300 isolated triplets (see Table 4.3), 45 of them are also classified as close triplets. The sample of isolated pairs and isolated triplets represents about the 7% and 3% of the galaxies in the local Universe, respectively. Meanwhile the close pairs and triplets identified represent about the 3% and 0.4%, respectively.

The distribution of the redshifts for isolated galaxies, isolated pairs and, isolated triplets (see Fig. 4.2) shows that there is not a preferred location.

Figs. 4.3, 4.4, and 4.5 show some examples of galaxies in the catalogue of isolated galaxies, isolated pairs, and isolated triplets, respectively.

For each galaxy in the catalogues, we provide its position, redshift, and quantification of the environment (see Table 4.1, Table 4.2, and Table 4.3). In the catalogue of isolated pairs and isolated triplets, we also identify close pairs and close triplets in the corresponding table.

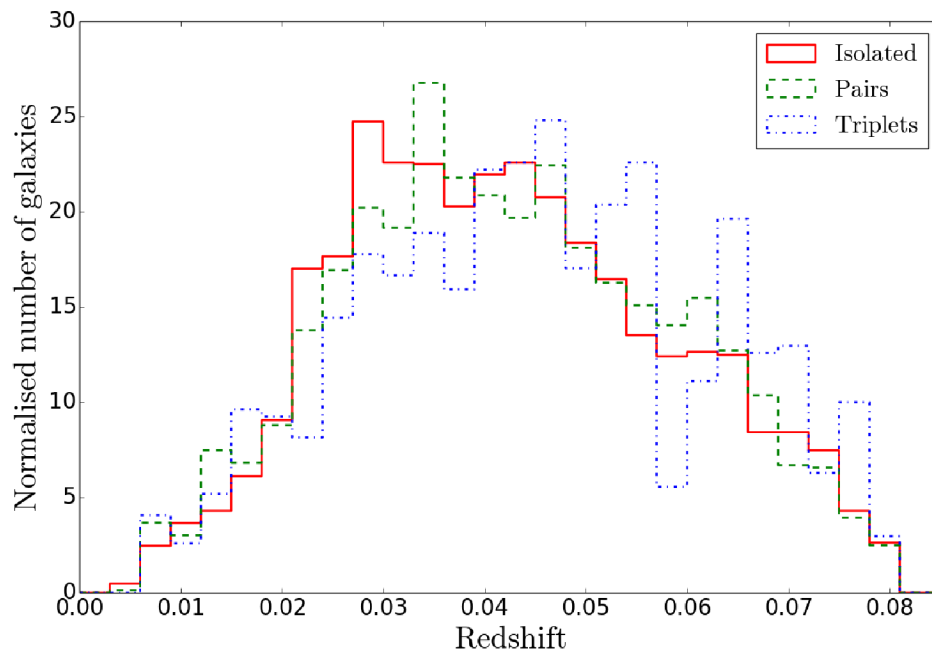


Figure 4.2: Redshift distribution for isolated galaxies (red solid histogram), isolated pairs (green dashed histogram), and isolated triplets (blue dash-dotted histogram).



Figure 4.3: SDSS three-colour images (field of view of $6'.7$, North is up, East is to the left) of twelve isolated galaxies in the SDSS-DR9 footprint.

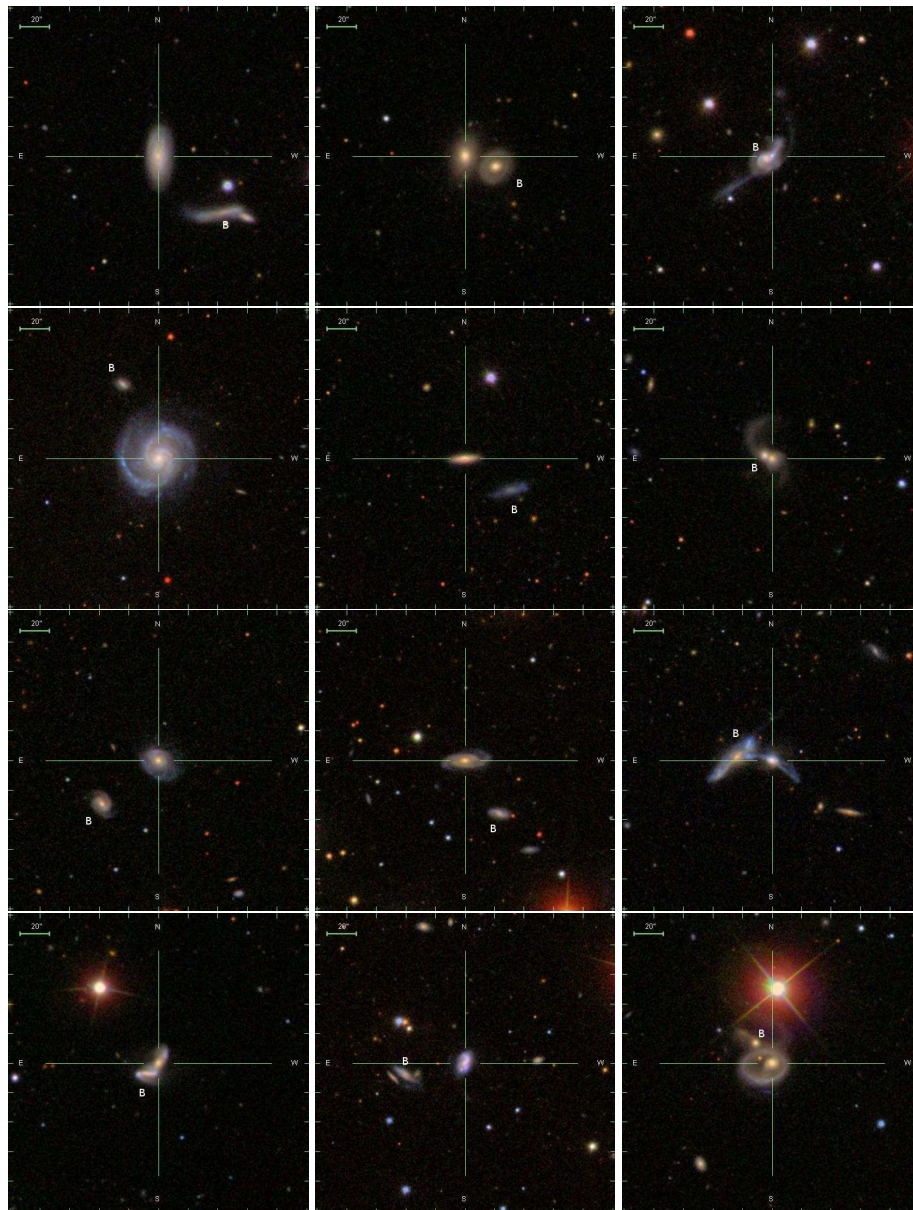


Figure 4.4: SDSS three-colour images (field of view of $3'4$, North is up, East is to the left) of twelve isolated pairs in the SDSS-DR9 footprint. The images are centred on the A galaxy. The B galaxy is labelled.

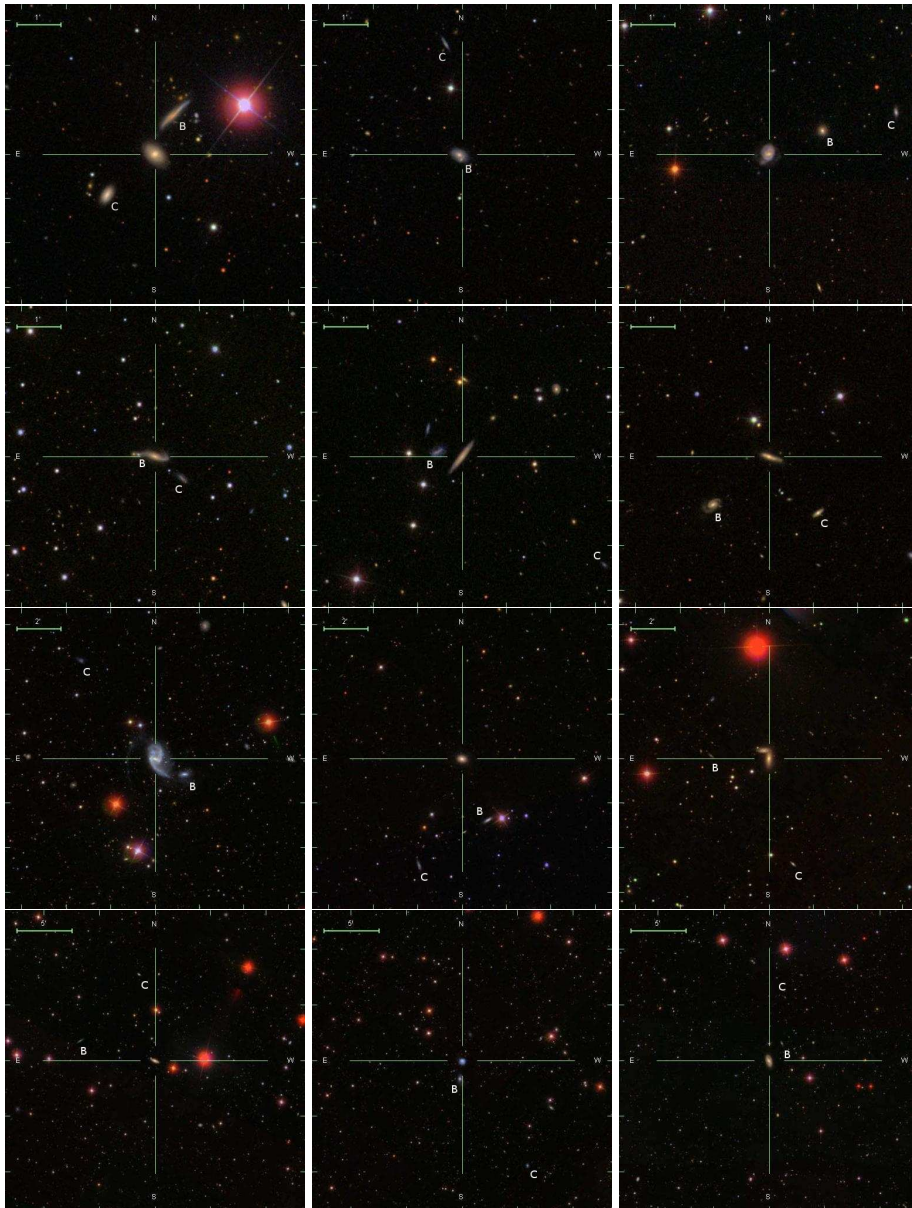


Figure 4.5: SDSS three-colour images (North is up, East is to the left) of twelve isolated triplets in the SDSS-DR9 footprint. The images are centred on the A galaxy. The B and C galaxies are labelled. The field of view of the images in the two upper rows is $6'7''$. The field of view of the images in the third row is $13'5''$. The field of view of the images in the lower rows is $27''$.

Table 4.1: SDSS-based catalogue of 3D isolated galaxies.

(1)	(2)	(3)	(4)	(5)	(6)	(7)	(8)	(9)
SIG	RA (deg)	DEC (deg)	z	k	f_{LSS}	d_{NN} (Mpc)	$\eta_{k,\text{LSS}}$	Q_{LSS}
1	204.00500	49.96092	0.00539	41	1	1.18	-0.63	-5.07
2	139.27202	25.42930	0.00551	21	1	1.23	-0.89	-6.46
3	154.11757	45.32154	0.00552	17	1	1.60	-0.91	-7.55
4	172.10004	9.40762	0.00568	35	1	1.66	-0.75	-5.83
5	187.90240	36.00747	0.00575	7	1	1.83	-1.12	-7.03
6	127.41145	52.07642	0.00585	10	0	2.41	-1.36	-8.02
7	175.10365	28.37389	0.00610	12	1	2.48	-1.40	-7.54
8	213.76544	36.45727	0.00629	22	1	2.50	-1.26	-5.21
9	227.17595	46.90694	0.00643	4	1	2.75	-1.63	-6.81
10	179.95589	21.44875	0.00658	10	1	2.80	-1.46	-5.75
...

Notes. The full table is available in electronic form at <http://amiga.iaa.es> and in CDS. The columns correspond to: (1) isolated galaxy identification; (2) J2000 Right Ascension in degrees; (3) J2000 Declination in degrees; (4) redshift of the galaxy; (5) k_{LSS} , number of LSS associations; (6) f_{LSS} , footprint flag: "1" if the galaxy has 5 Mpc field radius in the SDSS footprint, "0" if not; (7) d_{NN} , distance to the first nearest neighbour from 1 Mpc to 5 Mpc; (8) $\eta_{k,\text{LSS}}$, projected density estimation of the LSS; (9) Q_{LSS} , tidal strength estimation of the LSS.

Table 4.2: SDSS-based catalogue of 3D isolated pair galaxies.

(1)	(2)	(3)	(4)	(5)	(6)	(7)	(8)	(9)	(10)	(11)	(12)	(13)
SIP	index	RA (deg)	DEC (deg)	z	close	k	f_{LSS}	d_{NN} (Mpc)	$\eta_{k,\text{LSS}}$	Q_{LSS}	Q_{pair}	$\frac{Q_{\text{pair}}}{Q_{\text{total}}}$
1	1	135.10054	25.61475	0.00610	0	21	1	1.02	-1.13	-4.94	-4.39	0.78
1	2	134.50259	25.69789	0.00633	0	21	1	1.02	-1.13	-4.94	-4.39	0.78
2	1	175.07710	9.00988	0.00611	1	27	1	1.36	-0.99	-6.39	-3.22	1.00
2	2	174.96983	8.87449	0.00661	1	27	1	1.36	-0.99	-6.39	-3.22	1.00
3	1	238.55118	14.60718	0.00620	1	28	0	1.40	-0.75	-4.48	-2.90	0.97
3	2	238.68779	14.58401	0.00659	1	28	0	1.40	-0.75	-4.48	-2.90	0.97
4	1	169.53523	54.84130	0.00632	0	37	1	1.40	-0.50	-5.43	-6.22	0.14
4	2	170.87070	54.33746	0.00596	0	37	1	1.40	-0.50	-5.43	-6.22	0.14
5	1	182.44710	58.84927	0.00633	1	15	0	1.61	-0.90	-6.10	-3.58	1.00
5	2	182.24469	58.79212	0.00644	1	15	0	1.61	-0.90	-6.10	-3.58	1.00
...

Notes. The full table is available in electronic form at <http://amiga.iaa.es> and in CDS. The columns correspond to: (1) isolated pair identification; (2) index of the galaxy in the pair: "1" for the A galaxy, "2" for the B galaxy; (3) J2000 Right Ascension in degrees; (4) J2000 Declination in degrees; (5) redshift of the galaxy; (6) close pair: "1" if passes, "0" if fails; (7) k_{LSS} , number of LSS associations; (8) f_{LSS} , footprint flag: "1" if the A galaxy has 5 Mpc field radius in the SDSS footprint, "0" if not; (9) d_{NN} , distance from the A galaxy to the first nearest neighbour of the LSS (from 1 Mpc to 5 Mpc); (10) $\eta_{k,\text{LSS}}$, projected density estimation of the LSS; (11) Q_{LSS} , tidal strength estimation of the LSS; (12) Q_{pair} , tidal strength estimation on the A galaxy by the B galaxy; (13) $\frac{Q_{\text{pair}}}{Q_{\text{total}}}$, relation between Q_{pair} and the total tidal strengths on the A galaxy Q_{total} , from 0 to 1 if the isolated system amount from 0% to 100% to the total tidal strength.

Table 4.3: SDSS-based catalogue of 3D isolated triplet galaxies.

(1)	(2)	(3)	(4)	(5)	(6)	(7)	(8)	(9)	(10)	(11)	(12)	(13)
SIT	index	RA (deg)	DEC (deg)	z	close	k	f_{LSS}	d_{NN} (Mpc)	$\eta_{k,\text{LSS}}$	Q_{LSS}	Q_{triplet}	$\frac{Q_{\text{triplet}}}{Q_{\text{total}}}$
1	1	231.52316	9.20416	0.00633	0	25	1	1.04	-0.75	-5.03	-4.72	0.67
1	2	231.93532	9.69909	0.00607	0	25	1	1.04	-0.75	-5.03	-4.72	0.67
1	3	231.73071	9.78265	0.00631	0	25	1	1.04	-0.75	-5.03	-4.72	0.67
2	1	241.44124	41.34474	0.00664	1	4	1	1.73	-1.73	-8.09	-3.09	1.00
2	2	241.31084	41.18844	0.00678	1	4	1	1.73	-1.73	-8.09	-3.09	1.00
2	3	241.42453	41.38444	0.00648	1	4	1	1.73	-1.73	-8.09	-3.09	1.00
3	1	134.77768	53.75822	0.00760	0	6	0	1.78	-1.55	-5.29	-3.73	0.97
3	2	134.07739	54.13844	0.00792	0	6	0	1.78	-1.55	-5.29	-3.73	0.97
3	3	134.28633	53.81630	0.00776	0	6	0	1.78	-1.55	-5.29	-3.73	0.97
4	1	216.90269	41.25766	0.00892	0	20	1	1.81	-0.98	-5.73	-4.72	0.91
4	2	217.39275	40.89153	0.00900	0	20	1	1.81	-0.98	-5.73	-4.72	0.91
4	3	217.39229	40.93399	0.00881	0	20	1	1.81	-0.98	-5.73	-4.72	0.91
...

Notes. The full table is available in electronic form at <http://amiga.iaa.es> and in CDS. The columns correspond to: (1) isolated triplet identification; (2) index of the galaxy in the triplet: "1" for the A galaxy, "2" for the B galaxy, and "3" for the C galaxy; (3) J2000 Right Ascension in degrees; (4) J2000 Declination in degrees; (5) redshift of the galaxy; (6) close triplet: "1" if passes, "0" if fails; (7) k_{LSS} , number of LSS associations; (8) f_{LSS} , footprint flag: "1" if the A galaxy has 5 Mpc field radius in the SDSS footprint, "0" if not; (9) d_{NN} , distance from the A galaxy to the first nearest neighbour of the LSS (from 1 Mpc to 5 Mpc); (10) $\eta_{k,\text{LSS}}$, projected density estimation of the LSS; (11) Q_{LSS} , tidal strength estimation of the LSS; (12) Q_{triplet} , tidal strength estimation on the A by the Band C galaxies; (13) $\frac{Q_{\text{triplet}}}{Q_{\text{total}}}$, relation between Q_{triplet} and the total tidal strengths on the A galaxy Q_{total} , from 0 to 1 if the isolated system amount from 0% to 100% to the total tidal strength.

4.5.2 Relation to the Large Scale Structure

In order to understand the effects of the large scale environment on galaxy properties, we characterise the LSS around each primary galaxy up to 5 Mpc. We consider part of the LSS the neighbour galaxies within $\Delta v \leq 500 \text{ km s}^{-1}$ from 1 to 5 Mpc.

Not all the galaxies in the catalogues have 5 Mpc field radius completely covered by the SDSS footprint. To identify these galaxies, we add the column f_{LSS} with value "1" if the galaxy has 5 Mpc field radius in the SDSS footprint, and "0" if not, in Tables 4.1, 4.2, and 4.3.

There are 3,972 isolated galaxies, 1,205 isolated pairs, and 280 isolated triplets with no flags with respect to the SDSS footprint at 5 Mpc. Out of them, we find 801 isolated galaxies, 217 isolated pairs, and 46 isolated triplets with no neighbours within $\Delta v \leq 500 \text{ km s}^{-1}$ up to 5 Mpc.

The tidal strength engendered by all the galaxies in the LSS is defined as Q_{LSS} . The results of the quantification of the large scale environment for isolated, pair, and triplet galaxies are shown in Fig. 4.6.

For isolated pairs and isolated triplets, the tidal strength produced by galaxies of the same system, in comparison to the tidal strength exerted by galaxies in the LSS, leads to an evaluation of the role of the isolated systems with respect to the large scale environment. Hence, we define Q_{pair} and Q_{triplet} for pairs and triplets respectively, taking into account only the galaxies belonging to the same isolated system (the B galaxy for pairs, and the B and C galaxies in the case of triplets). We also define a Q_{total} which accounts the total amount of tidal strength exerted by galaxies in the pair and triplet, and by the large scale environment. Therefore, the ratios $\frac{Q_{\text{pair}}}{Q_{\text{total}}}$ and $\frac{Q_{\text{triplet}}}{Q_{\text{total}}}$ take values from 0 to 1 if the galaxies of the isolated system amount from 0% to 100% to the total tidal strengths. These ratios for isolated pairs and isolated triplets are tabulated in col. 13 in Table 4.2 and Table 4.3, respectively.

4.5.3 Morphology

According to the well known morphology-density relation (Dressler 1980; Dressler et al. 1997), cluster galaxies are more likely to show earlier morphological types, while field galaxies are more likely to have later morphological types. We aim to check if galaxies in the catalogues of isolated, pair, and triplets galaxies, follow the morphology-density relation.

As a first approximation of the galaxy morphology, we use the Inverse Concentration Index, an indicator of the morphological type defined as $ICI \equiv r_{50}/r_{90}$, where r_{50} and r_{90} are the Petrosian radii containing the 50% and 90% of the total galaxy flux, respectively, in the r -band. According to (Strateva et al. 2001), galaxies with a de Vaucouleurs profile show $ICI \approx 0.3$, while galaxies dominated by an exponential disk show $ICI \approx 0.43$. According to the distributions of the ICI for isolated galaxies, pairs, and triplets (see upper panels in Fig. 4.7) we select a limit value of 0.33 to distinguish between earlier and later types, if $ICI \leq 0.33$ and $ICI > 0.33$, respectively.

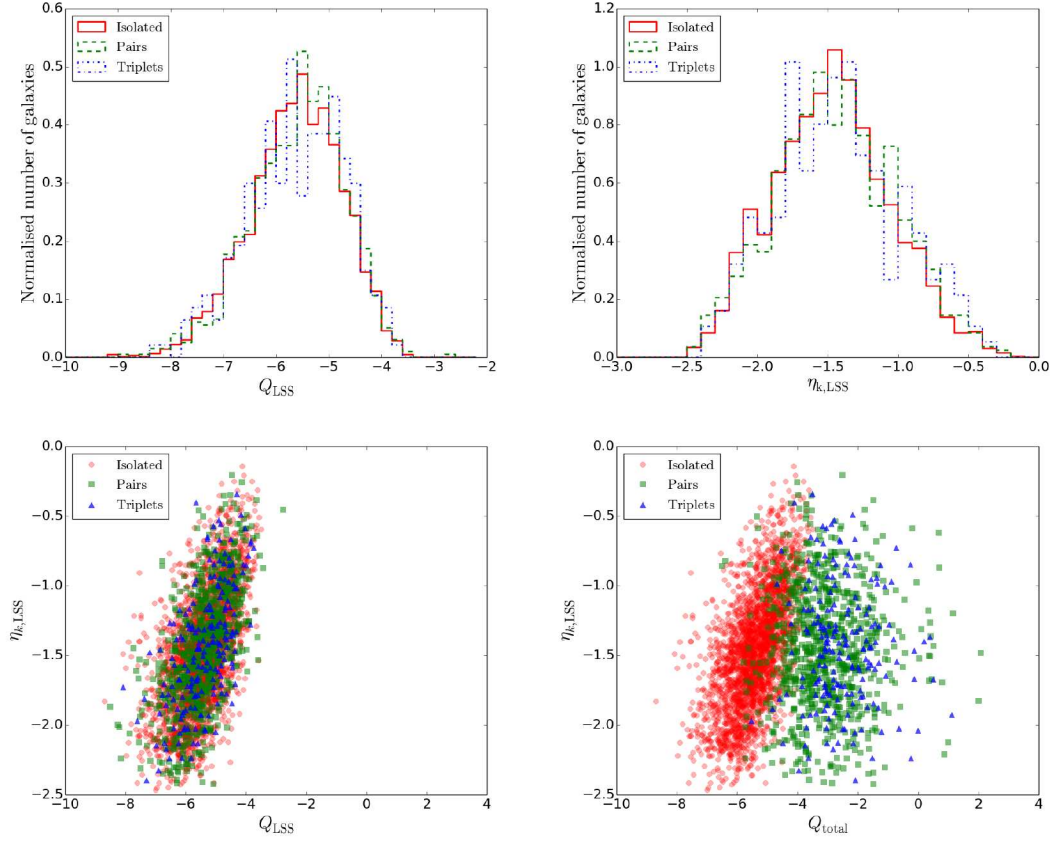


Figure 4.6: LSS isolation parameters for isolated galaxies, isolated pairs, and isolated triplets. (*upper left panel*): Distribution of the tidal strength Q_{LSS} for isolated galaxies (red solid histogram), isolated pairs (green dashed histogram), and isolated triplets (blue dash-dotted histogram). (*upper right panel*): Distribution of the projected density $\eta_{k,LSS}$ in the same colour scheme. (*lower left panel*): Projected density $\eta_{k,LSS}$ versus tidal strength Q_{LSS} diagram. Red circles, green squares, and blue triangles represent isolated galaxies, isolated pairs, and isolated triplets, respectively. (*lower right panel*): Projected density $\eta_{k,LSS}$ versus tidal strength Q_{total} diagram. Red circles, green squares, and blue triangles represent isolated galaxies, isolated pairs, and isolated triplets, respectively.

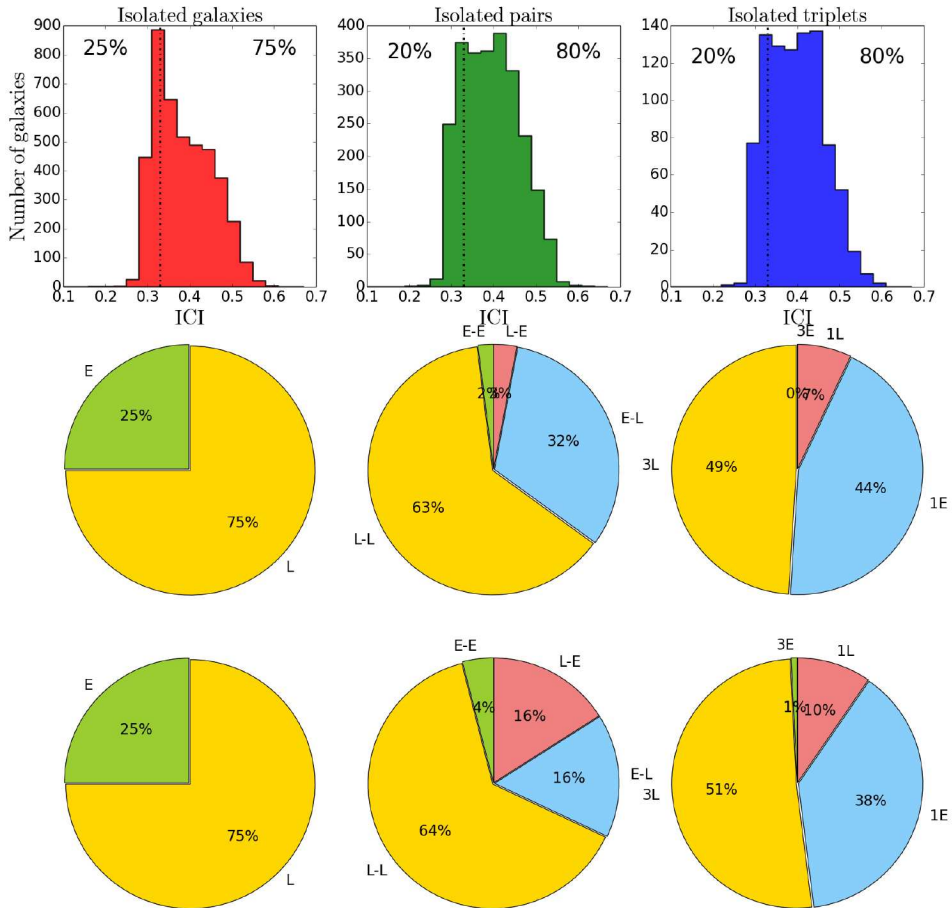


Figure 4.7: Distributions of the ICI for isolated galaxies (upper left panel), isolated pair galaxies (upper central panel), and isolated triplet galaxies (upper right panel). The dashed black line corresponds to the selected value $ICI = 0.33$ to separate between early- and late-type galaxies. The percentages of the morphological types found for isolated galaxies, isolated pairs, and isolated triplets are showed in middle left, middle central, and middle right panels, respectively. The estimated percentages of the morphological types for isolated galaxies (lower left panel), isolated pairs (lower central panel), and isolated triplets (lower right panel) are calculated from their respective distributions in the upper panels.

4.6 Discussion

4.6.1 The catalogues

As shown in Sect. 4.5.1, the catalogues of isolated galaxies, isolated pairs, and isolated triplets have been homogeneously selected using an automated method. The catalogue of isolated galaxies is composed of 4,191 galaxies with no neighbours within $\Delta v \leq 500 \text{ km s}^{-1}$ in a field radius of 1 Mpc. In the case of pairs and triplets, we identify 1,270 isolated pairs and 300 isolated triplets, with no neighbours within $\Delta v \leq 500 \text{ km s}^{-1}$ in a field radius of 1 Mpc.

In the upper and middle panels in Fig. 4.8, we show the mass ratio for galaxies in the isolated pairs and triplets catalogues. Stellar masses are calculated by fitting the spectral energy distribution, on the five SDSS bands, using the routine `kcorrect` (Blanton & Roweis 2007). The mass ratio for close and loose pairs presents similar trends. In isolated pairs, the mass of the B galaxy is typically 1/10 of the mass of the A galaxy. This means that isolated pairs usually show a hierarchical structure, therefore it is less probable to find a pair with two similar mass galaxies. Nevertheless we find clear differences for close triplets. The mass ratio of the A and C galaxies is much smaller (1/100) in comparison to the A and B galaxy. This result is also visible in some of the examples in Fig. 4.5, the C galaxy is usually very much smaller than the A and B galaxies, presenting also a hierarchical structure.

4.6.2 Relation with the Large Scale Structure

As introduced in Sect. 4.4, we use the projected density $\eta_{k,\text{LSS}}$ and tidal strength Q_{LSS} to quantify the large scale environment for isolated galaxies, isolated pairs, and isolated triplets.

The upper panels in Fig. 4.6 show that there is no difference in their relation with the LSS. This means that the isolated galaxies are as isolated, with respect to the large scale environment, as isolated pairs and triplets. This may suggest that they have a common origin in their formation and evolution.

When taking into account the physical associations of the galaxies in pairs (B) and triplets (B,C), which define the tidal strengths Q_{pair} and Q_{triplet} , respectively, their effects largely dominate (about 99.9%) the tidal strengths generated by the LSS (see also lower panel in Fig. 4.8). The tidal strengths Q_{pair} and Q_{triplet} are two orders of magnitude higher than the Q_{LSS} (see the lower right panel in Fig. 4.6).

We find a significant number of galaxies with no neighbours within $\Delta v \leq 500 \text{ km s}^{-1}$ up to 5 Mpc. One can expect that these galaxies would be located in voids. The smallest identifiable voids in the local Universe having radii $\sim 7 h^{-1} \text{ Mpc}$ (Tikhonov & Karachentsev 2006), with voids usually having characteristic radii of 10-40 $h^{-1} \text{ Mpc}$ (Sutter et al. 2012). Nevertheless, Fig. 4.9 and Fig. 4.10 show that in general, most of the isolated galaxies, isolated pairs, and isolated triplets, belong to the outer parts of filaments, walls, and clusters, and generally differ from the void population of galaxies.

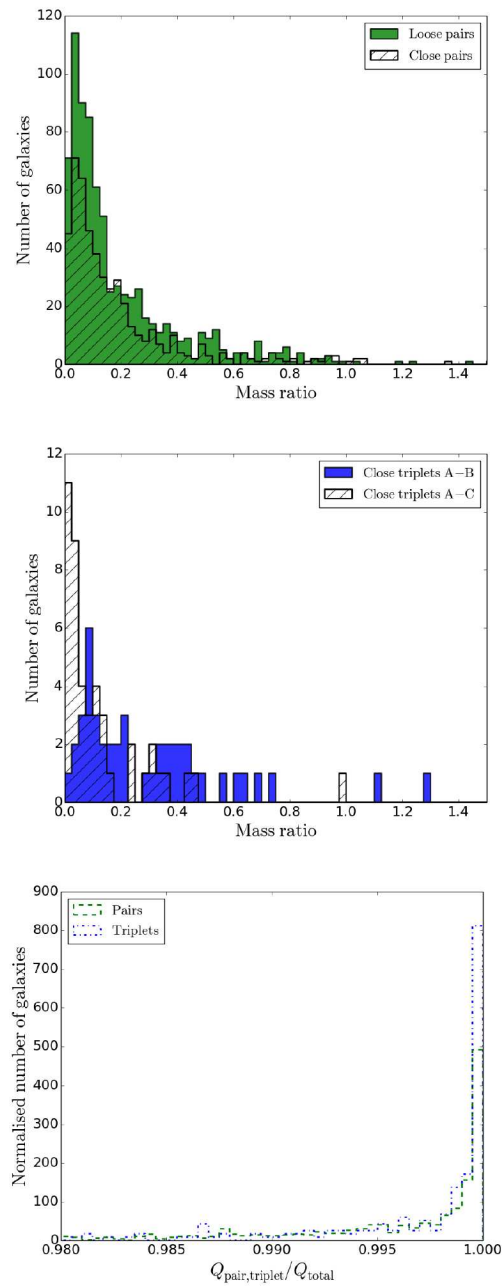


Figure 4.8: (*upper panel*): Distribution of the mass ratio between the A galaxy and the B galaxy in loose pairs (green filled histogram) and close pairs (black hatched histogram). (*middle panel*): Distribution of the mass ratio between the A and B galaxies (blue filled histogram), and between A and C galaxies (black hatched histogram) in close triplets. (*lower panel*): Distribution of the ratios $\frac{Q_{\text{pair}}}{Q_{\text{total}}}$ (green dashed histogram) and $\frac{Q_{\text{triplet}}}{Q_{\text{total}}}$ (blue dash-dotted histogram) for isolated pairs and isolated triplets, respectively.

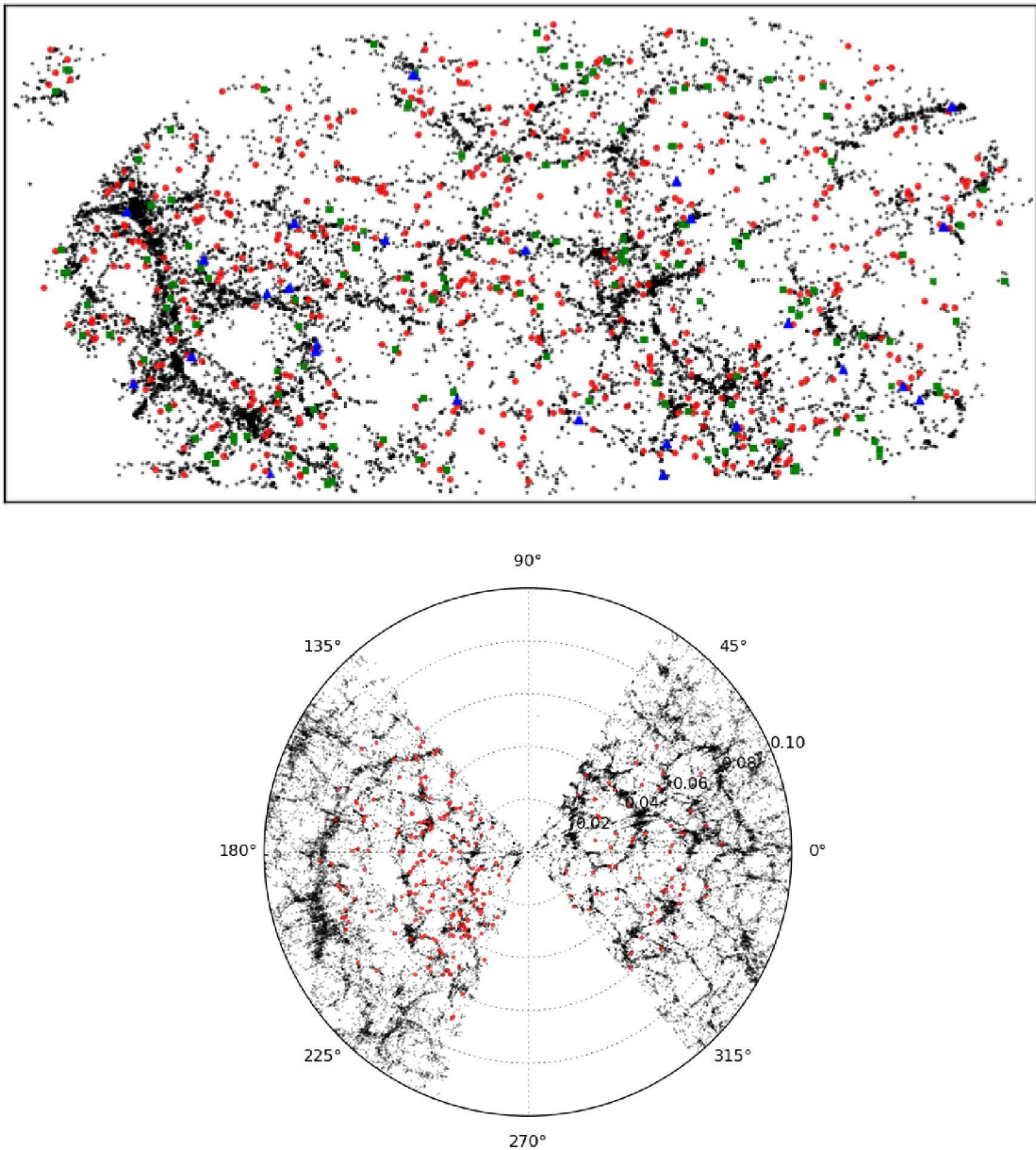


Figure 4.9: Distribution of isolated systems in the LSS (1). (*upper panel*): equidistant cylindrical projection of the LSS for galaxies in the redshift range $0.030 < z < 0.035$ (declination between -5 and 71 degrees, right ascension between 109 and 267 degrees, North is up, East is to the left). Red circles, green squares, and blue triangles represent isolated galaxies, isolated pairs, and isolated triplets, respectively. (*lower panel*): Pie chart projection of the LSS for galaxies within -2 and 2 degrees in declination. The over-plotted red circles represent isolated galaxies within the same declination range.

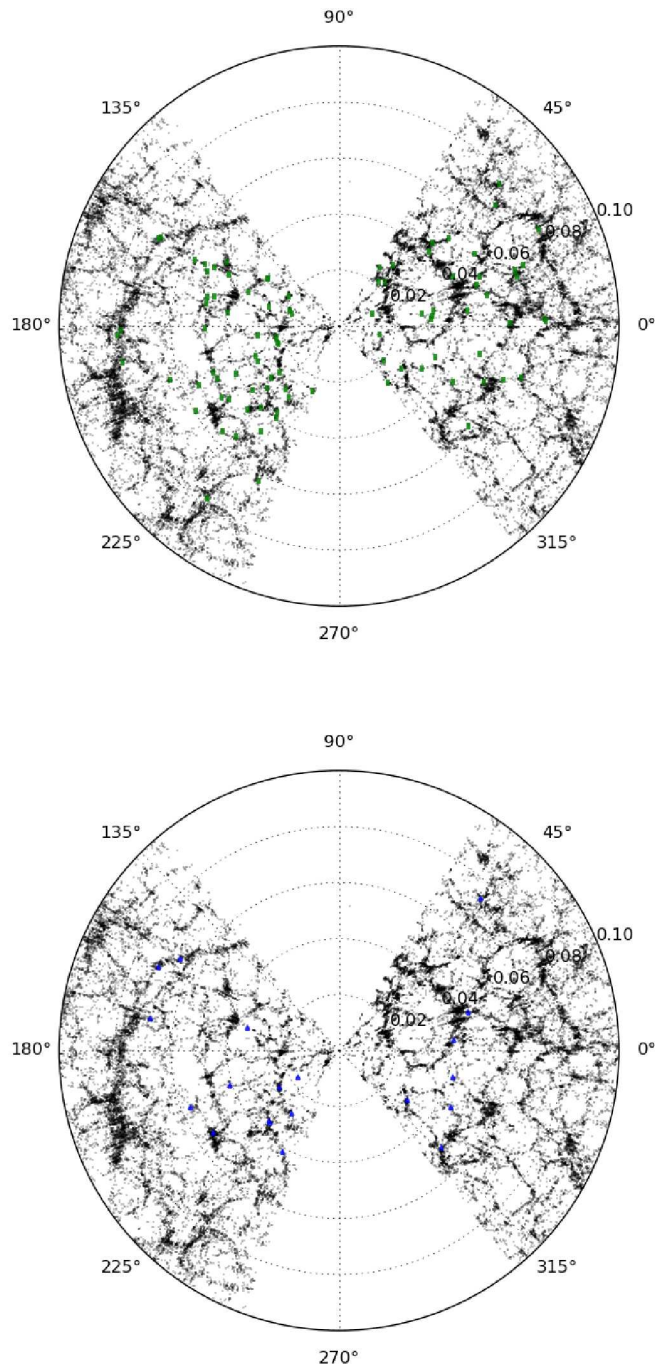


Figure 4.10: Distribution of isolated systems in the LSS (2). Same as the lower panel in Fig. 4.9 but for isolated pairs (green squares in the upper panel) and isolated triplets (blue triangles in the lower panel).

4.6.3 Euclidean Minimum Spanning Tree

Hierarchical clustering is a simple data mining technique which can examine the clustering at many different scales (March et al. 2010). The most common measure of similarity between clusters is when computing the single-linkage clustering turns out to be equivalent to the minimum Euclidean distance, finding the Euclidean Minimum Spanning Tree (MST), where the weight of the edge between each pair of points is the distance between them.

In order to connect isolated, pair and triplet galaxies with the Large Scale Structure, we compare their positions with respect to the MST of galaxies in the local Universe from the SDSS. To compute the hierarchical clustering of SDSS galaxies we use AstroML² (Vanderplas et al. 2012; Ivezić et al. 2013) Python module for machine learning and data mining.

Upper panel in Fig. 4.11 shows the hierarchical clustering of 34,274 galaxies from the SDSS within -1.25 and 1.25 degrees in declination, similar to Fig. 1.1, where the "SDSS Great Wall" (Gott et al. 2005) is visible in the northern Galactic cap. We can measure the amount of clustering at one determined scale by eliminating edges of a MST which are greater than a given length, therefore the results of this clustering approach for an edge cutoff of 2.9 Mpc are showed in lower left panel in Fig. 4.11. In Fig. 4.12 is shown that, in general, isolated galaxies are following the large structures, mainly distributed along filaments bordering superclusters. Isolated pairs and triplets tend to be located also following the LSS, but gradually in smaller large structures.

4.6.4 Morphology

The early- and late-type galaxies respectively account for 25% and 75% of the sample of isolated galaxies. In the samples of pair and triplet galaxies, these early and late-types represent, respectively, 20% and 80% of the galaxies. In order to see if some systems or some galaxy segregations are favoured by the formation or evolution of these isolated systems, we estimate what should be the expected numbers of randomly created early-type, late-type, and mixed-systems.

Starting from the percentages of early- and late-type galaxies in the original isolated pair sample, we can expect that about 64% of the pairs should be constituted by two late-type galaxies (L-L, see the lower central panel of Fig. 4.7), while only 4% should be early- early-type pairs (E-E). The expected percentage of randomly obtained mixed pairs (E-L or L-E) formed should consequently be 32%. If the formation and evolution of the isolated pairs favour some combinations of morphological types, the percentages of early-early, late-late, and mixed pairs in our observed sample should differ from the randomly expected ones. In the central middle panel of Fig. 4.7, it appears that the observed pairs display morphological type combinations which follow the percentages obtained for random combinations. This means that the formation or evolution of pairs do not segregate between the different morphological types, at least considering the sample of pairs as a whole.

The same conclusions are reached for the triplets (see the right column of Fig. 4.7) where the observed triplets and the randomly created ones are present in the same proportions.

²<http://www.astroml.org/>

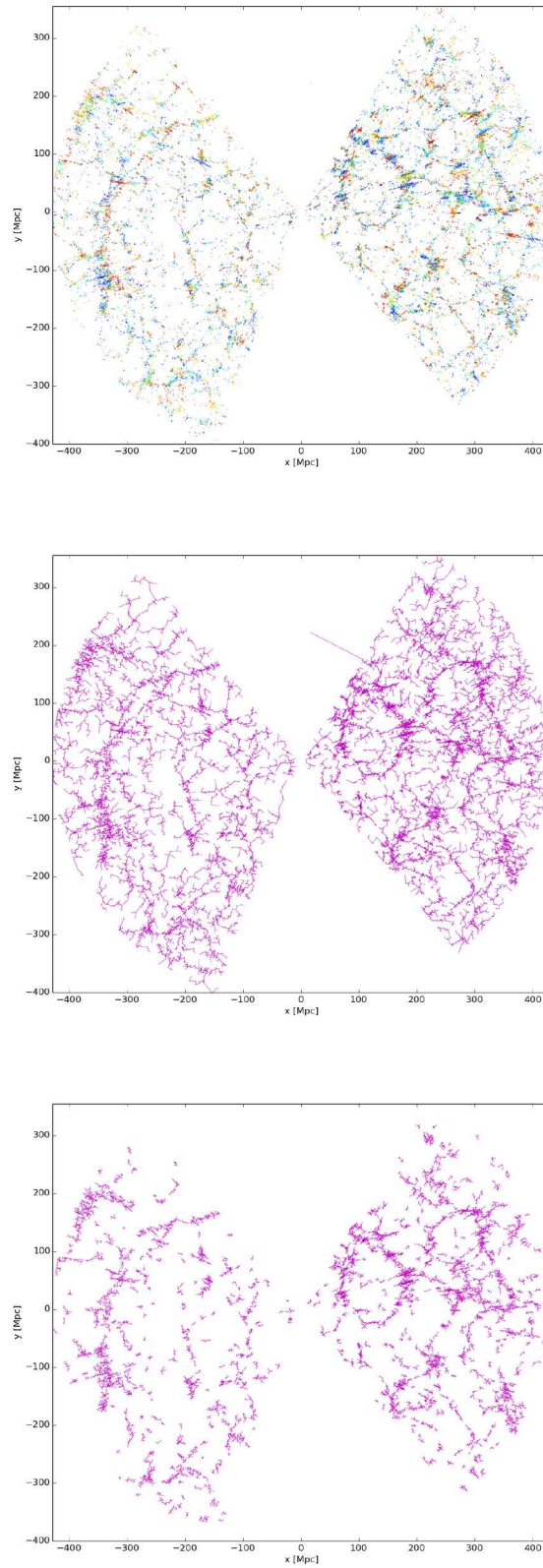


Figure 4.11: Computed MST for galaxies in the SDSS within -1.25 and 1.25 degrees in declination. (*upper panel*): 3-Dimensional map of the galaxy distribution of 34,274 galaxies from the SDSS. (*middle panel*): Result of the computed MST. (*lower panel*): Clustering approach of the computed MST.

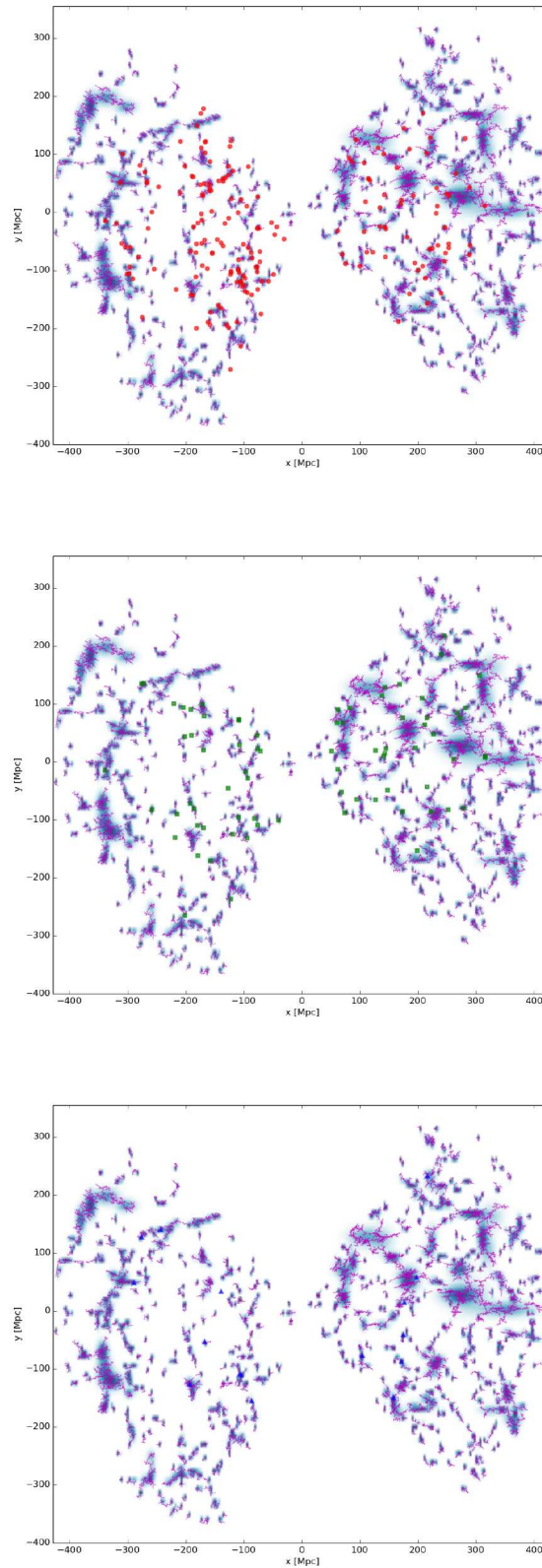


Figure 4.12: Isolated galaxies, isolated pairs and isolated triplets with respect to the computed MST for galaxies in the SDSS within -1.25 and 1.25 degrees in declination. (*upper panel*): Position of 188 isolated galaxies (red circles), within -1.25 and 1.25 degrees in declination, with respect to the clustering approach, along with a Gaussian Mixture Model fit showing high-density regions. (*middle panel*): Identical but for 76 isolated pairs (green squares). (*lower panel*): Identical but for 16 isolated triplets (blue triangles).

4.7 Summary and conclusions

We present catalogues of isolated galaxies, isolated pairs, and isolated triplets in the local Universe ($z \leq 0.08$ and $m_r \leq 15.7$ mag), automatically and homogeneously selected using the Ninth Data Release of the Sloan Digital Sky Survey (SDSS-DR9). The systems are isolated without neighbours within $\Delta v \leq 500 \text{ km s}^{-1}$ in a field radius of 1 Mpc. All the objects in the three final catalogues were visually inspected.

The relations of the isolated galaxies, isolated pairs, and isolated triplets with the Large Scale Structure (LSS) are characterised using the projected density $\eta_{k,\text{LSS}}$ and the tidal strength Q_{LSS} produced by the neighbours within $\Delta v \leq 500 \text{ km s}^{-1}$ up to 5 Mpc.

Our main conclusions are the following:

1. The catalogue of isolated galaxies is composed of 4,191 galaxies with no neighbours within $\Delta v \leq 500 \text{ km s}^{-1}$ in a field radius of 1 Mpc. The sample represents about the 12% of the total number of considered galaxies in the local Universe ($z \leq 0.080$ and $m_r \leq 15.7$ mag).
2. The catalogue of isolated pairs is constituted by 1,270 pairs, selected using the requirement that the faintest galaxy should be within $\Delta v \leq 170 \text{ km s}^{-1}$ and lie at a distance $d \leq 450 \text{ kpc}$ with respect to the brightest one. Of these, 494 pairs are identified as close pairs ($d \leq 160 \text{ kpc}$). The sample of isolated pairs represents about the 7% of the total number of considered galaxies in the local Universe ($z \leq 0.080$ and $m_r \leq 15.7$ mag).
3. Similarly, the catalogue of isolated triplets consists of 300 triplets, selected under the condition that the two faintest galaxies should be within $\Delta v \leq 170 \text{ km s}^{-1}$ and lie within $d \leq 450 \text{ kpc}$ from the brightest galaxy. Of them, 45 triplets are identified as close triplets (the two faintest galaxies should fulfill $d \leq 160 \text{ kpc}$). The sample of isolated triplets represents about the 3% of the total number of considered galaxies in the local Universe ($z \leq 0.080$ and $m_r \leq 15.7$ mag).
4. We find 801 isolated galaxies, 217 isolated pairs, and 46 isolated triplets, without neighbours within $\Delta v \leq 500 \text{ km s}^{-1}$ up to 5 Mpc. For the remaining primary galaxies in the three samples, we define the projected density $\eta_{k,\text{LSS}}$ and the tidal strength Q_{LSS} to quantify their large scale environment.
5. Most of the isolated galaxies, isolated pairs, and isolated triplets, belong to the outer parts of filaments, walls, and clusters, and generally differ from the void population of galaxies. We find no difference in their degree of interaction with the LSS, which may suggest that they have a common origin in their formation and evolution.
6. The physical companions in pairs and triplets play a prevailing role in the tidal strengths Q_{pair} and Q_{triplet} exerted on the primary galaxies. This local tidal strength due to the physical companions is two orders of magnitude higher than the tidal strength due to the LSS.

7. We provide catalogues of isolated galaxies, isolated pairs, and isolated triplets, with their positions, redshifts, and degrees of relation with their physical and LSS environments. The catalogues are publicly available to the scientific community.

Chapter 5

Conclusions

To understand the evolution of galaxies, it is necessary to have a reference sample where the effects of the environment are minimised and quantified. To identify and quantify the external influences which may play a role in the galaxy formation and evolution, we study the effects of the local and large scale environments in isolated galaxies.

In a first step, we carry out a revision of the isolation degree for a sample of galaxies in the Catalogue of Isolated Galaxies (CIG; [Karachentseva 1973](#)), which is the historically most significant sample of isolated galaxies in the local Universe. For the first time, the environment and the isolation degree of CIG galaxies are quantified using photometric and spectroscopic digital data from the SDSS. The use of the SDSS database provides linear photometry, improved sensitivity, and better spatial resolution than digitised photographic plates. Therefore we are able to identify faint companions that were not found in previous revisions of the CIG ([Verley et al. 2007c](#)). The availability of the spectroscopic data allows us to check the validity of the CIG isolation criterion within a field radius of 1 Mpc, and we conclude that it is not fully efficient. About 50% of the neighbours considered as potential companions in the photometric study are in fact background objects. On the other hand, we also find that about 92% of neighbour galaxies that show recession velocities similar to the corresponding CIG galaxy are not considered by the CIG isolation criterion as potential companions. These neighbours are most likely dwarf systems, with $D_i < 0.25 D_p$, and may have a considerable influence on the evolution of the central CIG galaxy.

In light of these results, we perform a detailed study of the 3-dimensional environment of the CIG galaxies using spectroscopic data from the SDSS, identifying and quantifying the effects of the satellite distribution, as well as the effects of the Large Scale Structure (LSS). We find that the CIG galaxies are distributed following the LSS of the local Universe, although presenting a large heterogeneity in their degree of connection with it, from galaxies in interaction with physical satellites to galaxies without neighbours in the first 3 Mpc around them. A clear segregation appears between early-type CIG galaxies in interaction and isolated late-type CIG galaxies. Isolated galaxies are in general bluer, with likely younger stellar populations and rather high star formation rates with respect to older, redder interacting CIG galaxies. Reciprocally, the satellites are redder and with older stellar populations around massive early-type CIG galaxies, while they have a younger stellar content around massive late-type CIG galaxies. This suggests

that the CIG is composed of a heterogeneous population of galaxies, sampling from old systems of galaxies to more recent, dynamical systems of galaxies. Interacting CIG galaxies might have a mild tendency (0.3-0.4 dex) to be more massive, which may indicate a higher frequency of having suffered a merger in the past.

According to the performed work on the CIG, we conclude that in the construction of catalogues of galaxies in relation to their environments (isolated, pairs, and triplets of galaxies), redshift surveys are required in order to distinguish small, faint, interacting satellites from a background projected galaxy population, so as to reach a more comprehensive 3-dimensional picture of the surroundings. Hence, in the last part of this thesis, we use spectroscopic data from the SDSS to automatically and homogeneously compile catalogues of 4,191 isolated galaxies, 1,270 isolated pairs, and 300 isolated triplets in the local Universe ($z \leq 0.080$) without being biased by projected neighbours. The physical companions in the pair and triplet samples usually account for more than 98% of the total tidal strength affecting the central galaxy. Most of the isolated galaxies, isolated pairs, and isolated triplets, belong to the outer parts of filaments, walls, and clusters, and generally differ from the void population of galaxies. We find no difference in their degree of interaction with the LSS, which may suggest that they have a common origin in their formation and evolution.

Appendix A

Interactive 3D visualisation software

Contents

A.1 Interactive 3D visualisation software: pie chart	108
A.2 Interactive 3D visualisation software: Mollweide projection	110

A.1 Interactive 3D visualisation software: pie chart

This visualisation software, exclusively based on free software, has been developed in collaboration with S. Duarte Puertas and E. Ramos Carmona.

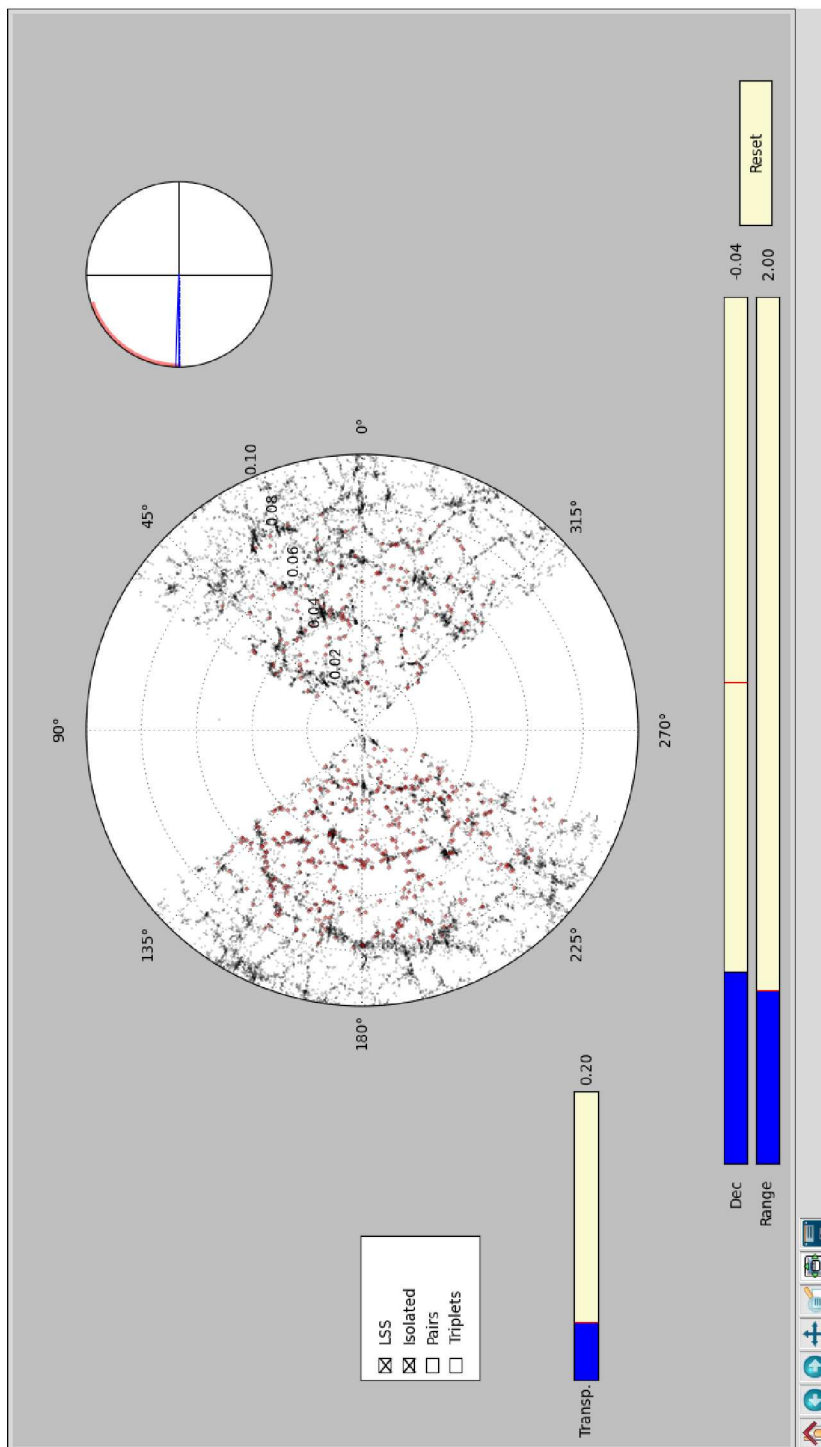


Figure A.1: Interactive 3D visualization software: pie chart

A.2 Interactive 3D visualisation software: Mollweide projection

This visualisation software, exclusively based on free software, has been developed in collaboration with S. Duarte Puertas and E. Ramos Carmona.

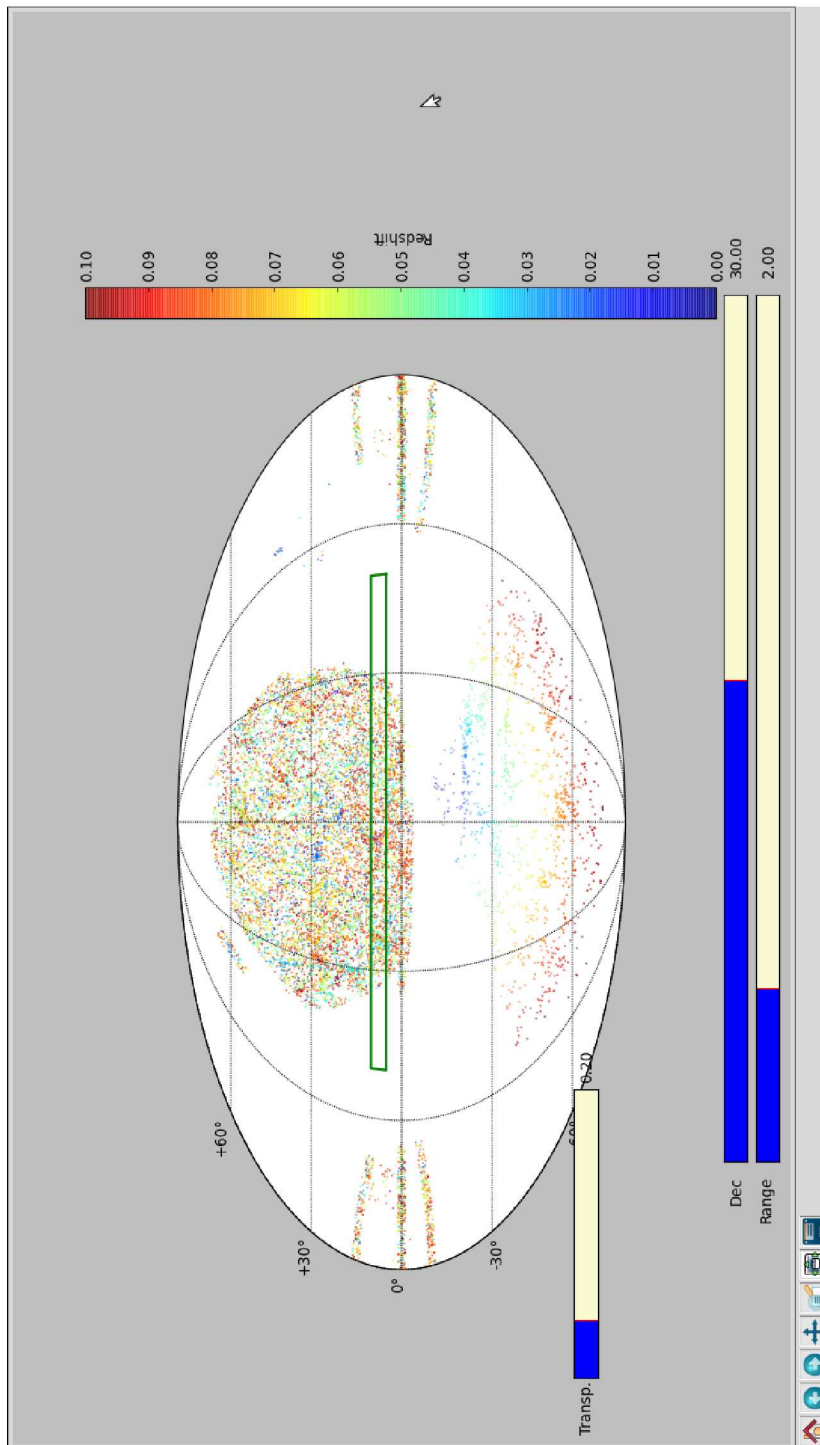


Figure A.2: Interactive 3D visualisation software: Mollweide projection

Appendix B

Collaborations

Contents

B.1	Effect of the interactions and environment on nuclear activity	114
B.2	The stellar mass-size relation for the most isolated galaxies in the local Universe	116
B.3	Highly perturbed molecular gas in the Abell 1367 ram pressure stripping spiral archetype CGCG 97-079	118

B.1 Effect of the interactions and environment on nuclear activity

In this collaboration I have provided helpful methods used in the pipeline to extract SDSS information, as well as the correction for SDSS diameters calculated in the present study has been used in the paper.



Effect of the interactions and environment on nuclear activity

J. Sabater,^{1,2*} P. N. Best¹ and M. Argudo-Fernández²

¹*Institute for Astronomy (IfA), University of Edinburgh, Royal Observatory, Blackford Hill, Edinburgh EH9 3HJ, UK*

²*Instituto de Astrofísica de Andalucía, CSIC, Apdo. 3004, E-18080 Granada, Spain*

Accepted 2012 December 18. Received 2012 December 18; in original form 2012 November 12

ABSTRACT

We present a study of the prevalence of optical and radio nuclear activity with respect to the environment and interactions in a sample of the Sloan Digital Sky Survey (SDSS) galaxies. The aim is to determine the independent effects of distinct aspects of source environment on the triggering of different types of nuclear activity. We defined a local density parameter and a tidal force estimator and used a cluster richness estimator from the literature to trace different aspects of environment and interaction. The possible correlations between the environmental parameters were removed using a principal component analysis. By far, the strongest trend found for the active galactic nuclei (AGN) fractions, of all AGN types, is with galaxy mass. We therefore applied a stratified statistical method that takes into account the effect of possible confounding factors like the galaxy mass. We found that (at fixed mass) the prevalence of optical AGN is a factor of 2–3 lower in the densest environments, but increases by a factor of ~ 2 in the presence of strong one-on-one interactions. These effects are even more pronounced for star-forming nuclei. The importance of galaxy interactions decreases from star-forming nuclei to Seyferts to low-ionization nuclear emission-line regions to passive galaxies, in accordance with previous suggestions of an evolutionary time-sequence. The fraction of radio AGN increases very strongly (by nearly an order of magnitude) towards denser environments, and is also enhanced by galaxy interactions. Overall, the results agree with a scenario in which the mechanisms of accretion into the black hole are determined by the presence and nature of a supply of gas, which in turn is controlled by the local density of galaxies and their interactions. A plentiful cold gas supply is required to trigger star formation, optical AGN and radiatively efficient radio AGN. This is less common in the cold-gas-poor environments of groups and clusters, but is enhanced by one-on-one interactions which result in the flow of gas into nuclear regions; these two factors compete against each other. In the denser environments where cold gas is rare, cooling hot gas can supply the nucleus at a sufficient rate to fuel low-luminosity radiatively inefficient radio AGN. However, the increased prevalence of these AGN in interacting galaxies suggests that this is not the only mechanism by which radiatively inefficient AGN can be triggered.

Key words: catalogues – galaxies: active – galaxies: evolution – galaxies: interactions – radio continuum: galaxies.

1 INTRODUCTION

Active galactic nuclei (AGN) are closely related to galaxy formation and evolution. The black holes that power AGN are found in all massive galaxies and their masses are tightly correlated with both the masses and the velocity dispersions of the stellar bulges (e.g. Ferrarese & Merritt 2000; Gebhardt et al. 2000; Marconi & Hunt 2003). AGN may play an important role in the feedback mechanisms

that control the growth of massive galaxies (see review by Cattaneo et al. 2009, and references therein). Interaction between galaxies can drive gas into the central region of the galaxy and trigger the AGN (Shlosman, Begelman & Frank 1990; Barnes & Hernquist 1991; Haan et al. 2009; Liu et al. 2011). However, a high fraction of AGN may be fuelled by secular processes (e.g. Silverman et al. 2011; Sabater et al. 2012).

The effect of the large-scale environment and of galaxy interactions on the triggering of an AGN has previously been studied by many authors, but contradictory results have been found. Quasars are thought to be associated with galaxy interactions (Sanders et al.

* E-mail: jsm@roe.ac.uk

B.2 The stellar mass-size relation for the most isolated galaxies in the local Universe

In this collaboration I have quantified the local environment for the AMIGA galaxies in the study and for galaxies in the catalogue of [Nair & Abraham \(2010\)](#). The identification of close similar redshift companions, up to three magnitude fainter, has been provided for both samples in order to check the stellar mass-size relation in function of the number of satellites.

The stellar mass–size relation for the most isolated galaxies in the local Universe[★]

M. Fernández Lorenzo,[†] J. Sulentic, L. Verdes-Montenegro
and M. Argudo-Fernández

Instituto de Astrofísica de Andalucía, Granada, IAA-CSIC Apdo. 3004, E-18080 Granada, Spain

Accepted 2013 June 6. Received 2013 May 6; in original form 2013 February 27

ABSTRACT

Disentangling processes governing the formation and evolution of galaxies is a fundamental challenge in extragalactic research. In this sense, the current belief that galaxies grow by the action of minor mergers makes the study of the stellar mass–size relation in different environments an important tool for distinguishing effects of internal and external processes. The aim of this work is to study the effects of environment on the growth in size of galaxies. As part of Analysis of the Interstellar Medium of Isolated GALaxies (AMIGA project), we examine the stellar mass–size relation for a sample of the most isolated galaxies in the local Universe interpreted as stellar systems where evolution has been mainly governed by internal processes. Effects of environment on the stellar mass–size relation are evaluated by comparing our results with samples of less isolated early- and late-type galaxies, as well as, for the first time, different spiral subtypes. Stellar masses in our sample were derived by fitting the SED of each galaxy with `KCORRECT`. We used two different size estimators, the half-light radius obtained with `SEXTRACTOR` and the effective radius calculated by fitting a Sérsic profile to the *i*-band image of each galaxy using `GALFIT`. We found good agreement between those size estimators when the Sérsic index fell in the range $2.5 < n < 4.5$ and $0.5 < n < 2.5$ for (visually classified) early- and late-type galaxies, respectively. We find no difference in the stellar mass–size relation for very isolated and less isolated early-type galaxies. We find that late-type isolated galaxies are ~ 1.2 times larger than less isolated objects with similar mass. Isolated galaxies and comparison samples were divided into six morphological ranges (E/S0, Spirals, Sb, Sbc, Sc and Scd–Sdm) and five stellar mass bins between $\log(M_*) = [9, 11.5]$. In all cases, the relation is better defined and has less scatter for the isolated galaxies. We find that as the morphological type becomes later the galaxy size (for a fixed stellar mass range) becomes larger. For the lowest stellar mass bins $\log(M_*) = [9, 10]$, we find good agreement between sizes of AMIGA and comparison spirals (both mostly composed of Scd–Sdm types). The isolated spiral galaxies in the high stellar mass bins $\log(M_*) = [10, 11]$ tend to be larger than less isolated galaxies. This difference in size is found for all spiral subtypes and becomes larger when we compare fully isolated galaxies with galaxies having two or more satellites (neighbours within 3 mag of difference at a distance less than 250 kpc from the galaxy). Our results suggest that massive spiral galaxies located in low-density environments, both in terms of major companions and satellites, have larger sizes than samples of less isolated galaxies. Hence, the environment has played a role in the growth in size of massive spiral galaxies.

Key words: galaxies: evolution – galaxies: fundamental parameters – galaxies: general – galaxies: interactions.

[★]Full Table 1 is only available in electronic form at the CDS via anonymous ftp to cdsarc.u-strasbg.fr (130.79.128.5) or via <http://cdsarc.u-strasbg.fr/viz-bin/qcat?J/MNRAS>, and at the AMIGA VO interface (<http://amiga.iaa.es>).

[†]E-mail: mirian@iaa.es

B.3 Highly perturbed molecular gas in the Abell 1367 ram pressure stripping spiral archetype CGCG 97-079

In this collaboration I have quantified the environment of CGCG 97-079, a late-type galaxy in the galaxy cluster Abell 1367, in order to distinguish tidal and ram pressure interaction effects in clusters.

The analysis of the HERA CO results for CGCG 97-079 reveals a displacement in its CO of several kpc from the optical disk. The galaxy also has long H alpha and radio continuum tails strongly indicating ram pressure stripping. There are some proposed scenarios which might explain the CO displacement, one of which is that it is currently undergoing an interaction with a close companion. The analysis of the tidal strengths impacting CGCG 97-079 would help to answer which of the effects (by the cluster as whole, by the neighbours or only by the proposed companion) could account for the observed displacement of molecular gas.

Appendix C

CasJobs queries

Contents

C.1 SQL queries	120
C.1.1 Query 1: cross-ID for CIG galaxies in the SDSS	120
C.1.2 Query 2: searching for photometric SDSS neighbours	120
C.1.3 Query 3: cleaning photometric SDSS neighbours	120
C.1.4 Query 4: searching for spectroscopic SDSS neighbours	120
C.1.5 Query 5: photometric data for spectroscopic SDSS neighbours	122

C.1 SQL queries

In this section, we outline the method by which we follow the SDSS recommendations to restrict our sample to clean, photometric detections by using the object flags assigned by the SDSS photometric pipeline. Flag codes are shown in Fig. C.1.

C.1.1 Query 1: cross-ID for CIG galaxies in the SDSS

<http://skyserver.sdss3.org/dr9/en/tools/crossid/crossid.asp>

Parameters: r 0.5 / all nearby primary

```
SELECT p.ra, p.dec, p.modelMag_r, p.petroR90_r
FROM #upload u
JOIN #x x ON x.up_id = u.up_id
JOIN PhotoPrimary p ON p.objID = x.objID
WHERE p.type=3 and p.modelMag_r > 0 and p.petroR90_r > 0
ORDER BY x.up_id
```

C.1.2 Query 2: searching for photometric SDSS neighbours

```
declare @name int, @ra float, @dec float, @r float;
DECLARE my_cursor cursor read_only
FOR
SELECT name,ra,dec,r FROM MYDB.Table_positions
OPEN my_cursor
WHILE(1=1)
BEGIN
FETCH NEXT from my_cursor into @name, @ra, @dec, @r
IF (@@fetch_status < 0) break
INSERT MYDB.MyTable_photo
SELECT @name, p.objID FROM
dbo.fGetNearbyObjEq(@ra,@dec,@r) as p
JOIN Galaxy as G ON p.objID = G.objID
WHERE G.modelMag_r > 11.0 and G.modelMag_r < 19.
and G.petroR90_r > 2.5
END
CLOSE my_cursor
DEALLOCATE my_cursor
```

C.1.3 Query 3: cleaning photometric SDSS neighbours

```
SELECT q.name, G.objID, G.specObjID, G.ra, G.dec, G.modelMag_r, G.petroR90_r
INTO photoneigh
FROM Galaxy as G, mydb.MyTable_photo as q
WHERE G.objID=q.objID
and G.petroRadErr_r != -9999 and G.petroRadErr_r != -1000
and (G.flags & dbo.fPhotoFlags('saturated')) = 0
and G.g > 0 and G.i > 0
and G.petroR90_g > 0 and G.petroR90_i > 0
and G.petroR90Err_g > 0 and G.petroR90Err_i > 0
and ((G.flags & 0x10000000) != 0)
and ((G.flags & 0x40000) = 0)
and ((G.flags & 0x80) = 0)
```

C.1.4 Query 4: searching for spectroscopic SDSS neighbours

```
declare @name int, @ra float, @dec float, @r float;
DECLARE my_cursor cursor read_only
FOR SELECT name,ra,dec,r FROM MYDB.Table_positions
```

C.1. SQL QUERIES

Table A1. This table briefly describes all flags that may affect the quality of the SDSS imaging data. The percentage of data with each flag is based on the SQL query in A1. The flags that have an asterisk (*) appended can be set in single band.

Name	Description	Data with this flag (%)
INTERP_PROBLEMS:		
PSF_FLUX_INTERP*	More than 20% of the PSF flux is from interpolated pixels.	14.7
BAD_COUNTS_ERR*	The object contains many interpolation affected pixels, thus there are too few good pixels to estimate a PSF error.	0
INTERP_CENTER	The interpolated pixel is within 3 pixels of the object center.	9.28
COSMIC_RAY (CR)	The object contains cosmic rays.	12.3
DEBLEND_PROBLEMS:		
PEAKCENTER*	The object uses the position of the peak pixel as its center.	0.549
NOTCHECKED	The object contains pixels that were not checked to see if they include local peaks.	1.20
DEBLEND_NOPEAK	The object is a CHILD but has no peak in at least one band.	11.9
psfErr_r	PSF flux error in r-band.	28.2
<i>Object status flags:</i>		
BINNED1*	The object was detected at $\geq 5\sigma$ in a 1×1 binned image.	97.2
BINNED2*	The object was detected in a 2×2 binned image.	2.97
BINNED4*	The object was detected in a 4×4 binned image.	0.105
DETECTED	The object was either detected in BINNED1, BINNED2, or BINNED4.	99.8
BRIGHT	The object was duplicate-detected at $> 200\sigma$, which usually means $r < 17.5$.	0
BLENDED*	The object was detected with multiple peaks, and thus there was an attempt to deblend it as a parent object.	9.15
NODEBLEND	The object was BLENDED, but there was no attempt to deblend it.	
CHILD	The object was the result of deblending a BLENDED object. It may still be BLENDED.	26.1
<i>Raw data problem flags:</i>		
SATURATED*	The object contains one or more saturated pixels.	4.42
EDGE	The object is too close to the edge of a field frame.	0.432
LOCAL_EDGE	Similar to EDGE, but one half of the CCD failed.	0
DEBLENDED.AT_EDGE	The object is so large that it is marked as EDGE in all fields and strips, and thus it is deblended anyway.	0.687
INTERP	The object contains one or more interpolated-over pixels.	42.1
MAYBE_CR	The object may be a cosmic ray.	1.33
MAYBE_EGHOST	The object may be a ghost produced by CCD electronics.	0.143
<i>Image problem flags:</i>		
CANONICAL_CENTER*	The measurements use the center in the r-band rather than the local band.	0
NOPROFILE*	The object is either too small or too close to the edge and thus it is hard to estimate the radial flux profile.	0
NOTCHECKED_CENTER	Similar to NOTCHECKED, but the affected pixels are close to object's center.	0
TOO_LARGE	The object is either too large to measure its profile or has a child greater than half of the frame.	2.64E-6
BADSKY	The local sky measurement is so bad and therefore the photometry is meaningless.	0
<i>Suspicious object flags:</i>		
DEBLENDED_AS_PSF	If the deblending algorithm found this child is unresolved.	12.7
TOO_FEW_GOOD_DETECTIONS	This object doesn't have detections with good centroid in all bands.	38.7
NO_PETRO	The code was not able to determine the Petrosian radius for this object.	26.4

Figure C.1: Code for SDSS photometric flags. Percentages correspond to SQL used in Wang et al. (2013), based on more than 341 million point sources (primary objects, including stars and galaxies) brighter than $m_r < 23$ extinction corrected.

```
OPEN my_cursor
WHILE(1=1)
BEGIN
FETCH NEXT from my_cursor into @name, @ra, @dec, @r
IF (@@fetch_status < 0) break
INSERT MYDB.MyTable_spec
SELECT @name, specObjID FROM
dbo.fGetNearbySpecObjEq(@ra,@dec,@r)
END CLOSE my_cursor
DEALLOCATE my_cursor
```

C.1.5 Query 5: photometric data for spectroscopic SDSS neighbours

```
SELECT q.name, p.objID, p.specObjID, p.ra, p.dec, p.modelMag_r, p.petroR90_r, s.z
INTO specphotoneigh
FROM Galaxy as p, mydb.MyTable_spec as q, SpecPhoto as s
WHERE p.specObjID=q.specObjID and s.specObjID=q.specObjID
and p.modelMag_r >= 11. and p.modelMag_r <= 21.
```

Appendix D

Tables

Contents

D.1 Summary of the samples used in the photometric and spectroscopic studies for CIG galaxies	124
D.2 Quantification of the local and large scale environment	125

D.1 Summary of the samples used in the photometric and spectroscopic studies for CIG galaxies

Table D.1: Summary of the samples used in the photometric and spectroscopic studies.

Number of entries	Definition of the sample
1050	CIG galaxies in the original catalogue (Karachentseva 1973)
799	CIG galaxies found in the photometric catalogue of the SDSS-DR9
789	CIG galaxies of 799 after deleting of 10 galaxies with unreliable photometric data from the SDSS-DR9
693	CIG galaxies of 789 after deleting of 96 galaxies with $v < 1500 \text{ km s}^{-1}$
636	CIG galaxies of 693 after deleting of 57 galaxies with a field radius of 1 Mpc not covered in the photometric SDSS-DR9 catalogue
411	CIG galaxies of 636 of which more than 80% have extended neighbours down to $m_r < 17.7 \text{ mag}$ that lie within a projected separation of 1 Mpc from the CIG galaxy with a measured redshift
1,241,442	Neighbours within 1 Mpc around N=636 CIG galaxies
66,387	Neighbours with redshift in the SDSS-DR9 within 1 Mpc around N=636 CIG galaxies
1,307,829	Neighbours within 1 Mpc around N=636 CIG galaxies after a first clean of saturated objects
1,305,130	Neighbours, out of 1,307,829, within 1 Mpc around N=636 CIG galaxies after clean for saturated objects
479,504	Neighbours, out of 1,305,130, within 1 Mpc around N=636 CIG galaxies after a second clean of saturated objects and star-galaxy separation
86	CIG galaxies of 636 without neighbours that violate Eqs. 1.1 and 1.2 within 1 Mpc
117	CIG galaxies of 636 without neighbours that violate Eqs. 1.1 and 1.2 within 1 Mpc
433	CIG galaxies of 636 with more than one neighbour that violate Eqs. 1.1 and 1.2 within 1 Mpc
13	CIG galaxies of 433 with more than ten neighbour that violate Eqs. 1.1 and 1.2 within 1 Mpc
59	CIG galaxies of 636 within the original search area used by Karachentseva 1973
4	CIG galaxies of 59 without neighbours that violate Eqs. 1.1 and 1.2 within the original search area used by Karachentseva 1973
550	CIG galaxies of 636 with neighbours that violate Eqs. 1.1 and 1.2 within 1 Mpc
433	CIG galaxies of 550 with a tidal strength $Q_{\text{Kar,p}} < -2$
340	CIG galaxies of 550 with a tidal strength $Q_{\text{Kar,p}} < -2$ and a local number density $\eta_{k,p} < 2.7$
426	CIG galaxies of 636 (86+340) without neighbours that violate Eqs. 1.1 and 1.2 within 1 Mpc and with tidal strength $Q_{\text{Kar,p}} < -2$ and local number density $\eta_{k,p} < 2.7$
231	CIG galaxies of 636 without neighbours that violate Eq. 1.2 and for which, additionally, the approximate factor 4 in size was replaced in Eq. 1.1 by a factor 3 in magnitude within 1 Mpc
2,109	Neighbours of 479,504 identify as potential companions that violate Eqs. 1.1 and 1.2 within 1 Mpc
479,415	Neighbours of 479,504 within 1 Mpc around N=636 CIG galaxies after deletion of 89 saturated stars
121,872	Neighbours of 479,415 that violate Eq. 1.1 within 1 Mpc
3,433	Neighbours of 479,415 that violate Eq. 1.2 within 1 Mpc
2,020	Neighbours of 479,415 that violate Eqs. 1.1 and 1.2 within 1 Mpc
347	CIG galaxies of 411 without neighbours that violate Eqs. 1.1 and 1.2, and with $ \Delta v \leq 500 \text{ km s}^{-1}$ within 1 Mpc
35	CIG galaxies of 411 within the original search area used by Karachentseva 1973
32	CIG galaxies of 35 without neighbours that violate Eqs. 1.1 and 1.2, and with $ \Delta v \leq 500 \text{ km s}^{-1}$ within the original search area used by Karachentseva 1973
3	CIG galaxies of 35 with neighbours that violate Eqs. 1.1 and 1.2, and with $ \Delta v \leq 500 \text{ km s}^{-1}$ within the original search area used by Karachentseva 1973
105	CIG galaxies of 411 without neighbours with $ \Delta v \leq 500 \text{ km s}^{-1}$ within 1 Mpc
126	CIG galaxies of 411 without neighbours with $ \Delta v \leq 250 \text{ km s}^{-1}$ within 1 Mpc
308	CIG galaxies of 411 with at least one neighbour with $ \Delta v \leq 500 \text{ km s}^{-1}$ within 1 Mpc
103	CIG galaxies of 411 without neighbours with $ \Delta v \leq 500 \text{ km s}^{-1}$ within 1 Mpc when estimating upper limit for redshift incompleteness
10	CIG galaxies of 411 with changes in the isolation parameters when estimating upper limit for redshift incompleteness
70,169	Neighbours with redshift in the SDSS-DR9 within 1 Mpc around N=411 CIG galaxies
30,222	Neighbours of 70,169 that violate Eq. 1.1 within 1 Mpc
845	Neighbours of 70,169 that violate Eq. 1.2 within 1 Mpc

D.2. QUANTIFICATION OF THE LOCAL AND LARGE SCALE ENVIRONMENT

643	Neighbours of 70,169 that violate Eqs. 1.1 and 1.2 within 1 Mpc
75	Neighbours of 70,169 that violate Eqs. 1.1 and 1.2, and with $ \Delta v \leq 500 \text{ km s}^{-1}$ within 1 Mpc
791	CIG galaxies with tidal strength $Q < -2$ and local number density $\eta_k < 2.4$ according to Verley et al. (2007b)
620	CIG galaxies of 636 in common between Verley et al. (2007b)
486	CIG galaxies of 620 with also fulfill tidal strength $Q_{\text{Kar,p}} < -2$ and local number density $\eta_{k,p} < 2.7$

D.2 Quantification of the local and large scale environment

Table D.2: Quantification of the environment. The columns correspond to: (1) galaxy identification according to the CIG; (2) Q_{sat} , tidal strength estimation for satellites using the escape speed method; (3) $Q_{\text{sat,sup}}$, tidal strength estimation for satellites using the Gaussian distribution method; (4) k_{sat} , number of satellites selected following the escape speed method; (5) $k_{\text{sat,sup}}$, number of satellites selected following the Gaussian distribution method; (6) Q_{LSS} , tidal strength estimation of the LSS; (7) $\eta_{k,\text{LSS}}$, local number density estimation of the LSS; (8) k_{LSS} , number of LSS associations; (9) $\frac{Q_{\text{sat}}}{Q_{\text{LSS}}}$, relation between Q_{sat} and Q_{LSS} , from 0 to 1 if the considered satellites amount from 0% to 100% to the total tidal strength; (10) $\frac{Q_{\text{sat,sup}}}{Q_{\text{LSS}}}$, relation between $Q_{\text{sat,sup}}$ and Q_{LSS} , from 0 to 1 if the considered satellites amount from 0% to 100% to the total tidal strength.

(1)	(2)	(3)	(4)	(5)	(6)	(7)	(8)	(9)	(10)
CIG	Q_{sat}	$Q_{\text{sat,sup}}$	k_{sat}	$k_{\text{sat,sup}}$	Q_{LSS}	$\eta_{k,\text{LSS}}$	k_{LSS}	$\frac{Q_{\text{sat}}}{Q_{\text{LSS}}}$	$\frac{Q_{\text{sat,sup}}}{Q_{\text{LSS}}}$
11	NULL	NULL	0	0	-6.12	-1.43	5	NULL	NULL
33	NULL	NULL	0	0	-4.79	-0.21	18	NULL	NULL
56	-4.37	-4.37	1	1	-4.06	0.04	37	0.49	0.49
60	NULL	NULL	0	0	-4.75	0.78	31	NULL	NULL
198	-3.01	-3.01	1	1	-2.90	-0.81	11	0.78	0.78
199	NULL	NULL	0	0	-5.77	-0.97	8	NULL	NULL
203	NULL	NULL	0	0	-5.65	-1.94	2	NULL	NULL
204	NULL	NULL	0	0	-3.41	-0.25	18	NULL	NULL
205	NULL	NULL	0	0	-5.52	-1.26	5	NULL	NULL
207	NULL	NULL	0	0	-4.49	-0.36	27	NULL	NULL
210	NULL	NULL	0	0	-4.06	-1.32	7	NULL	NULL
211	-3.30	-3.07	1	2	-3.07	-1.23	6	0.59	1.00
212	NULL	NULL	0	0	-6.12	-0.58	14	NULL	NULL
213	NULL	NULL	0	0	-4.55	-0.41	3	NULL	NULL
214	NULL	NULL	0	0	-5.69	-1.53	4	NULL	NULL
216	NULL	NULL	0	0	-6.20	-1.95	2	NULL	NULL
217	NULL	NULL	0	0	-5.79	-1.62	3	NULL	NULL
219	NULL	NULL	0	0	-4.39	-1.09	7	NULL	NULL
220	NULL	NULL	0	0	-4.68	-1.32	7	NULL	NULL
221	NULL	NULL	0	0	-4.07	-1.15	7	NULL	NULL
222	NULL	NULL	0	0	-4.80	-1.40	4	NULL	NULL
223	NULL	NULL	0	0	-4.88	-1.70	3	NULL	NULL
225	NULL	NULL	0	0	-3.69	-1.40	5	NULL	NULL
226	NULL	NULL	0	0	-4.05	-0.86	9	NULL	NULL
227	NULL	NULL	0	0	-3.54	-1.10	7	NULL	NULL
228	NULL	-4.11	0	1	-4.01	-0.22	19	NULL	0.79
229	NULL	NULL	0	0	NULL	NULL	0	NULL	NULL
231	NULL	NULL	0	0	-5.02	-0.77	7	NULL	NULL
232	-2.04	-2.04	2	2	-2.04	-0.60	17	1.00	1.00
233	NULL	NULL	0	0	-4.24	-0.89	10	NULL	NULL
234	NULL	NULL	0	0	-4.88	-2.01	2	NULL	NULL
236	NULL	NULL	0	0	-6.16	-2.03	2	NULL	NULL
237	-3.14	-3.12	2	3	-3.04	0.84	20	0.79	0.83
238	NULL	NULL	0	0	-4.03	-1.27	11	NULL	NULL
241	NULL	NULL	0	0	-4.60	-0.96	7	NULL	NULL
242	NULL	NULL	0	0	-4.92	-0.81	36	NULL	NULL

(1)	(2)	(3)	(4)	(5)	(6)	(7)	(8)	(9)	(10)
CIG	Q_{sat}	$Q_{\text{sat,sup}}$	k_{sat}	$k_{\text{sat,sup}}$	Q_{LSS}	$\eta_{k,\text{LSS}}$	k_{LSS}	$\frac{Q_{\text{sat}}}{Q_{\text{LSS}}}$	$\frac{Q_{\text{sat,sup}}}{Q_{\text{LSS}}}$
243	NULL	NULL	0	0	-4.31	-0.19	56	NULL	NULL
244	NULL	NULL	0	0	-4.30	-0.14	29	NULL	NULL
245	NULL	NULL	0	0	NULL	NULL	0	NULL	NULL
247	NULL	NULL	0	0	-6.30	-1.05	14	NULL	NULL
248	NULL	NULL	0	0	-6.03	-1.34	4	NULL	NULL
249	NULL	NULL	0	0	-6.39	-1.44	2	NULL	NULL
250	-3.64	-3.47	1	2	-3.46	-0.25	8	0.66	0.98
252	NULL	NULL	0	0	-3.10	-0.49	14	NULL	NULL
254	NULL	NULL	0	0	-4.39	-1.12	3	NULL	NULL
257	NULL	NULL	0	0	-4.68	-1.40	6	NULL	NULL
258	NULL	NULL	0	0	-4.97	-0.86	11	NULL	NULL
260	NULL	NULL	0	0	-4.41	-0.75	16	NULL	NULL
261	NULL	NULL	0	0	-4.31	-1.47	4	NULL	NULL
262	NULL	NULL	0	0	-5.06	-0.86	19	NULL	NULL
263	NULL	NULL	0	0	-4.16	-0.55	19	NULL	NULL
264	NULL	NULL	0	0	-4.76	-0.77	12	NULL	NULL
268	NULL	NULL	0	0	-4.14	-0.50	25	NULL	NULL
269	NULL	NULL	0	0	-3.82	-1.08	8	NULL	NULL
270	NULL	-3.71	0	1	-2.95	-1.16	8	NULL	0.17
271	NULL	NULL	0	0	-4.42	-0.47	13	NULL	NULL
272	NULL	NULL	0	0	-6.48	-1.93	2	NULL	NULL
273	NULL	NULL	0	0	-3.67	-0.44	18	NULL	NULL
274	-4.28	-4.28	1	1	-4.21	-1.39	5	0.85	0.85
276	NULL	NULL	0	0	-5.24	-1.12	7	NULL	NULL
278	-3.85	-3.85	1	1	-3.81	-1.21	5	0.91	0.91
279	NULL	NULL	0	0	-4.92	-0.50	9	NULL	NULL
280	NULL	NULL	0	0	-4.48	-1.03	17	NULL	NULL
281	NULL	NULL	0	0	-6.15	-1.35	4	NULL	NULL
282	NULL	NULL	0	0	-3.95	-0.49	15	NULL	NULL
283	NULL	NULL	0	0	-4.43	-0.40	9	NULL	NULL
284	NULL	NULL	0	0	NULL	NULL	0	NULL	NULL
286	NULL	NULL	0	0	-4.71	-1.75	3	NULL	NULL
287	NULL	NULL	0	0	-4.78	-1.01	8	NULL	NULL
288	NULL	NULL	0	0	-6.50	NULL	1	NULL	NULL
289	NULL	NULL	0	0	-4.97	-1.23	11	NULL	NULL
290	NULL	NULL	0	0	-4.75	-0.79	16	NULL	NULL
292	NULL	NULL	0	0	-5.04	-0.16	17	NULL	NULL
293	NULL	-4.37	0	1	-4.31	-1.11	14	NULL	0.87
294	NULL	NULL	0	0	-3.73	-0.66	9	NULL	NULL
296	NULL	-2.88	0	1	-2.87	-1.22	8	NULL	0.98
298	NULL	NULL	0	0	-4.01	-0.42	25	NULL	NULL
299	NULL	NULL	0	0	-4.55	0.38	35	NULL	NULL
302	NULL	NULL	0	0	-4.00	0.06	54	NULL	NULL
303	-3.38	-3.38	2	2	-3.34	0.06	27	0.91	0.91
304	NULL	NULL	0	0	-3.25	-0.97	11	NULL	NULL
305	NULL	NULL	0	0	-5.65	-1.21	7	NULL	NULL
306	NULL	NULL	0	0	-5.33	-1.97	2	NULL	NULL
307	NULL	NULL	0	0	-5.75	NULL	1	NULL	NULL
308	NULL	NULL	0	0	-3.50	0.80	49	NULL	NULL
310	NULL	NULL	0	0	-4.26	-0.90	6	NULL	NULL
311	NULL	NULL	0	0	-5.36	-1.74	2	NULL	NULL
312	NULL	NULL	0	0	-3.80	-0.56	15	NULL	NULL
313	NULL	NULL	0	0	-5.36	-1.61	3	NULL	NULL
314	NULL	NULL	0	0	-5.60	-0.82	14	NULL	NULL
316	NULL	NULL	0	0	-4.24	-0.28	22	NULL	NULL
317	NULL	NULL	0	0	-5.58	-1.20	14	NULL	NULL
318	NULL	NULL	0	0	NULL	NULL	0	NULL	NULL
319	-3.30	-3.11	1	2	-3.08	-0.02	11	0.60	0.93
321	NULL	NULL	0	0	-4.69	NULL	1	NULL	NULL
322	NULL	NULL	0	0	-6.35	-0.72	17	NULL	NULL

D.2. QUANTIFICATION OF THE LOCAL AND LARGE SCALE ENVIRONMENT

(1)	(2)	(3)	(4)	(5)	(6)	(7)	(8)	(9)	(10)
CIG	Q_{sat}	$Q_{\text{sat,sup}}$	k_{sat}	$k_{\text{sat,sup}}$	Q_{LSS}	$\eta_{k,\text{LSS}}$	k_{LSS}	$\frac{Q_{\text{sat}}}{Q_{\text{LSS}}}$	$\frac{Q_{\text{sat,sup}}}{Q_{\text{LSS}}}$
323	-3.34	-3.34	1	1	-3.31	-0.75	12	0.93	0.93
325	NULL	NULL	0	0	-5.65	-1.35	7	NULL	NULL
327	NULL	NULL	0	0	-4.93	-0.56	27	NULL	NULL
328	NULL	NULL	0	0	-5.16	0.05	12	NULL	NULL
329	NULL	NULL	0	0	-5.21	-1.41	5	NULL	NULL
330	NULL	NULL	0	0	-3.78	-0.48	15	NULL	NULL
331	NULL	NULL	0	0	NULL	NULL	0	NULL	NULL
332	NULL	NULL	0	0	-4.56	-0.31	16	NULL	NULL
333	NULL	NULL	0	0	-3.93	-1.70	3	NULL	NULL
334	NULL	NULL	0	0	-4.72	-0.63	28	NULL	NULL
335	NULL	NULL	0	0	-4.53	-0.55	9	NULL	NULL
336	NULL	NULL	0	0	-3.16	0.22	28	NULL	NULL
337	NULL	NULL	0	0	-3.92	-0.84	9	NULL	NULL
338	-5.42	-5.42	1	1	-5.27	-0.17	14	0.71	0.71
339	NULL	-2.89	0	1	-2.77	-0.37	10	NULL	0.76
340	NULL	NULL	0	0	-3.92	-0.79	17	NULL	NULL
341	NULL	NULL	0	0	-3.68	-1.12	3	NULL	NULL
342	NULL	NULL	0	0	-4.54	-0.87	18	NULL	NULL
343	NULL	NULL	0	0	-3.57	-0.12	12	NULL	NULL
344	NULL	NULL	0	0	-4.42	-1.01	9	NULL	NULL
348	NULL	-2.83	0	1	-2.83	-1.33	3	NULL	1.00
349	NULL	NULL	0	0	-5.10	-1.14	6	NULL	NULL
350	NULL	NULL	0	0	-4.31	-1.45	5	NULL	NULL
351	NULL	NULL	0	0	-5.01	-1.17	5	NULL	NULL
352	NULL	NULL	0	0	-5.65	-0.42	49	NULL	NULL
353	NULL	NULL	0	0	-4.79	-0.78	11	NULL	NULL
355	-3.70	-3.70	1	1	-3.63	-0.28	11	0.85	0.85
358	NULL	NULL	0	0	-5.22	-0.69	8	NULL	NULL
359	NULL	NULL	0	0	-5.48	-1.31	4	NULL	NULL
360	NULL	NULL	0	0	-4.61	-1.06	8	NULL	NULL
361	NULL	NULL	0	0	-4.34	-0.28	16	NULL	NULL
364	NULL	NULL	0	0	-5.39	-1.27	7	NULL	NULL
365	NULL	NULL	0	0	-4.09	-0.68	9	NULL	NULL
366	NULL	NULL	0	0	-4.18	-0.76	23	NULL	NULL
367	-2.86	-2.86	1	1	-2.84	-0.40	7	0.95	0.95
368	NULL	NULL	0	0	-4.47	-1.75	2	NULL	NULL
370	NULL	NULL	0	0	-4.80	-1.74	3	NULL	NULL
372	NULL	NULL	0	0	-4.98	-1.32	5	NULL	NULL
373	NULL	NULL	0	0	-4.25	-0.84	6	NULL	NULL
374	NULL	NULL	0	0	-4.76	-1.47	4	NULL	NULL
375	NULL	NULL	0	0	-4.18	-1.35	7	NULL	NULL
378	NULL	NULL	0	0	-6.04	-1.63	2	NULL	NULL
379	NULL	NULL	0	0	-4.58	-0.86	11	NULL	NULL
380	NULL	NULL	0	0	-5.17	-0.54	4	NULL	NULL
381	NULL	NULL	0	0	-5.35	-0.81	14	NULL	NULL
384	NULL	NULL	0	0	-3.97	-1.04	3	NULL	NULL
385	-4.78	-4.78	1	1	-4.36	-0.13	16	0.38	0.38
386	NULL	NULL	0	0	-5.46	-1.42	5	NULL	NULL
387	NULL	NULL	0	0	-5.85	-1.32	4	NULL	NULL
391	NULL	NULL	0	0	-4.27	-1.55	4	NULL	NULL
392	NULL	NULL	0	0	-5.07	-1.27	7	NULL	NULL
394	NULL	NULL	0	0	-4.08	-0.99	13	NULL	NULL
395	NULL	NULL	0	0	-4.18	-1.61	3	NULL	NULL
397	NULL	NULL	0	0	-5.16	0.45	18	NULL	NULL
398	NULL	NULL	0	0	-4.09	-1.06	7	NULL	NULL
399	NULL	NULL	0	0	-5.32	-1.33	8	NULL	NULL
400	-2.90	-2.90	2	2	-2.90	-0.96	9	1.00	1.00
401	-1.31	-1.31	1	1	-1.31	-0.76	19	1.00	1.00
403	NULL	NULL	0	0	-3.72	-0.57	11	NULL	NULL
405	NULL	NULL	0	0	-4.85	-0.56	15	NULL	NULL

(1)	(2)	(3)	(4)	(5)	(6)	(7)	(8)	(9)	(10)
CIG	Q_{sat}	$Q_{\text{sat,sup}}$	k_{sat}	$k_{\text{sat,sup}}$	Q_{LSS}	$\eta_{k,\text{LSS}}$	k_{LSS}	$\frac{Q_{\text{sat}}}{Q_{\text{LSS}}}$	$\frac{Q_{\text{sat,sup}}}{Q_{\text{LSS}}}$
406	NULL	NULL	0	0	-5.58	-1.18	10	NULL	NULL
408	NULL	NULL	0	0	-3.96	-1.08	2	NULL	NULL
409	NULL	NULL	0	0	-4.02	0.50	38	NULL	NULL
410	NULL	NULL	0	0	-4.40	-0.53	25	NULL	NULL
412	NULL	NULL	0	0	-3.81	-0.71	8	NULL	NULL
413	NULL	NULL	0	0	-4.33	0.39	23	NULL	NULL
414	NULL	NULL	0	0	-4.99	-1.29	5	NULL	NULL
415	NULL	NULL	0	0	-4.46	-1.20	5	NULL	NULL
416	NULL	-4.00	0	2	-4.00	-1.50	4	NULL	1.00
417	NULL	NULL	0	0	-5.35	-1.29	8	NULL	NULL
418	NULL	NULL	0	0	-5.63	-0.85	11	NULL	NULL
419	NULL	NULL	0	0	-5.19	-1.64	3	NULL	NULL
420	NULL	NULL	0	0	-5.72	-0.96	10	NULL	NULL
423	-1.64	-1.64	2	2	-1.64	-0.46	23	1.00	1.00
424	NULL	NULL	0	0	-4.18	-0.62	19	NULL	NULL
425	NULL	NULL	0	0	-3.99	-0.46	17	NULL	NULL
426	NULL	NULL	0	0	-4.89	-0.74	27	NULL	NULL
427	NULL	NULL	0	0	-5.88	-1.71	3	NULL	NULL
430	NULL	NULL	0	0	-4.31	-0.68	8	NULL	NULL
431	NULL	NULL	0	0	-5.23	-1.05	2	NULL	NULL
432	NULL	NULL	0	0	-4.23	-1.39	5	NULL	NULL
437	-3.58	-3.58	1	1	-3.57	-0.88	16	0.98	0.98
438	NULL	NULL	0	0	-3.79	-0.02	14	NULL	NULL
439	NULL	NULL	0	0	-3.70	-0.34	31	NULL	NULL
440	NULL	NULL	0	0	-2.63	0.26	11	NULL	NULL
441	NULL	NULL	0	0	-5.01	-0.53	13	NULL	NULL
443	NULL	NULL	0	0	-5.85	-1.11	10	NULL	NULL
445	NULL	NULL	0	0	-3.67	-0.45	10	NULL	NULL
446	NULL	NULL	0	0	-4.57	-0.42	16	NULL	NULL
450	NULL	NULL	0	0	-4.36	-0.66	12	NULL	NULL
451	NULL	NULL	0	0	-6.82	NULL	1	NULL	NULL
453	NULL	NULL	0	0	-4.10	-0.23	36	NULL	NULL
456	NULL	NULL	0	0	-5.72	-1.70	3	NULL	NULL
457	NULL	NULL	0	0	-7.15	NULL	1	NULL	NULL
458	NULL	NULL	0	0	-5.23	-1.52	4	NULL	NULL
459	NULL	NULL	0	0	-5.66	-1.67	3	NULL	NULL
460	NULL	NULL	0	0	-4.92	-1.00	10	NULL	NULL
462	NULL	NULL	0	0	-5.46	-0.68	17	NULL	NULL
463	NULL	NULL	0	0	-5.01	-0.66	11	NULL	NULL
466	NULL	NULL	0	0	-5.04	-1.41	7	NULL	NULL
467	NULL	NULL	0	0	-4.78	-1.01	6	NULL	NULL
468	NULL	NULL	0	0	-4.93	-0.69	7	NULL	NULL
473	NULL	NULL	0	0	-5.11	-1.27	6	NULL	NULL
474	NULL	-2.86	0	1	-2.85	-0.43	10	NULL	0.98
475	NULL	NULL	0	0	-4.16	-1.41	3	NULL	NULL
476	NULL	NULL	0	0	-5.34	-1.08	17	NULL	NULL
478	NULL	NULL	0	0	-3.90	-0.89	10	NULL	NULL
479	NULL	NULL	0	0	-5.33	-1.46	3	NULL	NULL
480	NULL	NULL	0	0	-4.62	-0.79	12	NULL	NULL
482	NULL	NULL	0	0	-4.31	-1.43	3	NULL	NULL
485	NULL	NULL	0	0	-5.46	-0.84	8	NULL	NULL
487	NULL	NULL	0	0	-5.31	-1.09	8	NULL	NULL
489	NULL	NULL	0	0	-4.96	-0.64	12	NULL	NULL
490	NULL	NULL	0	0	-5.68	-1.36	8	NULL	NULL
491	NULL	NULL	0	0	-6.64	-1.29	3	NULL	NULL
492	NULL	NULL	0	0	-5.16	-1.15	9	NULL	NULL
493	NULL	NULL	0	0	-4.06	NULL	1	NULL	NULL
494	NULL	NULL	0	0	-4.30	-0.51	15	NULL	NULL
495	NULL	-5.20	0	1	-5.15	-0.85	11	NULL	0.89
497	NULL	NULL	0	0	-5.55	-1.57	3	NULL	NULL

D.2. QUANTIFICATION OF THE LOCAL AND LARGE SCALE ENVIRONMENT

(1)	(2)	(3)	(4)	(5)	(6)	(7)	(8)	(9)	(10)
CIG	Q_{sat}	$Q_{\text{sat,sup}}$	k_{sat}	$k_{\text{sat,sup}}$	Q_{LSS}	$\eta_{k,\text{LSS}}$	k_{LSS}	$\frac{Q_{\text{sat}}}{Q_{\text{LSS}}}$	$\frac{Q_{\text{sat,sup}}}{Q_{\text{LSS}}}$
499	NULL	NULL	0	0	-4.88	-1.30	4	NULL	NULL
500	NULL	NULL	0	0	-4.41	-1.12	12	NULL	NULL
501	NULL	NULL	0	0	-6.96	NULL	1	NULL	NULL
504	NULL	NULL	0	0	-5.01	-0.50	9	NULL	NULL
507	NULL	NULL	0	0	-4.14	-0.79	14	NULL	NULL
508	NULL	NULL	0	0	-4.46	-0.94	11	NULL	NULL
510	NULL	NULL	0	0	-4.82	-0.84	21	NULL	NULL
513	NULL	NULL	0	0	-4.25	-1.50	4	NULL	NULL
515	NULL	NULL	0	0	-4.44	-0.75	43	NULL	NULL
516	NULL	NULL	0	0	-4.25	-0.49	17	NULL	NULL
517	-3.60	-3.60	1	1	-3.55	-0.80	4	0.89	0.89
519	NULL	NULL	0	0	-5.43	NULL	1	NULL	NULL
520	NULL	-4.11	0	1	-4.11	-1.73	2	NULL	1.00
521	NULL	NULL	0	0	-5.29	-0.29	71	NULL	NULL
522	NULL	NULL	0	0	-6.75	-1.47	4	NULL	NULL
525	NULL	NULL	0	0	-4.32	-0.61	18	NULL	NULL
526	NULL	NULL	0	0	-4.91	-1.27	5	NULL	NULL
528	NULL	-4.16	0	1	-4.03	-0.89	10	NULL	0.74
529	NULL	NULL	0	0	-5.95	-1.29	6	NULL	NULL
532	NULL	NULL	0	0	-5.17	-1.28	6	NULL	NULL
537	NULL	NULL	0	0	-6.34	-1.46	3	NULL	NULL
539	-2.75	-2.75	1	1	-2.75	-1.21	4	1.00	1.00
541	NULL	NULL	0	0	NULL	NULL	0	NULL	NULL
542	NULL	NULL	0	0	NULL	NULL	0	NULL	NULL
544	NULL	NULL	0	0	-5.62	-1.42	6	NULL	NULL
545	NULL	NULL	0	0	-4.81	-0.93	8	NULL	NULL
546	NULL	NULL	0	0	NULL	NULL	0	NULL	NULL
548	NULL	NULL	0	0	-4.87	-0.34	12	NULL	NULL
550	NULL	NULL	0	0	-4.32	-0.87	9	NULL	NULL
553	NULL	NULL	0	0	-4.29	-0.42	31	NULL	NULL
554	NULL	-2.48	0	1	-2.47	-0.96	12	NULL	0.98
557	-2.86	-2.65	1	2	-2.64	0.14	7	0.60	0.98
558	NULL	NULL	0	0	-5.19	-1.41	5	NULL	NULL
560	NULL	NULL	0	0	-5.96	-1.19	7	NULL	NULL
561	NULL	NULL	0	0	-4.69	0.17	26	NULL	NULL
563	NULL	NULL	0	0	-4.27	-1.08	11	NULL	NULL
565	NULL	NULL	0	0	-3.81	-0.35	22	NULL	NULL
566	NULL	NULL	0	0	-4.98	-0.61	17	NULL	NULL
567	NULL	NULL	0	0	-4.43	-1.15	5	NULL	NULL
568	NULL	NULL	0	0	-3.23	0.07	14	NULL	NULL
570	NULL	NULL	0	0	-5.86	-1.33	8	NULL	NULL
571	NULL	NULL	0	0	-5.36	-0.58	13	NULL	NULL
572	NULL	NULL	0	0	-3.29	-0.29	18	NULL	NULL
575	NULL	NULL	0	0	-4.61	0.22	16	NULL	NULL
576	NULL	NULL	0	0	-4.03	-0.31	27	NULL	NULL
578	-4.10	-4.10	1	1	-4.09	-1.06	5	0.98	0.98
579	NULL	NULL	0	0	-4.06	-0.38	41	NULL	NULL
580	NULL	NULL	0	0	-4.41	-0.62	32	NULL	NULL
581	NULL	NULL	0	0	-3.29	-0.19	24	NULL	NULL
582	NULL	NULL	0	0	-4.87	-1.52	4	NULL	NULL
583	NULL	NULL	0	0	-4.13	-0.57	7	NULL	NULL
585	NULL	NULL	0	0	-4.70	-0.95	15	NULL	NULL
586	NULL	NULL	0	0	-4.70	-0.76	24	NULL	NULL
587	NULL	NULL	0	0	-4.45	-0.98	5	NULL	NULL
589	NULL	-3.07	0	1	-3.06	-1.04	5	NULL	0.98
591	NULL	NULL	0	0	-4.61	-0.41	25	NULL	NULL
592	NULL	-4.82	0	1	-4.45	0.22	41	NULL	0.43
594	NULL	NULL	0	0	-4.92	-1.54	4	NULL	NULL
595	-0.34	-0.34	1	1	-0.34	-0.04	22	1.00	1.00
596	NULL	-3.32	0	1	-2.99	0.28	26	NULL	0.47

(1)	(2)	(3)	(4)	(5)	(6)	(7)	(8)	(9)	(10)
CIG	Q_{sat}	$Q_{\text{sat,sup}}$	k_{sat}	$k_{\text{sat,sup}}$	Q_{LSS}	$\eta_{k,\text{LSS}}$	k_{LSS}	$\frac{Q_{\text{sat}}}{Q_{\text{LSS}}}$	$\frac{Q_{\text{sat,sup}}}{Q_{\text{LSS}}}$
598	NULL	NULL	0	0	-5.34	-1.43	5	NULL	NULL
599	NULL	NULL	0	0	-4.41	-1.23	5	NULL	NULL
600	NULL	NULL	0	0	-3.59	0.07	18	NULL	NULL
601	NULL	NULL	0	0	-4.34	-1.18	11	NULL	NULL
602	NULL	NULL	0	0	-3.47	-1.08	8	NULL	NULL
603	NULL	NULL	0	0	-4.38	-0.89	16	NULL	NULL
605	-2.62	-2.62	1	1	-2.62	-1.02	9	1.00	1.00
606	NULL	-1.64	0	1	-1.64	-1.62	3	NULL	1.00
607	NULL	NULL	0	0	-4.01	-0.67	18	NULL	NULL
608	NULL	NULL	0	0	-5.39	NULL	1	NULL	NULL
609	NULL	-4.27	0	2	-4.12	0.69	55	NULL	0.71
611	NULL	NULL	0	0	-3.74	0.20	35	NULL	NULL
612	-2.79	-2.79	1	1	-2.76	-0.74	8	0.93	0.93
613	NULL	NULL	0	0	-4.18	-1.13	3	NULL	NULL
614	NULL	NULL	0	0	-2.86	-0.35	11	NULL	NULL
616	NULL	NULL	0	0	-4.63	-1.40	4	NULL	NULL
617	NULL	NULL	0	0	-5.18	-1.31	5	NULL	NULL
618	-2.12	-2.12	1	1	-2.12	-1.59	3	1.00	1.00
619	NULL	NULL	0	0	-3.82	-1.08	5	NULL	NULL
620	NULL	NULL	0	0	-5.03	-1.40	5	NULL	NULL
622	NULL	NULL	0	0	-5.63	-0.74	19	NULL	NULL
623	NULL	NULL	0	0	-4.94	-0.97	14	NULL	NULL
625	NULL	-2.75	0	1	-2.73	-0.15	26	NULL	0.95
626	NULL	NULL	0	0	-4.13	0.16	71	NULL	NULL
628	NULL	NULL	0	0	-3.91	-1.38	5	NULL	NULL
630	NULL	-4.12	0	1	-4.11	-0.74	11	NULL	0.98
631	NULL	NULL	0	0	-5.20	0.56	54	NULL	NULL
633	NULL	NULL	0	0	-4.91	0.12	65	NULL	NULL
634	-3.13	-3.13	1	1	-3.13	0.51	87	1.00	1.00
635	NULL	NULL	0	0	-3.96	-0.40	16	NULL	NULL
636	NULL	NULL	0	0	-6.58	NULL	1	NULL	NULL
637	-3.32	-3.32	1	1	-3.32	-0.26	78	1.00	1.00
639	NULL	NULL	0	0	-4.68	-0.77	13	NULL	NULL
640	NULL	NULL	0	0	-5.71	-1.61	3	NULL	NULL
641	NULL	NULL	0	0	-6.69	NULL	1	NULL	NULL
643	NULL	NULL	0	0	-3.81	-0.40	20	NULL	NULL
644	-3.90	-3.90	1	1	-3.87	-1.34	7	0.93	0.93
645	NULL	NULL	0	0	-4.66	-1.18	11	NULL	NULL
646	NULL	NULL	0	0	-5.21	-1.05	3	NULL	NULL
647	NULL	NULL	0	0	-3.79	-1.02	8	NULL	NULL
648	NULL	NULL	0	0	-4.31	-0.91	27	NULL	NULL
650	NULL	NULL	0	0	-3.84	-0.34	25	NULL	NULL
653	-4.18	-4.18	1	1	-3.91	-0.25	15	0.54	0.54
655	NULL	NULL	0	0	-4.60	-0.82	13	NULL	NULL
658	NULL	NULL	0	0	-3.99	-0.48	22	NULL	NULL
659	NULL	NULL	0	0	-4.26	-1.43	5	NULL	NULL
665	NULL	NULL	0	0	-4.82	-0.76	9	NULL	NULL
667	NULL	NULL	0	0	-5.43	-1.43	4	NULL	NULL
668	NULL	NULL	0	0	-4.21	-0.85	21	NULL	NULL
672	NULL	NULL	0	0	-4.24	-1.58	3	NULL	NULL
674	NULL	NULL	0	0	NULL	NULL	0	NULL	NULL
675	NULL	NULL	0	0	-4.60	-0.77	20	NULL	NULL
676	NULL	NULL	0	0	-4.76	-1.01	4	NULL	NULL
678	NULL	NULL	0	0	-5.45	-1.41	5	NULL	NULL
679	NULL	NULL	0	0	-6.36	-1.72	3	NULL	NULL
680	NULL	NULL	0	0	-4.23	-0.76	26	NULL	NULL
681	NULL	NULL	0	0	-5.52	-1.41	5	NULL	NULL
683	NULL	NULL	0	0	-4.22	-0.79	18	NULL	NULL
685	NULL	NULL	0	0	-4.15	-1.64	3	NULL	NULL
689	NULL	NULL	0	0	-5.41	-0.87	10	NULL	NULL

D.2. QUANTIFICATION OF THE LOCAL AND LARGE SCALE ENVIRONMENT

(1)	(2)	(3)	(4)	(5)	(6)	(7)	(8)	(9)	(10)
CIG	Q_{sat}	$Q_{\text{sat,sup}}$	k_{sat}	$k_{\text{sat,sup}}$	Q_{LSS}	$\eta_{k,\text{LSS}}$	k_{LSS}	$\frac{Q_{\text{sat}}}{Q_{\text{LSS}}}$	$\frac{Q_{\text{sat,sup}}}{Q_{\text{LSS}}}$
690	NULL	NULL	0	0	-6.46	-1.55	4	NULL	NULL
693	NULL	NULL	0	0	-5.53	-1.40	6	NULL	NULL
694	-2.74	-2.74	1	1	-2.74	-1.48	3	1.00	1.00
695	NULL	NULL	0	0	-4.05	-0.61	17	NULL	NULL
696	NULL	-2.39	0	1	-2.39	-0.56	7	NULL	1.00
698	NULL	NULL	0	0	-6.06	-1.12	4	NULL	NULL
701	-1.19	-1.19	1	1	-1.19	0.82	2	1.00	1.00
702	NULL	NULL	0	0	NULL	NULL	0	NULL	NULL
703	-5.41	-5.41	1	1	-5.40	-1.38	4	0.98	0.98
704	NULL	NULL	0	0	-4.15	-0.21	22	NULL	NULL
705	NULL	NULL	0	0	-5.22	-0.69	9	NULL	NULL
714	NULL	NULL	0	0	-5.02	-0.49	36	NULL	NULL
716	NULL	NULL	0	0	-3.96	-1.44	5	NULL	NULL
717	NULL	NULL	0	0	-4.41	-1.18	8	NULL	NULL
719	NULL	NULL	0	0	-3.32	-0.50	26	NULL	NULL
721	-3.73	-3.73	2	2	-3.45	0.36	18	0.52	0.52
722	-3.58	-3.58	1	1	-3.57	-0.32	8	0.98	0.98
723	NULL	NULL	0	0	-3.79	-0.42	14	NULL	NULL
724	NULL	NULL	0	0	-3.01	-0.85	17	NULL	NULL
725	NULL	NULL	0	0	-4.86	-1.41	6	NULL	NULL
726	NULL	NULL	0	0	-3.54	-0.31	43	NULL	NULL
731	NULL	NULL	0	0	-4.57	-1.16	15	NULL	NULL
733	NULL	NULL	0	0	-4.81	-0.15	14	NULL	NULL
735	NULL	NULL	0	0	-4.24	0.05	40	NULL	NULL
739	NULL	-3.54	0	1	-3.51	-0.98	4	NULL	0.93
741	NULL	NULL	0	0	-3.80	-1.54	4	NULL	NULL
743	NULL	NULL	0	0	-6.91	NULL	1	NULL	NULL
747	NULL	NULL	0	0	-3.09	-1.19	6	NULL	NULL
749	NULL	NULL	0	0	-5.05	-1.06	6	NULL	NULL
751	NULL	NULL	0	0	-5.17	-0.63	13	NULL	NULL
752	NULL	NULL	0	0	-5.46	-1.42	4	NULL	NULL
757	NULL	NULL	0	0	-4.69	-0.60	8	NULL	NULL
761	NULL	NULL	0	0	-6.49	NULL	1	NULL	NULL
762	NULL	NULL	0	0	-4.69	-0.36	6	NULL	NULL
767	NULL	NULL	0	0	-4.43	-2.04	2	NULL	NULL
771	0.10	0.10	3	3	0.10	0.85	30	1.00	1.00
780	NULL	NULL	0	0	-4.40	0.06	2	NULL	NULL
795	NULL	NULL	0	0	-4.20	-0.93	23	NULL	NULL
807	NULL	NULL	0	0	-4.73	-1.29	6	NULL	NULL
893	NULL	NULL	0	0	-4.38	-0.37	43	NULL	NULL
924	NULL	-3.00	0	1	-3.00	-0.54	11	NULL	1.00
931	NULL	NULL	0	0	-4.98	-0.63	19	NULL	NULL
932	NULL	NULL	0	0	-4.61	-0.65	13	NULL	NULL
937	NULL	NULL	0	0	-4.30	-0.07	21	NULL	NULL
943	NULL	NULL	0	0	-7.48	-1.59	2	NULL	NULL
980	NULL	NULL	0	0	-5.27	-1.48	2	NULL	NULL
1008	NULL	NULL	0	0	-4.66	-1.71	3	NULL	NULL
1014	NULL	NULL	0	0	-5.89	-1.72	3	NULL	NULL
1029	NULL	NULL	0	0	-4.80	NULL	1	NULL	NULL
1030	NULL	NULL	0	0	-4.66	-0.82	16	NULL	NULL

List of Figures

1.1	SDSS galaxy map	19
1.2	Mollweide projection of the Large Scale Structures in the local Universe	21
1.3	Histogram of the CIG recession velocities.	25
1.4	Optical images of AMIGA galaxies.	26
1.5	$(g - r)$ colour–magnitude diagram for galaxies in the CIG.	27
1.6	Emission line diagnostic diagrams	28
1.7	Magnitude differences from Verley et al. (2007c)	29
1.8	Quantification of the environment from Verley et al. (2007b)	30
2.1	Diagram of the methodology	35
2.2	Star-galaxy separation	37
2.3	Photometric isolation parameters	42
2.4	Velocity difference distributions	44
2.5	Visualisation of photometric results	48
2.6	Isolation parameters in comparison to Verley et al. (2007b)	50
2.7	Photometric vs. spectroscopic estimates of the isolation parameters	53
2.8	Spectroscopic isolation parameters	54
3.1	Escape speed method	62
3.2	Gaussian distribution of physical satellites	63
3.3	3-Dimensional view of the environment	66
3.4	LSS isolation parameters	67
3.5	Characterisation of satellites versus the background population	69
3.6	Comparison of satellites with Verley et al. (2007c)	70
3.7	The ten most isolated CIG galaxies in the SDSS-DR9 footprint	72
3.8	CIG galaxy properties as a function of the environment	75
3.9	Properties of satellites as a function of primary stellar mass	76
4.1	Selection of physical pairs and triplets	84
4.2	Redshift distribution for isolated, pair, and triplet galaxies	86
4.3	Example images for isolated galaxies	87
4.4	Example images for isolated pairs	88
4.5	Example images for isolated triplets	89
4.6	LSS isolation parameters for isolated galaxies, isolated pairs, and isolated triplets	94
4.7	Distribution of the <i>ICI</i> for isolated galaxies, isolated pairs, and isolated triplets.	95
4.8	Mass ratios for isolated pairs and triplets galaxies	97
4.9	Distribution of isolated systems with respect to the LSS (1)	98
4.10	Distribution of isolated systems with respect to the LSS (2)	99
4.11	Euclidean Minimum Spanning Tree (1)	101
4.12	Euclidean Minimum Spanning Tree (2)	102
A.1	Interactive 3D visualisation software: pie chart	109
A.2	Interactive 3D visualisation software: Mollweide projection	111
C.1	Code for SDSS photometric flags.	121

List of Tables

2.1	Estimation of apparent diameters from the SDSS	38
2.2	Revision of the isolation degree using photometric data	41
2.3	Means and standard deviations of the isolation parameters for the CIG and for the comparison samples	41
2.4	Revision of the isolation degree using spectroscopic data	45
4.1	SDSS-based catalogue of 3D isolated galaxies	90
4.2	SDSS-based catalogue of 3D isolated pair galaxies	91
4.3	SDSS-based catalogue of 3D isolated triplet galaxies	92
D.1	Summary of samples used in the study	124
D.2	Quantification of the local and large scale environment	125

Bibliography

- Añorve, C., López-Cruz, O., Ibarra-Medel, H., & León-Tavares, J. 2009, in American Institute of Physics Conference Series, Vol. 1201, American Institute of Physics Conference Series, ed. S. Heinz & E. Wilcots, 131–134
- Aars, C. E., Marcum, P. M., & Fanelli, M. N. 2001, *AJ*, 122, 2923
- Abazajian, K., Adelman-McCarthy, J. K., Agüeros, M. A., et al. 2003, *AJ*, 126, 2081
- Abazajian, K. N., Adelman-McCarthy, J. K., Agüeros, M. A., et al. 2009, *ApJS*, 182, 543
- Abell, G. O. 1958, *ApJS*, 3, 211
- Abell, G. O., Corwin, Jr., H. G., & Olowin, R. P. 1989, *ApJS*, 70, 1
- Adams, M. T., Jensen, E. B., & Stocke, J. T. 1980, *AJ*, 85, 1010
- Adams, S. M., Zaritsky, D., Sand, D. J., et al. 2012, *AJ*, 144, 128
- Agustsson, I. & Brainerd, T. G. 2010, *ApJ*, 709, 1321
- Ahn, C. P., Alexandroff, R., Allende Prieto, C., et al. 2012, *ApJS*, 203, 21
- Allam, S. S., Tucker, D. L., Lee, B. C., & Smith, J. A. 2005, *AJ*, 129, 2062
- Anderhalden, D., Schneider, A., Macciò, A. V., Diemand, J., & Bertone, G. 2013, *J. Cosmology Astropart. Phys.*, 3, 14
- Arakelian, M. A. & Magtesian, A. P. 1981, *Astrofizika*, 17, 53
- Athanassoula, E. 1984, *Phys. Rep.*, 114, 321
- Athanassoula, E. 2003, in *IAU Symposium*, Vol. 208, *Astrophysical Supercomputing using Particle Simulations*, ed. J. Makino & P. Hut, 177
- Baldry, I. K., Balogh, M. L., Bower, R. G., et al. 2006, *MNRAS*, 373, 469
- Balogh, M. L., Christlein, D., Zabludoff, A. I., & Zaritsky, D. 2001, *ApJ*, 557, 117
- Bell, E. F., McIntosh, D. H., Katz, N., & Weinberg, M. D. 2003, *ApJS*, 149, 289
- Bell, E. F., Phleps, S., Somerville, R. S., et al. 2006, *ApJ*, 652, 270
- Bernardi, M., Shankar, F., Hyde, J. B., et al. 2010, *MNRAS*, 404, 2087
- Bertin, E. & Arnouts, S. 1996, *A&AS*, 117, 393
- Blanton, M. R., Kazin, E., Muna, D., Weaver, B. A., & Price-Whelan, A. 2011, *AJ*, 142, 31
- Blanton, M. R. & Moustakas, J. 2009, *ARA&A*, 47, 159
- Blanton, M. R. & Roweis, S. 2007, *AJ*, 133, 734

- Bozek, B., Wyse, R. F. G., & Gilmore, G. 2013, *ApJ*, 772, 109
- Brosch, N. & Shaviv, G. 1982, *ApJ*, 253, 526
- Byrd, G. G. & Howard, S. 1992, *AJ*, 103, 1089
- Calvi, R., Poggianti, B. M., Fasano, G., & Vulcani, B. 2011, *MNRAS*, L354
- Choi, J.-H., Weinberg, M. D., & Katz, N. 2007a, in *Bulletin of the American Astronomical Society*, Vol. 39, American Astronomical Society Meeting Abstracts, 126.02
- Choi, Y.-Y., Park, C., & Vogeley, M. S. 2007b, *ApJ*, 658, 884
- Choi, Y.-Y., Woo, J.-H., & Park, C. 2009, *ApJ*, 699, 1679
- Colbert, J. W., Mulchaey, J. S., & Zabludoff, A. I. 2001, *AJ*, 121, 808
- Colless, M., Dalton, G., Maddox, S., et al. 2001, *MNRAS*, 328, 1039
- Cooper, M. C., Griffith, R. L., Newman, J. A., et al. 2012, *MNRAS*, 419, 3018
- Courtois, H. M., Pomarède, D., Tully, R. B., Hoffman, Y., & Courtois, D. 2013, *AJ*, 146, 69
- Coziol, R., Torres-Papaqui, J. P., Plauchu-Frayn, I., et al. 2011, *Rev. Mexicana Astron. Astrofis.*, 47, 361
- Crook, A. C., Huchra, J. P., Martimbeau, N., et al. 2007, *ApJ*, 655, 790
- Dahari, O. 1984, *AJ*, 89, 966
- Dariush, A., Cortese, L., Eales, S., et al. 2011, *MNRAS*, 418, 64
- Dawson, K. S., Schlegel, D. J., Ahn, C. P., et al. 2013, *AJ*, 145, 10
- Diaferio, A. & Geller, M. J. 1997, *ApJ*, 481, 633
- Dressler, A. 1980, *ApJ*, 236, 351
- Dressler, A., Oemler, Jr., A., Couch, W. J., et al. 1997, *ApJ*, 490, 577
- Durbala, A., Buta, R., Sulentic, J. W., & Verdes-Montenegro, L. 2009, *MNRAS*, 397, 1756
- Durbala, A., Sulentic, J. W., Buta, R., & Verdes-Montenegro, L. 2008, *MNRAS*, 390, 881
- Edman, J. P., Barton, E. J., & Bullock, J. S. 2012, *MNRAS*, 424, 1454
- Einasto, M. & Einasto, J. 1987, *MNRAS*, 226, 543
- Eisenstein, D. J., Weinberg, D. H., Agol, E., et al. 2011, *AJ*, 142, 72
- Ellison, S. L., Patton, D. R., Simard, L., et al. 2010, *MNRAS*, 407, 1514
- Elyiv, A., Melnyk, O., & Vavilova, I. 2009, *MNRAS*, 394, 1409
- Elyiv, A. A., Karachentsev, I. D., Karachentseva, V. E., Melnyk, O. V., & Makarov, D. I. 2013, *Astrophysical Bulletin*, 68, 1
- Espada, D., Verdes-Montenegro, L., Huchtmeier, W. K., et al. 2011, *A&A*, 532, A117
- Fernández Lorenzo, M., Sulentic, J., Verdes-Montenegro, L., & Argudo-Fernández, M. 2013, *MNRAS*, 434, 325
- Fernández Lorenzo, M., Sulentic, J., Verdes-Montenegro, L., et al. 2012, *A&A*, 540, A47
- Ferrero, I., Abadi, M. G., Navarro, J. F., Sales, L. V., & Gurovich, S. 2012, *MNRAS*, 425, 2817
- Fuse, C., Marcum, P., & Fanelli, M. 2012, *AJ*, 144, 57

BIBLIOGRAPHY

- González, R. E., Kravtsov, A. V., & Gnedin, N. Y. 2013, *ApJ*, 770, 96
- Gott, III, J. R., Jurić, M., Schlegel, D., et al. 2005, *ApJ*, 624, 463
- Grützbauch, R., Conselice, C. J., Varela, J., et al. 2011, *MNRAS*, 411, 929
- Guo, Q., Cole, S., Eke, V., & Frenk, C. 2011, *MNRAS*, 417, 370
- Guo, Q., Cole, S., Eke, V., & Frenk, C. 2012, *MNRAS*, 427, 428
- Hernández-Toledo, H. M., Vázquez-Mata, J. A., Martínez-Vázquez, L. A., Choi, Y.-Y., & Park, C. 2010, *AJ*, 139, 2525
- Hickson, P. 1982, *ApJ*, 255, 382
- Hogg, D. W., Blanton, M. R., Brinchmann, J., et al. 2004, *ApJ*, 601, L29
- Hoyte, F., Vogeley, M. S., & Pan, D. 2012, *MNRAS*, 426, 3041
- Hubble, E. 1929, *Proceedings of the National Academy of Science*, 15, 168
- Huchra, J. & Thuan, T. X. 1977, *ApJ*, 216, 694
- Huchra, J. P., Macri, L. M., Masters, K. L., et al. 2012, *ApJS*, 199, 26
- Hwang, H. S. & Park, C. 2010, *ApJ*, 720, 522
- Ivezić, Ž., Connolly, A., Vanderplas, J., & Gray, A. 2013, *Statistics, Data Mining and Machine Learning in Astronomy* (Princeton University Press)
- Kaiser, N. 1987, *MNRAS*, 227, 1
- Karachentsev, I. D. 1972, *Soobshcheniya Spetsial'noj Astrofizicheskoy Observatorii*, 7, 1
- Karachentsev, I. D., Makarov, D. I., Karachentseva, V. E., & Melnyk, O. V. 2010, in *Astronomical Society of the Pacific Conference Series*, Vol. 421, *Galaxies in Isolation: Exploring Nature Versus Nurture*, ed. L. Verdes-Montenegro, A. Del Olmo, & J. Sulentic, 69
- Karachentsev, I. D., Makarov, D. I., Karachentseva, V. E., & Melnyk, O. V. 2011, *Astrophysical Bulletin*, 66, 1
- Karachentseva, V. E. 1973, *Astrofizicheskie Issledovaniia Izvestiya Spetsial'noj Astrofizicheskoy Observatorii*, 8, 3
- Karachentseva, V. E., Karachentsev, I. D., & Melnyk, O. V. 2011, *Astrophysical Bulletin*, 66, 389
- Karachentseva, V. E., Karachentsev, I. D., & Sharina, M. E. 2010a, *Astrophysics*, 53, 462
- Karachentseva, V. E., Karachentsev, I. D., & Shcherbanovskiy, A. L. 1979, *Astrofizicheskie Issledovaniia Izvestiya Spetsial'noj Astrofizicheskoy Observatorii*, 11, 3
- Karachentseva, V. E., Mitronova, S. N., Melnyk, O. V., & Karachentsev, I. D. 2010b, *Astrophysical Bulletin*, 65, 1
- Karachentseva, V. E., Mitronova, S. N., Melnyk, O. V., & Karachentsev, I. D. 2010c, in *Astronomical Society of the Pacific Conference Series*, Vol. 421, *Galaxies in Isolation: Exploring Nature Versus Nurture*, ed. L. Verdes-Montenegro, A. Del Olmo, & J. Sulentic, 11
- Kauffmann, G., White, S. D. M., Heckman, T. M., et al. 2004, *MNRAS*, 353, 713
- Komatsu, E., Smith, K. M., Dunkley, J., et al. 2011, *ApJS*, 192, 18
- Koposov, S., Belokurov, V., Evans, N. W., et al. 2008, *ApJ*, 686, 279
- Leon, S. & Verdes-Montenegro, L. 2003, *VizieR Online Data Catalog*, 341, 10391
- Leon, S., Verdes-Montenegro, L., Sabater, J., et al. 2008, *A&A*, 485, 475

- Lisenfeld, U., Espada, D., Verdes-Montenegro, L., et al. 2012, *A&A*, 538, C1
- Lisenfeld, U., Verdes-Montenegro, L., Sulentic, J., et al. 2007, *A&A*, 462, 507
- MacArthur, L. A., Ellis, R. S., Treu, T., & Moran, S. M. 2010, *ApJ*, 709, L53
- Makarov, D. & Karachentsev, I. 2011, *MNRAS*, 412, 2498
- March, W. B., Ram, P., & Gray, A. G. 2010, in Proceedings of the 16th ACM SIGKDD international conference on Knowledge discovery and data mining, KDD '10 (New York, NY, USA: ACM), 603–612
- Marcum, P. M., Aars, C. E., & Fanelli, M. N. 2004, *AJ*, 127, 3213
- Márquez, I. & Moles, M. 1999, *A&A*, 344, 421
- Melnyk, O. V., Karachentseva, V. E., Karachentsev, I. D., Makarov, D. I., & Chilingarian, I. V. 2009, *Astrophysics*, 52, 184
- Morgan, I., Smith, R. M., & Phillipps, S. 1998, *MNRAS*, 295, 99
- Nair, P. B. & Abraham, R. G. 2010, *ApJS*, 186, 427
- Niemi, S.-M., Heinämäki, P., Nurmi, P., & Saar, E. 2010, *MNRAS*, 405, 477
- Odehahn, S. C. 1995, *PASP*, 107, 770
- Odehahn, S. C., Cohen, S. H., Windhorst, R. A., & Philip, N. S. 2002, *ApJ*, 568, 539
- Odehahn, S. C., Windhorst, R. A., Driver, S. P., & Keel, W. C. 1996, *ApJ*, 472, L13
- Pan, D. C., Vogeley, M. S., Hoyle, F., Choi, Y.-Y., & Park, C. 2012, *MNRAS*, 421, 926
- Park, C., Choi, Y., Vogeley, M. S., Gott, I. J. R., & Blanton, M. R. 2007, *ApJ*, 658, 898
- Petrosian, V. 1976, *ApJ*, 209, L1
- Pisano, D. J., Wilcots, E. M., & Liu, C. T. 2002, *ApJS*, 142, 161
- Planck Collaboration, Ade, P. A. R., Aghanim, N., et al. 2013a, *ArXiv e-prints*
- Planck Collaboration, Ade, P. A. R., Aghanim, N., et al. 2013b, *ArXiv e-prints*
- Prada, F., Vitvitska, M., Klypin, A., et al. 2003, *ApJ*, 598, 260
- Sabater, J., Best, P. N., & Argudo-Fernández, M. 2013, *MNRAS*, 430, 638
- Sabater, J., Leon, S., Verdes-Montenegro, L., et al. 2008, *A&A*, 486, 73
- Sabater, J., Verdes-Montenegro, L., Leon, S., Best, P., & Sulentic, J. 2012, *A&A*, 545, A15
- Sales, L. & Lambas, D. G. 2005, *MNRAS*, 356, 1045
- Schlegel, D. J., Finkbeiner, D. P., & Davis, M. 1998, *ApJ*, 500, 525
- Skrutskie, M. F., Cutri, R. M., Stiening, R., et al. 2006, *AJ*, 131, 1163
- Smee, S., Gunn, J. E., Uomoto, A., et al. 2012, *ArXiv e-prints*
- Solomon, P. M. & Sage, L. J. 1988, *ApJ*, 334, 613
- Strateva, I., Ivezić, Ž., Knapp, G. R., et al. 2001, *AJ*, 122, 1861
- Strauss, M. A., Weinberg, D. H., Lupton, R. H., et al. 2002, *AJ*, 124, 1810
- Strauss, M. A. & Willick, J. A. 1995, *Phys. Rep.*, 261, 271

BIBLIOGRAPHY

- Sulentic, J. W., Verdes-Montenegro, L., Bergond, G., et al. 2006, *A&A*, 449, 937
- Sutter, P. M., Lavaux, G., Wandelt, B. D., & Weinberg, D. H. 2012, *ApJ*, 761, 44
- Tikhonov, A. V. & Karachentsev, I. D. 2006, *ApJ*, 653, 969
- Tollerud, E. J., Boylan-Kolchin, M., Barton, E. J., Bullock, J. S., & Trinh, C. Q. 2011, *ApJ*, 738, 102
- Tollerud, E. J., Bullock, J. S., Strigari, L. E., & Willman, B. 2008, *ApJ*, 688, 277
- Tonry, J. L., Blakeslee, J. P., Ajhar, E. A., & Dressler, A. 2000, *ApJ*, 530, 625
- Toribio, M. C., Solanes, J. M., Giovanelli, R., Haynes, M. P., & Masters, K. L. 2011, *ApJ*, 732, 92
- Trujillo, I., Rudnick, G., Rix, H.-W., et al. 2004, *ApJ*, 604, 521
- Tully, R. B. 1987, *ApJ*, 321, 280
- Vanderplas, J., Connolly, A., Ivezić, Ž., & Gray, A. 2012, in *Conference on Intelligent Data Understanding (CIDU)*, 47–54
- Varela, J., Moles, M., Márquez, I., et al. 2004, *A&A*, 420, 873
- Vavilova, I. B., Melnyk, O. V., & Elyiv, A. A. 2009, *Astronomische Nachrichten*, 330, 1004
- Verdes-Montenegro, L., Sulentic, J., Lisenfeld, U., et al. 2005, *A&A*, 436, 443
- Verley, S., Combes, F., Verdes-Montenegro, L., Bergond, G., & Leon, S. 2007a, *A&A*, 474, 43
- Verley, S., Leon, S., Verdes-Montenegro, L., et al. 2007b, *A&A*, 472, 121
- Verley, S., Odewahn, S. C., Verdes-Montenegro, L., et al. 2007c, *A&A*, 470, 505
- Vettolani, G., de Souza, R., & Chincarini, G. 1986, *A&A*, 154, 343
- Wang, J., Frenk, C. S., Navarro, J. F., Gao, L., & Sawala, T. 2012, *MNRAS*, 424, 2715
- Wang, W. & White, S. D. M. 2012, *MNRAS*, 424, 2574
- Wang, Y., Brunner, R. J., & Dolence, J. C. 2013, *MNRAS*
- Xu, C. & Sulentic, J. W. 1991, *ApJ*, 374, 407
- York, D. G., Adelman, J., Anderson, J. J. E., et al. 2000, *AJ*, 120, 1579
- Zwicky, F. & Kowal, C. T. 1968, "Catalogue of Galaxies and of Clusters of Galaxies", Volume VI, ed. Zwicky, F., Herzog, E., & Wild, P.